The Sliding Wear of UHMWPE against Ceramics in Solutions Containing Proteins

By

Melissa Kernick

A thesis submitted to the faculty of engineering, University of Cape Town in fulfillment of the degree of Master of Science in Engineering

Department of Materials Engineering

University of Cape Town

August 1996

Abstract

The sliding wear behaviour of ultrahigh molecular weight polyethylene (UHMWPE) sliding against partially stabilised zirconia (PSZ) and alumina ceramic counterfaces in various lubricating media was investigated. Wear tests were conducted in order to investigate the effect that the addition of proteins to the lubricating solutions had on the wear behaviour of the UHMWPE against a smooth counterface of PSZ . The lubricants selected were physiological saline solution, distilled water and physiological saline solution containing small additions of synovial fluid and up to 15% by volume of albumen solution. The effect of the addition of proteins to the lubricating solutions on the production of wear debris was also studied.

The effect of changing the counterface roughness from R_a of 0.01μm to 0.06μm was also investigated. The wear behaviour of UHMWPE against alumina ceramics in distilled water was compared to that of UHMWPE against PSZ in similar conditions.

The results showed that the addition of protein to the lubricating solution reduced the wear rates over sliding distances of 35km after which wear rates resembled those found from distilled water. The polymer pins tested in distilled water lost material form the surface in the form of sheets that were readily lost once shear had taken place. The polymer pins tested in the protein solutions lost material in the form of stringers from the pin surfaces. At increased sliding distances, cracking of the polymer wear pin surfaces was also observed for the pins tested in distilled water, cracking was more widespread for increased protein contents in the lubricating solutions.

The mode of polymer removal from the wear pins is through debonding at the interface of the deformed surface layers and the bulk material. The mode of material removal for UHMWPE in distilled water is one of macroscopic asperity wear whereby the polymer asperity peaks are significantly larger than those on the wearing counterface. Plastic strain is built up in the polymer peaks during sliding wear and polymer are removed when the plastic failure strain of the polymer peak is reached. These debonded regions are lost in the form of sheet debris. In the protein containing solutions the debonded regions

appeared as stringers. After long exposure times in albumen containing solutions deep cracking of the polymer wear pin surface was observed. Polymer removal from the wear pins tested in the protein containing lubricants was concluded to be a result of the weakening of the intermolecular forces between the oriented long chain molecules on the surface which are then sheared from the pin surface in the form of stringers.

Transfer of UHMWPE to the PSZ surfaces occurred in an uneven manner and no coherent transfer layer was observed. Analysis of the ceramic counterfaces which had been tested in the protein solutions revealed the presence of a film of protein on the surface of the ceramic counterface.

The size and morphology of the polymer debris was found to be dependent on the composition of the lubricating solutions. The debris characteristic of the albumen containing solutions was found to be smaller and spherical in shape when compared with that typical of the distilled water solution which was generally larger and flake like in morphology. The morphology of the debris retrieved from the tests conducted in distilled water suggests that this debris was produced by polymer shearing from the interface of the deformed zone and the bulk material. The morphology of the finer particles is indicative of having been formed from rolled up stringers or the break up of larger wear particles or from the loss of transferred particles on the counterface.

Increasing the counterface roughness was found to increase the wear rates in all solutions by about 3.4 times. More polymer transfer was observed on the ceramic counterfaces with transferred polymer acting as preferential sites for further transfer. No coherent transfer layer was observed. It was concluded that increasing the counterface roughness results in more polymer particles being trapped by asperities on the rougher counterfaces.

The wear rates of the UHMWPE sliding against PSZ were lower than those found for the UHMWPE sliding against alumina counterfaces. This was attributed to the better surface

finish of the PSZ counterfaces and the lack of porosity of the PSZ counterfaces when compared with the alumina counterfaces.

It was concluded that the addition of proteins to the lubricating solutions does have an effect on the wear rates. Furthermore the addition of proteins to the lubricating solutions influences the dominant wear mode and the way in which debris is formed, in addition to having an effect on the size and morphology of the debris that is formed as a result of the wear process.

Acknowledgements

My most heartfelt thanks goes to the following people. Professor Allen for his unfailing patience especially with my last minute decisions. To Glen Newins, Nick Dreeze and Reggie Hendricks for their technical help and to Bernard Greeves and James Peterson for their extremely prompt photographic work. Thanks also to Drs. Grobblar, Scher, Pollack and Hanna for their help in the supply of synovial fluid. And to Wynand Louw for XPS, SIMS and AES analyses. And to Candy, Suzie and Mom for helping me through the rough spots, I can't thank you enough.

Thank you to Boart Longyear Research Centre and Eskom for financial assistance that made this project possible.

Contents

Abstract ii

Introduction 1

Aims of Research Project 2

Chapter 1 - Structure and Properties of UHMWPE 3

1.1 Polymer Structure

1.1.1 Introduction 3

1.1.2 Crystallites 3

1.1.3 The Unit Cell 4

1.2 Polymer Morphology in the Melt Crystallised State 4

1.3 Molecular Orientation 7

1.4 The Amorphous Region 10

1.5 Mechanical Properties 11

1.6 Electrical Properties 13

Chapter 2 - Friction and Wear 14

2.1 Friction 14

2.1.1 Introduction 14

2.1.2 True Area of Contact 15

2.1.3 Adhesion Theory of Friction 17

2.1.4 Elastic Plastic Transition 19

2.1.5 Junction Growth 20

2.1.6 Sliding Friction of Plastics 20

2.2 Wear 22

2.2.1 Introduction 22

2.2.2 Adhesive Wear 23

2.2.3 Abrasive Wear 24

2.2.4 Fatigue Wear 25

2.2.5 Corrosive Wear 26

2.3 Polymer Properties Affecting Friction and Wear 27

2.3.1 Introduction 27

2.3.2 Viscoelasticity 27

2.3.3 Mechanical Properties 28

2.4 Wear of UHMWPE 29

2.4.1 Introduction 29

2.4.2 Wear Modes 29

2.4.3 Counterface Roughness 30

2.4.4 Grinding Direction 31

2.4.5 Morphology 32

2.5 Wear in Prosthetic Implants 33

2.5.1 Introduction 33

2.5.2 Materials in Use 35

2.5.3 UHMWPE Wear in Implants 37

2.5.4 Wear Debris Effects 38

2.6 Lubrication 40

2.6.1 Introduction 40

2.6.2 Hydrodynamic Lubrication 40

2.6.3 Elastohydrodynamic Lubrication 41

2.6.4 Thin Film or Mixed Lubrication 42

2.6.5 Boundary Lubrication 42

2.7 Lubrication of Implants 44

2.7.1 Introduction 44

2.7.2 Articular Cartilage 45

2.7.3 Synovial Fluid 45

2.7.4 Lubrication Action of Joints 47

2.7.5 The Effect of Protein on the Lubricating Function of Synovial Fluid

Chapter 3 - Experimental Methods 49

3.1 Test Materials 49

3.2 Test Apparatus 52

3.2.1 Specimen Location 55

3.2.2 Loading Mechanism 55

3.2.3 Coolant Bath 55

3.3 Test Parameters 56

3.4 Experimental Measurements 60

3.4.1 Measurement of Specific Wear Rate 60

3.4.2 Measurement of Counterface Roughness 60

3.4.3 Measurement of Frictional Forces 60

3.4.4 Collection of Wear Debris 62

3.4.5 Test Reproducibility 63

3.5 Polymer Characterisation 64

3.5.1 Scanning Electron Microscopy 64

3.5.2 Energy Dispersive Spectroscopy (EDS) 64

3.5.3 Optical Microscopy 64

3.5.4 Scratch Tests 65

3.6 Counterface Characterisation 66

3.6.1 Optical Microscopy 66

3.6.2 Scanning Electron Microscopy 66

3.6.3 X-Ray Photoelectron Microscopy (XPS) 66

3.6.4 Secondary Ion Mass Spectroscopy 66

3.6.5 Auger Electron Spectroscopy 66

3.7 Wear Debris Analysis 68

3.7.1 Scanning Electron Microscopy (SEM) 68

3.7.2 Energy Dispersive Spectroscopy (EDS) 68

Chapter 4 - Results 69

4.1 Introduction 69

4.2 Wear **70**

4.2.1 Wear Studies on Zirconia Counterfaces with Average Initial Surface Roughness 0.01μm 74

4.2.2 Wear Studies for Increasing Counterface Roughness 80

4.2.3 Wear Studies on Two Ceramic Counterfaces 82

4.2.4 Summary 83

4.3 Friction **84**

4.4 Polymer Behaviour **85**

4.4.1 SEM Examination of Worn Polymer Pin Surfaces 85

Part 1 Distilled Water Lubrication 87

Part 2 5% Synovial Fluid Lubricant 88

Part 3 5% Albumen Lubricant 89

Part 4 10% Albumen Lubricant 90

Part 5 15% Albumen Lubricant 91

Part 6 Distilled Water Lubricant against Rough (0.06μm) PSZ Counterface Surfaces 93

Part 7 Alumina Counterfaces 95

4.4.2 Scratch Tests of UHMWPE Surfaces 96

4.4.3 Investigation of Subsurface Deformation of UHMWPE by Polarised Light 97

4.5 Nature of the Wear Scar **99**

4.5.1 Optical Examination of Wear Scar 99

4.5.2 SEM Examination of Counterface Wear Tracks 103

4.5.3 Analysis of Wear Scar 108

Section I XPS Analysis of Wear Scar 108

Section II SIMS Analysis of Wear Scar 111

Section III AES Analysis of Wear Scar 112

4.6 Nature of the Wear Debris **114**

4.6.1 Morphology of Wear Debris 114

4.6.2 Morphology Analysis 118
4.6.3 Size Distribution Analysis of UHMWPE Wear Debris in Albumen Solutions 121
Chapter 5 - Discussion **127**
5.1 Introduction **127**
5.2 Friction and Wear Behaviour of UHMWPE **128**
5.2.1 Saline Lubricated Sliding Wear 128
5.2.2 Water Lubricated Sliding Wear 128
5.2.2.1 The Effect of Changing the Counterface Roughness on Wear Rates 130
5.2.2.2 The Effect of Changing the Counterface on the Coefficient of Friction 131
5.2.3 Protein Lubricated Sliding Wear 132
5.2.3.1 Transfer Layer Formation 132
5.2.3.2 UHMWPE Behaviour 134
5.2.3.3 The Effect of Changing the Counterface Roughness 136
5.3 Production of Wear Debris **138**
Chapter 6 Conclusions **141**
Appendices **143**
Appendix A Other Materials Used for Implants **143**
A.1 Particle Filled Materials 143
A.2 Fibre Reinforced Materials 143
A.3 Ceramic Fibre Reinforced Ceramics 145
A.4 Hydroxyapatite-reinforced Polyethylene 146
A.6 Carbon Composite Ceramics 147
A.7 Boroaluminosilicate Ceramics 147
A.8 Silica, Aluminium Nitride and Aluminium Oxide 147
Appendix B Amino Acids **148**

Appendix C Polysaccharides 151

Appendix D Glycoproteins 152

Appendix E Properties of UHMWPE (Chirulen) 153

References 155

INTRODUCTION

In recent years, ultrahigh molecular weight polyethylene (UHMWPE) has been established as one of the foremost engineering polymers in sliding wear applications The excellent mechanical, physical and chemical properties of this material coupled with its biocompatibility has ensured widespread use. Applications range from seals and bushings in water powered mining equipment to prosthetic hip and knee implants. The majority of research into behaviour and mechanisms of the sliding wear of UHMWPE has been conducted against metallic surfaces, mainly stainless alloys. However, the increasing use of engineering ceramic materials such as alumina and partially stabilised zirconia (PSZ), particularly in prosthetics, has necessitated further sliding wear studies using these materials.

Whilst it has been shown that the establishment of a coherent UHMWPE transfer layer on the counterface is necessary to ensure low wear rates, any loss of UHMWPE as debris has important consequences in bioengineering. UHMWPE debris is one of the most common causes of failure in total hip replacements (THR'S)[1-12]. Particles of UHMWPE wear debris are transported to the hard and soft tissue adjacent to the prosthesis where they activate inflammatory cells or macrophages. The activated macrophages stimulate osteoclasts to form local bone resorption around the implant [13]. This results in osteolysis or bone loss and ultimately leads to the failure of the implant [2-12]. These tissue reactions are dependent on the size and morphology of the wear debris. However relatively little research has been conducted into the size distribution of the UHMWPE wear debris formed during sliding wear and the conditions which control its production. This work is an attempt to address this issue.

The Aims of this Research Project

The objective of this work was to study the tribological behaviour of UHMWPE during reciprocating sliding wear against ceramic materials under fluid lubricating conditions, and to ascertain the conditions which control the production and size of UHMWPE debris.

The specific aims of this project were :

(i) to investigate the sliding wear behaviour of UHMWPE against PSZ and alumina ceramic counterfaces in various lubricating conditions which simulate those found in the human body

(ii) to determine the effect of the various lubricants on the formation of transfer films and the size and shape of the wear debris generated.

(iii) to qualitatively determine the size distribution of the wear debris generated for a given test.

(iv)to investigate the influence of counterface roughness (R_a), on the wear behaviour of UHMWPE when sliding against ceramic counterfaces.

CHAPTER 1

LITERATURE REVIEW

STRUCTURE AND PROPERTIES OF UHMWPE

1.1 Polymer Structure

1.1.1 Introduction

Polyethylene is an aliphatic hydrocarbon of the type $-CH_2-CH_2-CH_2-$. It is a thermoplastic and is semicrystalline. Properties such as strength, stiffness, impact strength, solubility and hardness are affected by the degree of crystallinity of the polyethylene [14].

The molecular structure of polyethylene must be considered during any investigation into its wear behaviour and the formation of wear debris.

1.1.2 Crystallites

Semicrystalline polymers are considered to be made up of crystallites which are separated from one another by amorphous material [15]. Crystallites are small relative to the length of a fully extended polymer chain, are independent of molar mass and rarely exceed 100nm in size. Crystallites are formed as shown in Figure 1.1.

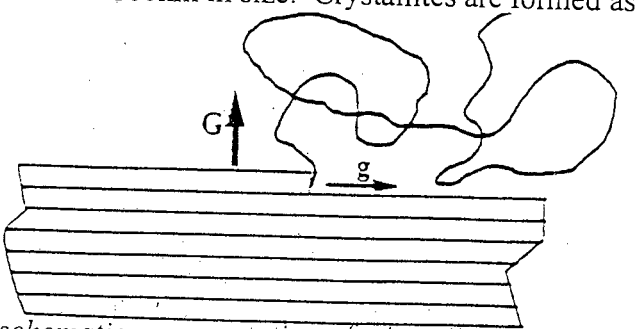

Figure 1.1 A schematic representation of a lamellar crystallite in the process of growth on a face transverse to the chain axis. For polyethylene the chain axes are normal to the diagram. Growth rates along the edge and normal to it are indicated by g and G respectively [16].

A point is reached where the chain growing into a crystallite becomes strained as the rest of the molecule becomes tightly entangled. Incorporating more segments of the chain at this stage would require work to be done against stress. This work soon equals the decrease in free energy which would result from further crystallisation. This effectively impedes further crystallisation. Separated sections of the same chain may become involved in the simultaneous development of two different crystallites. Thus each crystallite is surrounded by an amorphous band of polymer [15,16].

1.1.3 The Unit Cell

Polyethylene molecules crystallising from the molten state assume a planar zigzag arrangement along a single bonded carbon backbone as shown in Figures 1.2 and 1.3 This is the lowest Gibbs free energy state [14,17].

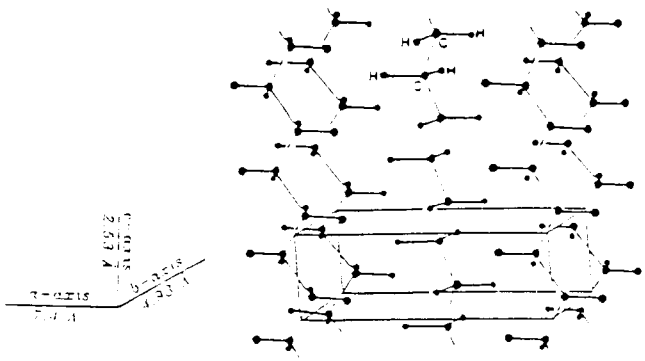

Figure 1.2 A model of the packing in the crystal structure of polyethylene (PE). Dimensions of the orthorhombic unit cell are shown [17].

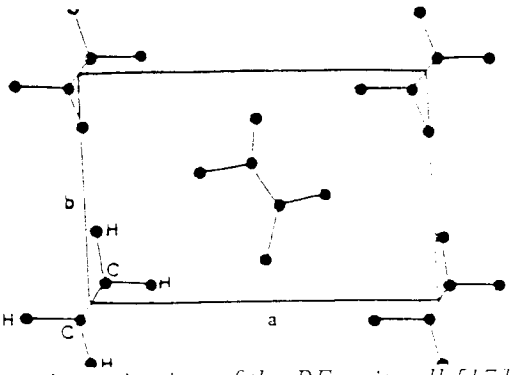

Figure 1.3 A c-axis projection of the PE unit cell [17].

Polyethylene has an orthorhombic unit cell as described by lattice vectors a, b and c. The a and b vectors characterise the side-by-side packing of the molecules. The c vector is normal to these and is parallel to the molecular axis. The length of the c-axis is determined by the crystallographic repeat unit [14,17].

1.2 Polymer Morphology in the Melt Crystallised State

The predominant morphology of polyethylene is spherulitic in nature. A typical structure of a spherulite is shown in Figure 1.4 .

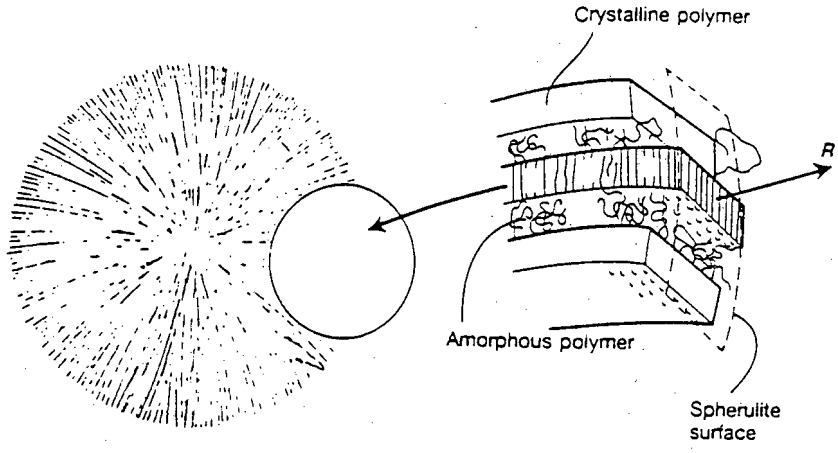

Figure 1.4 *A typical spherulite showing a magnified view of chain-folded lamellae. R is the spherulitic radius or b axis. The a and c axes are perpendicular to the b axis [After 14].*

The spherulite is made up of helically twisted lamellae that radiate from a common centre of nucleation. Amorphous material is trapped between fold surfaces, as well as being trapped between the spherulites themselves. The unit cell of polyethylene is orthorhombic with the b axis as the radial growth axis. The number, size and fine structure of the spherulite depend on the temperature of crystallisation. Crystallisation at a low temperature results in a large number of small spherulites. This is because spherulitic growth is limited by interference from neighbouring growing spherulites [17]. The lamellae are typically 5 - 40nm thick and are separated by regions of non-crystalline material [18]. There are three major motional processes in polyethylene which are known as the α, β and γ relaxations [19]. The α process is significant in possible solid state diffusion [20] and is assigned 180° jumps of chain steps in the crystallites [21]. This motion effectively involves a rotation and a translation of one repeat unit as shown in Figure 1.5.

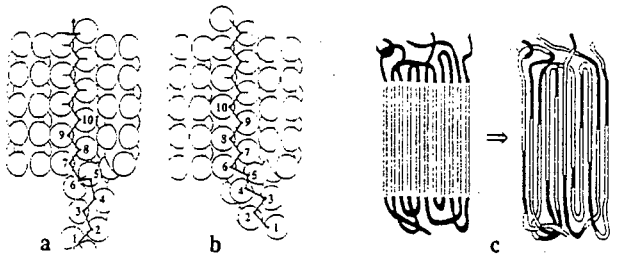

Figure 1.5 *(a) A schematic view of polyethylene chains on a crystallite near an amorphous region. The repeat units of one chain extending into the amorphous region are marked by numbers. (b) Same as (a) after one elementary step of the dynamic α process motion of the selected chain. Note the translation and the 180° rotation of the chain. (c) A schematic of chain diffusion in polyethylene. At one point in time all the chains outside of the crystallites are marked. Through many jumps of the type depicted in (a) and (b), the marked segments diffuse far into the crystallites [22].*

In high molecular weight polyethylene the chain motion process does result in large scale chain diffusion which is significantly hindered by constraints in the amorphous region [22].

The stress-strain behaviour of polymers is strongly connected with the polymer morphology. Typical stress-strain curves are associated with spherulitic, stacked lamellar and needle-like crystal morphologies. Oriented micellular morphologies can be found in thermoplastic semicrystalline homopolymers when they are crystallised under high strain rates and high undercoolings [23]. Crystallites of about $10x10x10nm^3$ form micellular units which are strongly interconnected by a large number of strained tie molecules. This morphology can also be characterised by a needle-like crystalline morphology in which the aspect ratio of the needle-crystals (l/d where l = length of the needle crystal, d = diameter) is about 1 and crystals are embedded in an oriented amorphous matrix. High molecular weight material tends to favour the formation of this morphology. This is because the nucleation density under extensional flow conditions is high and the crystal growth rate is low. (The crystal

growth rate is low as a result of the high entanglement density of the molecules when comparing them to molecules of the lower molecular weight material). Kestenbach et al., found that drawn UHMWPE films are best described by an oriented ringed micellular morphology [24]. The shearing of a micellular crystal is assumed to free a formerly extended amorphous chain segment from its crystalline junction. During reloading, the average length of the amorphous chain segments between the networks link positions will have increased. This leads to lower stresses of an equivalent level of strain as show in Figure 1.6.

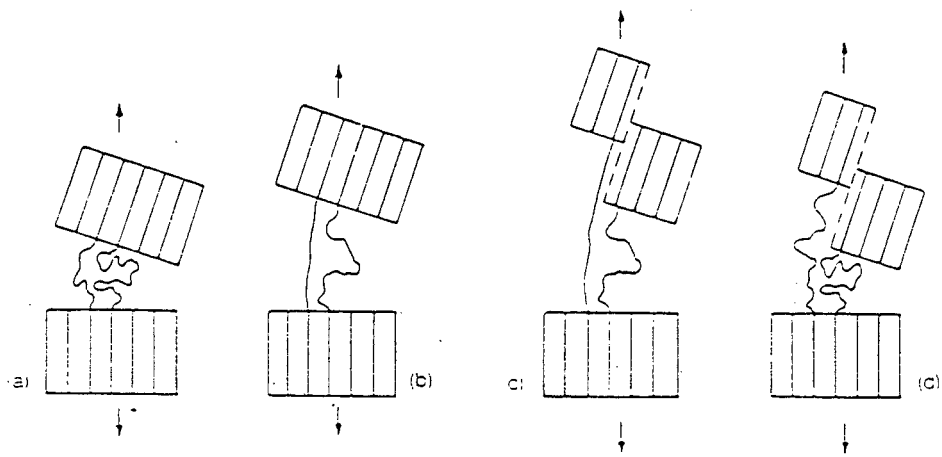

Figure 1.6 *Structural model of the deformation of the micellular morphology (a) unstrained; (b) strained to the extension of one tie molecule; (c) plastic deformation of the micellular crystal; (d) unloading. Note that the length of the left tie molecule has increased [24].*

1.3 Molecular Orientation

When a bulk polymer is crystallised in the absence of external forces, there is no preferred orientation of crystallites or molecules. However, when a linear polymer is subjected to drawing, stretching or rolling resulting in mechanical deformation and cold work, crystallites and molecular chains tend to align parallel to the direction of deformation. Two processes occur simultaneously during uniaxial drawing, strengthening from the unfolding and parallel arrangement of macromolecules along

the draw axis and fracture caused by the rupture of stressed ties chains and the splitting of crystallites [25]. Bulk crystallised polymers with a spherulitic structure which is composed of lamellar crystals growing from central nuclei, are changed upon drawing into a fibre structure. Suehiro et al. [26], postulated that, if an unfolded extended chain is released from the restraining force associated with molecular potential, it will refold to form a crystallite, the size of which is determined by the draw temperature. This results in a fibre structure which is made up of a sequential arrangement of crystallites which are interconnected by tie molecules. Any mechanically unfolded extended chains will be buried by the folded crystallites. Pigeon et al. [27] have shown that, during the roll-drawing processes, the extended chains in the crystalline phase are almost completely oriented at a draw ratio of 7 and that the trans C-C bonds in the amorphous phase orient more readily in the draw direction than the gauche effects. Peterlin suggested that the following structural metamorphosis occurs during deformation: A multilayer lamellar crystal is destroyed with chain tilting, slipping and breaking off of blocks of folded chains, with subsequent re-formation of folded chains in the fibre [28]. The molecules in the structure of semicrystalline polymers are stretched and aligned during deformation at temperatures above those of their glass transition temperatures (T_g) [29]. The deformation of the chain-folded domains in surface layers is shown Figure 1.7. The observation of kink bands [30] suggests that mechanical twinning is one of the underlying processes for the orientation of crystal lamellae. During this process the chains are tilted by a stepwise rotation of segments within the crystals into a new crystallographic position. This process is known as "c-twinning". Mechanical twinning proceeds by the migration of a twin boundary through the crystallite and the remaining parts of the crystallite shear mutually, as shown in Figure 1.8.

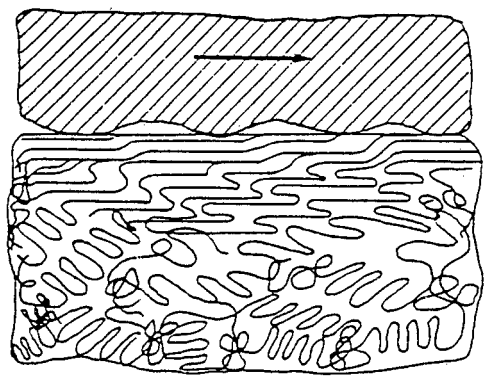

Figure 1.7 *Stretching and reorientation of polymer molecules in semicrystalline polymers above T_g during adhesive wear [after 29].*

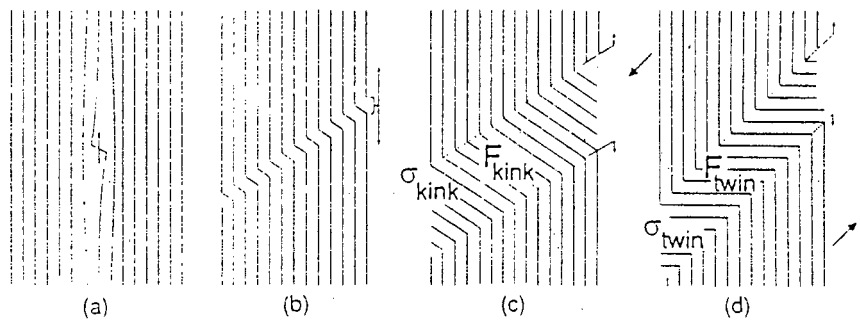

Figure 1.8 *A schematic of the possible mechanism of c-twin nucleation. (a) Single kink within a crystal can move along a chain (mechanically activated). (b) The arrangement of kinks within a kink block is energetically favourable. (c) Extending the trans sequences results in a shear deformation of the whole crystal but increases the free energy of the block not being arranged in a crystal lattice. (d) Beyond a certain length of all-trans part locking to a twinned crystal lattice at the expense of surface free energy is energetically favourable [31]*

A c-twinning process is seen to prepare the crystallites for the action of subsequent c-slip processes as can be seen in Figure 1.9.

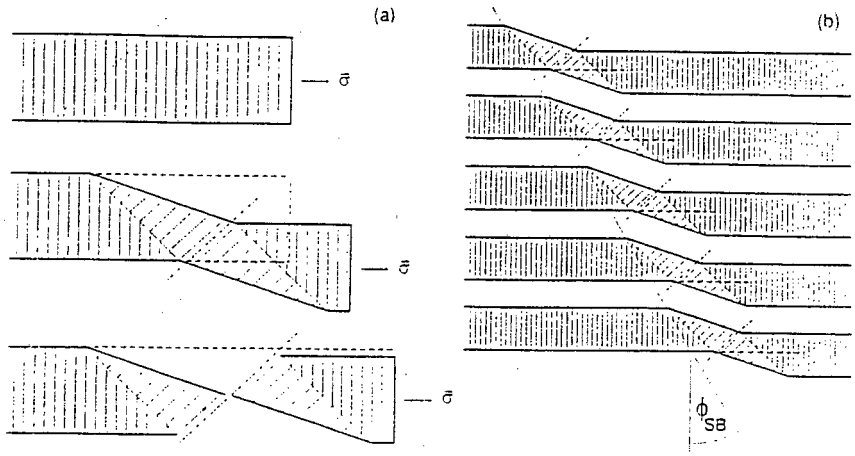

Figure 1.9 *(a) A twin starting within a lamella prepares it for c-slip. (b) Within a stack of lamellae the process must run co-operatively producing a shear band the angle ϕ_{sb} of which depends on crystallinity[31].*

Pietralla [31] concluded that twinning results in gradual deformation combined with a large orientational step. C-twinning tilts the chains within the lamellae, begins to destroy them and brings the crystallites into orientations suited for c-slip.

1.4 The Amorphous Region

In polymeric materials the molecular morphology in the amorphous regions depends on the parameters of the resulting heterogeneous structure and on the mechanism of crystallisation. The amorphous regions contain chain segments of three types fixed to the crystallite surface. These are tie chains, loops and free ends as seen in Figure 1.10 (a) [32]. There are three different subtypes of loops, which are dependent on the length and positions of the loop ends on the crystallite surface. These are regular folds, loose loops with adjacent re-entry, and random re-entrant loops (Figure 1.10(b)) [33]. There is a certain amount of orientation in the amorphous region on drawing. Elyasevich et al. [34] showed that the amorphous region of oriented HDPE prepared from a crystallised material contains pores to the order of 80nm and the volume fraction of these pores increases for increasing orientation.

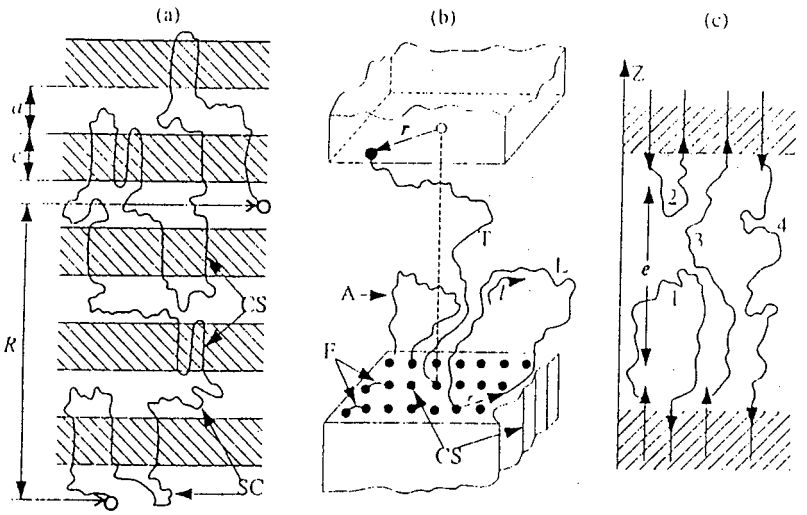

Figure 1.10 *Macromolecule in stacked lamellar model. (a) Stacked-lamellae. 'c' is the thickness of lamella, 'a' is the thickness of the amorphous region, 'R' is end-to-end distance of macromolecule, 'SC' is chain segments in amorphous region, 'CS' is Crystal stems. (b) Different types of chain segments. 'F' is regular folds, 'A' is adjacent re-entrant loops, 'L' is random re-entrant loops, 'T' is tie chains; 'r' and 'l' are parameters of chain segment state. (c) Different types of loops (n = 1,2), and tie chains (n = 3,4) distinguished by the direction of vector round at the entrance and exit of the surface of the crystallite. 'Z' is the axis of drawing and 'e' is the unit vector of the macromolecule round [35].*

1.5 Mechanical Properties

The mechanical properties of UHMWPE are the single largest factor which determine the choice of UHMWPE as an implant material. Materials used for prosthetic implants are subjected to demanding loading and environmental conditions. The requirements of a material functioning as an acetabular cup can be summarised as follows:

1. The average lifespan should ideally be 30 years or more
2. The material should be fatigue resistant in the physiological environment
3. The material should be biocompatible

4. The material should be able to withstand loading without substantial dimensional changes and no brittle failure
5. There should be minimal creep
6. There should be minimal stress corrosion
7. The material should maintain its properties in the physiological environment, i.e. it should be stable at 37°C and should not react to the presence of synovial fluid or blood plasma

The mechanical properties of polyethylene are particularly dependent on the molecular weight and the degree of branching of the polymer. Other factors influencing the observed mechanical properties of polyethylene are: the rate of testing, the temperature of the test, the method of specimen preparation and the size and shape of the specimen. These must therefore be kept constant for results of any tests to be comparable [36].

The general effects of changing the rate of testing, temperature and the density of the polymer are shown in Figure 1.11. Lowering the test temperature or increasing the testing rate produces a pronounced "hump", with the apex being the yield point. Up to the yield point, the deformations are recoverable and the behaviour of the polymer is considered Hookean. Working the sample results in strain softening as a result of spherulitic breakdown or crystalline melting. This causes the polymer to extend under constant stress. During this period the polymer chains become aligned and this induces crystallisation. This in turn causes the stiffening of the sample which can be seen by the upward sweep of the stress-strain curve [36].

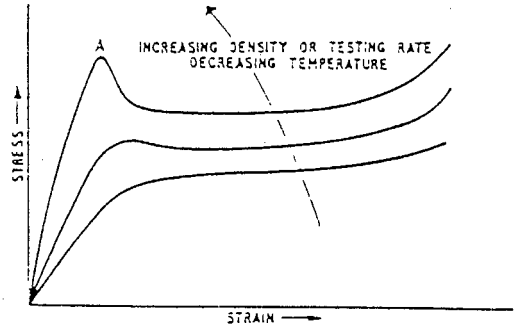

Figure 1.11 The effect if changing the rate of testing, the temperature and the density of the polymer [36].

Elongation to break is dependent on the density of the material. High density polymers tend to be more brittle than those of lower molecular weight. Polyethylene will deform continuously under load (i.e. it will creep). The mechanical properties of UHMWPE define the way in which the UHMWPE reacts to a wear situation and these will be dealt with in greater detail in section 2.4.

1.6 Electrical Properties

Polyethylene (PE) has good insulating properties when compared to other dielectric materials. It is non-polar, and therefore its power factor and dielectric constant are almost independent of temperature and frequency. The dielectric constant is linearly dependent on density. The oxidation of PE with the formation of carbonyl groups can cause a large increase in the power factor and therefore antioxidants are added to reduce this effect [36]. It is important to consider the electrical properties of an implant materials because they are subject to an ionic environment. Furthermore, the presence of proteins in the physiological environment can be complicated by the electrical properties of a polymer substrate because, the way in which proteins adsorb onto a polymer surface is largely determined by the polarity and the charge on the polymer surface [37].

CHAPTER 2
LITERATURE REVIEW

FRICTION AND WEAR

2.1 Friction

2.1.1 Introduction

When a polymer slides over a rigid substrate, the force of friction between the two materials is a result of the action of two mechanisms; an adhesion mechanism and a deformation mechanism [38]. The adhesion mechanism arises from the interaction of the intermolecular forces across the interface, which necessitates work being done to break these forces so that sliding can occur. The deformation mechanism arises from the mechanical interaction of the two surfaces. The deformation component is the contribution to the total frictional force from the ploughing of asperities of the harder solid through the surface of the softer polymer. Surface melting, material transfer, reorientation and chemical degradation can contribute to the adhesion component of friction, while viscoelastic ploughing and elastic tearing can contribute to the deformation component of friction [39].

2.1.2 True Area of Contact

Real surfaces are not atomically smooth, so when two surfaces come into contact, the asperities on the respective surfaces and the deformation properties of the materials under loading determine the true area of contact. The interaction of a smooth and undeformable surface which is put into contact with a rough and deformable surface is shown in Figure 2.1.

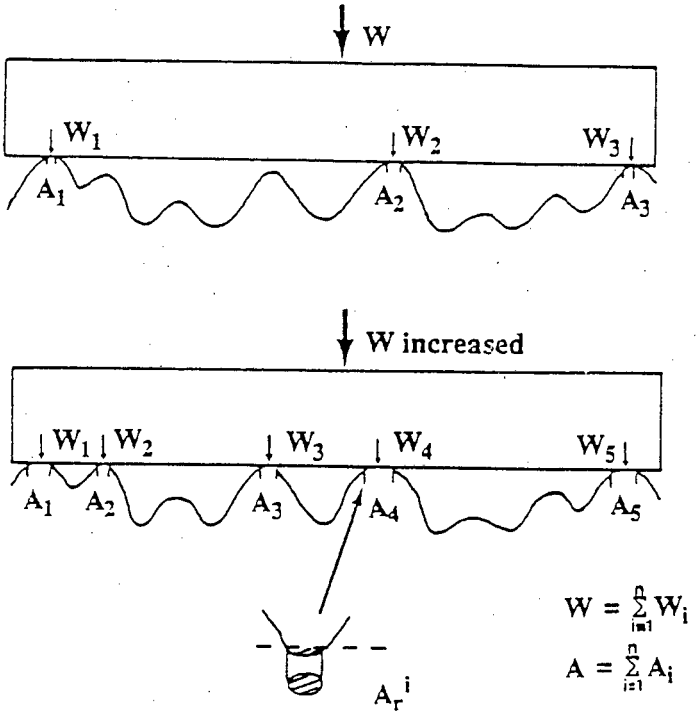

Figure 2.1 The interaction of a rough and deformable surface with a smooth and undeformable surface [40].

As the load is increased, existing contacts will grow in size and new contacts will be formed as the asperities in the lower levels come into contact with the smooth surface. This contact is controlled by the deformation properties of the two materials as well as their topographical characteristics [40]. Assuming a Gaussian distribution of asperity heights : plasticity index , $\psi = (E/P_0)(\sigma/\beta)^{1/2}$

where E = Young's modulus

P_0= plastic yield pressure

σ = mean deviation of asperity height

β = asperity tip radius

The first term describes the mechanical properties and the second, the surface topography [40].

For polymeric materials in contact, viscoelastic and relaxation phenomena result in a time dependence of the contact area. These phenomena also result in hysterisis losses during loading and unloading cycles [41].

So, $Ar = \Sigma Ar_i << A_0$ A_0 = apparent area of contact

Ar = real area of contact

Generally, if asperities are the same height and the load W is increased, the area of contact in the range where the asperities deform elastically is proportional to $W^{2/3}$. If the number of asperity contacts increase with load so that the averages size of each asperity contact remains constant (i.e. A_r/number of contacts, is constant), then the area of contact will be proportional to W. If plastic deformation takes place, the area of contact will be proportional to W for either of the idealised distribution cases because the yield pressure for each asperity contact will be a material constant P_0 [39,40].

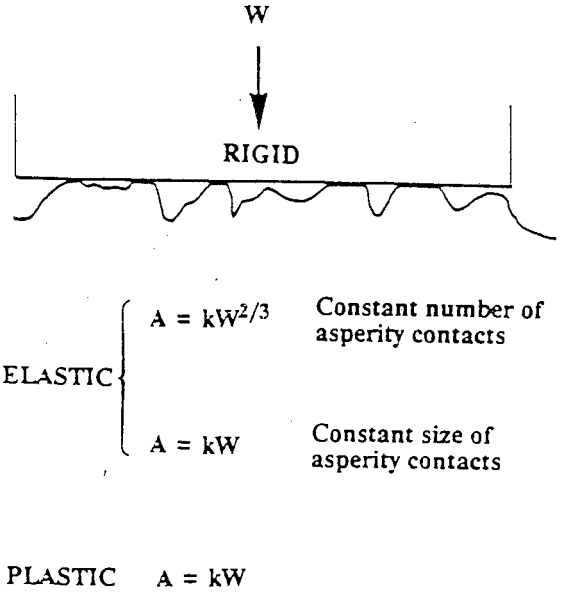

Figure 2.2 The area of contact between two surfaces in terms of asperity deformation [39].

When contact is made, adhesion occurs. Frictional resistance to sliding arises from the shearing of the cold-welded junctions which have formed the contact. Benabdallah [42] found that for UHMWPE sliding against a metallic plate the relation between τ, the shear strength, and the real contact pressure, P, was represented by a regression of the order 3. Three stages were identified

1. A decrease in τ when asperities deform elastically
2. The transitional τ remains almost constant when P approaches the same value as the yield stress of the UHMWPE material
3. An increase in τ when asperities deform plastically.

It was also found that the initial roughness of the plastic sample plays a significant role in determining the static yield strength [42].

2.1.3 Adhesion Theory of Friction

Solids adhere to one another and a force is thus required to make one body slide across another. This force is known as the frictional force which is associated with μ, the coefficient of friction. The following observations concerning frictional force were made by Amontons:

(a) The frictional force is independent of area

(b) The frictional force is directly proportional to the normal load.

Polymers do not obey Amontons' laws to any large extent and for a wide variety of loads, friction has been found to vary with load as follows:

$$F = kX^n$$

or

$$\mu = F/X = k\,X^{(n-1)}$$

where F is the frictional force,

X is the normal load

μ is the coefficient of friction

and n is a constant

for branched polyethylene, n-1 is about -0.26

Generally friction decreases for increasing load. The true area of contact must equal a constant multiplied by load X. If there is an exponential distribution of asperity heights independent of the mode of deformation of the asperities, or the shape of the asperities, then there must be exact proportionality between the load and the true area of contact [43].

Deformations associated with the deformation component of friction are usually in excess of 1μm. This component of friction is a result of the work done to slide two surfaces against each other. Thus, the measured frictional force, F (at a constant sliding velocity) is given by $F\Delta = W_f$, where W_f is the work done to move surfaces a distance Δ. This work may be expended by bringing about either plastic or viscoelastic deformations in the surfaces. The deformation component of friction is thus sub-divided into ploughing friction and hysterisis friction. Ploughing friction occurs when a harder material ploughs through a softer material. Ploughing friction is a measure of the energy dissipated by bringing about permanent plastic deformations to one or both of these materials. Hysterisis friction occurs when energy is dissipated, bringing about viscoelastic deformation by a molecular relaxation process [38].

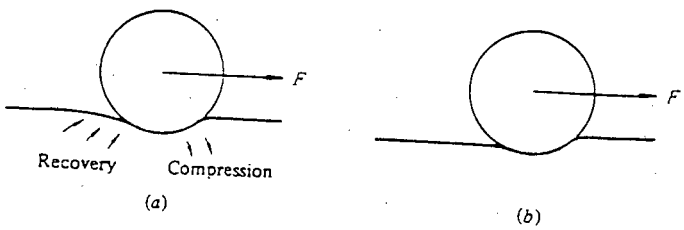

Figure 2.3 *Deformation friction (a) hysterisis friction (b) ploughing friction [38].*

For a sphere in rolling or sliding motion across a well lubricated surface the coefficient of friction is found to be:

$\mu_r = 3/16(3/4)^{1/3}\alpha([1-\nu^2]/R^2E)^{1/3}W^{1/3}$

R is the radius of the sphere

α is the fraction of input energy dissipated elastically and this varies with speed

W is the applied load /unit length

Or alternatively

$\mu_r = ([1-\nu^2]/R^2E)^{1/3}W^{1/3}\phi_5\tan\psi$

$\phi_5\tan\psi$ is a polynomial of $\tan\psi$ which is a function of the speed of sliding

The variation of the hysterisial component with velocity is shown in Figure 2.4.

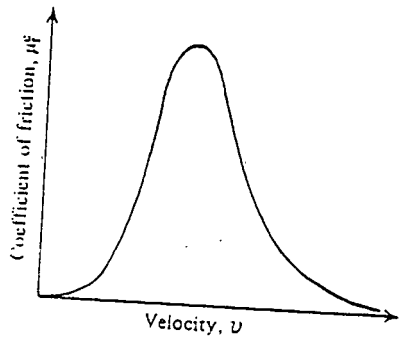

Figure 2.4 The variation of hysterisial component with velocity [38].

For ploughing friction,

$F = (32h\pi^3R^3)\text{-}1/2W^{3/2}$

$\mu = k'W^{1/2}$

where F is the frictional force

R is the radius of the spherical indentor

W is the applied load/unit length

and μ is the coefficient of friction

This shows that the coefficient of friction is very sensitive to the applied load

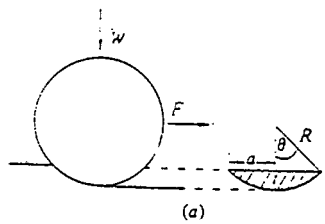

Figure 2.5 Ploughing friction for a spherical indenter [38].

2.1.4 Elastic Plastic Transition

The onset of plastic flow occurs when the mean pressure over an asperity is given by $P = 1.1\sigma_y$. Thus yielding commences at a mean pressure of 0.39h ($h = 2.82\sigma_y$). The value δ at which yielding commences is given by:

$\delta \approx Rh^2/E'^2$, where $E'^2 = E/(1\text{-}\nu^2)$.

where R is the radius of the spherical indentor

h is the effective hardness of the counterface

E is Young's Modulus

and ν is Poisson's ratio

From this the plasticity index ψ can be derived. The plasticity index describes the potential for forming plastic contacts and is given by:

$\psi = E'/h\ (\sigma/R)^{1/2}$

and $\Omega_p/\Omega = \exp.\ (-1/\psi^2)$ where Ω_p is the area of plastic contact.

Ω is the total area of contact

Therefore, for $\psi > 1.5$, contact is predominantly plastic and for $\psi < 0.5$, contact is predominantly elastic [38].

E'/h for LDPE = 8 , for HDPE = 12 and for steel = 200

2.1.5 Junction Growth

The nature of the contact, whether it is elastic or plastic, is likely to cause variations in behaviour when a load is applied tangential to the interface. Sliding cannot occur until the material at or near the interface yields. This results in what is known as von Mises yield criterion. This states : $\sigma^2 + \alpha\tau^2 = k$,τ and σ are tangential and normal stresses, k and α are constants.

If the junction is plastic and has yielded before the application of a tangential stress, then $\sigma^2 = k$. Applying a tangential force will then result in : $\sigma^2 + \alpha\tau^2 > k$.

This means that the system must yield under the action of the normal force until σ is reduced.

However, polymers behave in a predominantly elastic manner during sliding wear, therefore the normal stress is likely to reduce the value of τ which causes yielding rather than junction growth. (Increasing τ will act to increase the contact area resulting in junction growth which is characteristic of plastic contact).

Friction forces up to this point have been examined in terms of static friction, i.e. the force required for initial motion. Once sliding occurs, friction is still present in the form of sliding or kinetic friction [38].

2.1.6 Sliding Friction of Plastics

For most rigid plastics the static, μ_s and kinetic, μ_k coefficients of friction are similar. Linear PE has a significantly lower value of μ_k than of μ_s. This is because a transfer process takes place. Polymer transfer onto the counterface takes place rapidly once

sliding has been initiated. As this process continues, the transfer film becomes smooth. The initial sliding orients this polymer so that the polymer chains lie parallel to the sliding direction. Because of the molecularly smooth profile of polyethylene, the forces required to form this smooth oriented film are low. This results in a reduction of the frictional forces during sliding because, effectively a smooth polymer surface slides against another smooth polymer surface [38].

2.2 Wear

2.2.1 Introduction

Wear is a continuous inexorable process associated with two or more materials moving in contact with one another. It involves the displacement of material from a surface and this may occur by several mechanisms [43]. The most common modes are:

- **adhesive wear**
- **abrasive wear**
- **surface fatigue**
- **corrosive wear**

2.2.2 Adhesive Wear

This is the most important of the wear processes as it occurs in all wear situations. When two surfaces touch and support a normal load, atoms come into contact and so the forces between the atoms interact [44,45]. For ceramics these interatomic forces will be valency bonds, for polymers they may be Van der Waal's forces, electrostatic forces or hydrogen bonds. Increasing the applied load, increases the likelihood of strong interatomic bonding. When two surfaces are atomically clean, extremely strong bonding may occur [45]. Gong et al. [46] suggested that, if the chemical activity of the counterface is strong, the chemical bonds between the first layer of the transfer film and the substrate will result in strong adhesion between the first layer of the film and the substrate. However, the adhesion between the second and third layers of the transfer film will still be poor. This can result in the transfer layer being detached from the surface of the counterface. For sliding to occur the interfacial bonds must be broken and shear must take place in order to rupture the adhesive bonds at the interface. An adhesive interaction is developed at the interface during this shear process.

The strength of the individual structural elements in the surface layers of the material may be overcome at the onset of sliding. This results in fracture at the start of the frictional interaction [47]. In practice, the adhesive bonds seldom rupture at the interface and the bonds of the cohesively weaker material rupture instead. The fracture products that result from this process form a third body and a transferred layer may be deposited on the surface of the cohesively stronger material. Fracture does not always occur and sometimes the softer material will "find" a flaw in the harder material and cause this portion of the harder material to be removed. The transferred fragment may be back-transferred, or alternatively it may be abraded by other features of the rubbing surface. It may also become involved in the sliding process as a third body. For ceramic fragments, these are likely to cause the breakdown of any transfer film and this results in increased wear. The wear mechanism will then be abrasive [45]. For polymer fragments, the third body will form part of the transferred layer which is deposited on the cohesively stronger material. There is usually a running in

period of polymer wear following which steady state wear (in which the wear rate almost always becomes constant) is established.

2.2.3 Abrasive Wear

Abrasive wear occurs if a hard particle cuts or grooves one of the rubbing surfaces. It is most marked if the abrading particle is sharp and so acts as a small cutting tool. Abrasive wear can be in the form of two or three body wear [45].

Two body wear occurs when a rough surface or fixed abrasive particles cut a softer surface. Plastic flow of the softer surface then occurs around the asperities of the harder surface. Three body wear occurs when loose particles (usually in the form of wear debris) move relative to one another while sliding across a wearing surface. These cause the removal of materials by acting as small cutting tools [45].

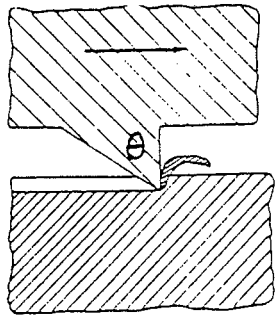

Figure2.6 Two body abrasive wear[49].

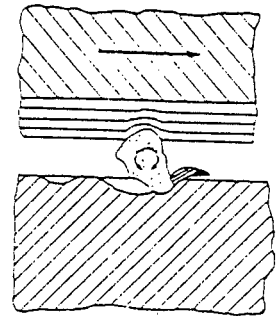

***Figure 2.7** Three body abrasive wear [49].*

For rigid polymers, abrasive wear of the hard surface asperities penetrating the surface and removing polymer by shearing or cutting may be characterised by the following relationship [48]:

$z = k\,(W/H)\tan\theta$ = volume of material removed/unit sliding distance

W = normal load

H = hardness

θ = base angle of indenting asperity

k = probability of the formation of a wear particle

In metals, plastic deformation occurs at all angles of θ, while for polymers plastic deformation only occurs when θ is greater than 30° i.e. when the apex angle is small

[49]. Thus plastic deformation only becomes the predominant mode when the indenting asperities are sharp.

Generally the deformation of polymers is part plastic, part elastic with the relative proportions depending on the roughness of the polymer surface. In abrasive wear the product $S\varepsilon$ (where S is the breaking stress and ε is the elongation to break) is important. This is because for low values of strain the work required to produce a wear fragment is proportional to $S\varepsilon$. When friction and hardness are constant, the wear rates of a polymer are believed to be some function of $1/S\varepsilon$ [43].

Cohesive energy density (CED-which is a measure of the strength of the secondary bonding in polymeric materials) of a polymer can also influence this mode of wear. The rate of thermoplastic polymer abrasive wear is inversely proportional to the root of their cohesive energies. This however only holds true if the predominant mode of deformation is plastic [43]. Abrasive wear has been described by Lancaster [50] as a combination of cutting and fatigue. Rough surfaces with sharp asperities which act as cutting tools contribute to the cutting component of abrasive wear. Rough surfaces with rounded asperities contribute to the friction component.

2.2.4 Fatigue Wear

As with adhesive wear, if there is very strong interfacial adhesion the surface layers may become detached in a single traversal. But frequently in the presence of appreciable adhesion, several traversals of the same portion of the surface may be required before a fragment can become detached. Sometimes failure is initiated at the surface by a surface flaw. These traversals over the same region involve a series of compression and recovery cycles. Associated with these cycles, are tensile stresses over the contact region resulting from adhesion and tangential movement [45]. In polymeric fatigue tribo-cracking of the polymer molecules may be due to mechanical and thermal effects.

As the counterface surface becomes smoother and the polymer more elastic, fatigue wear becomes more important. With ceramic-polymer systems it should be possible to design a system to operate below the fatigue limit. It should however be taken into

account that surfaces are not ideally smooth, and thus some asperities will experience stresses well above the fatigue limit. The environment can also have an effect on crack propagation [43]. Shallow pits and small cracks have been observed to align perpendicular to the sliding direction in the UHMWPE after prolonged sliding [43].

2.2.5 Corrosive Wear

Corrosive wear or stress corrosion is associated with a chemically active medium in the presence of an applied stress. Cracking can occur at stresses far below critical in the presence of environmental factors. Chemical degradation - possibly in the form of chain scission can profoundly influence polymer wear [43].

This is an important wear process but it is unclear as to the exact role of the chemical reactions as they differ depending on the chemical content of the tribological system.

2.3 Polymer Properties Affecting Friction and Wear

2.3.1 Introduction

The mechanical properties of a polymer are dependent on the chemical and physical nature of the polymer. The mechanical properties are also affected by the environment in which the polymer is used. Properties such as chain branching and cross-linking, chain length and crystallinity of the polymer are linked to its mechanical properties.

The mobility of polymer molecules has a critical effect in the friction and wear behaviour of the polymer. Crosslinking results in a more tightly bound network which in turn results in decreased elongation to break and increased hardness. The presence of crosslinks prevents the easy drawing out of the molecules which occurs during the formation of a transfer film on the counterface [51,52].

Orientation effects can change the mechanical properties of a polymer and subsequently affect wear rates at certain orientations of the polymer molecules. Free solidified polymer melts and pressed sheets are largely free from orientation. Drawn or hydrostatically extruded polymers are anisotropic. Anisotropic polymers have high wear rates when the chains are oriented normal to the direction of sliding. This is because the polymers are strong in the direction of orientation. Polymers are weak in the direction normal to orientation and sliding against this direction makes the polymers more susceptible to wear.

2.3.2 Viscoelasticity

Viscoelastic is the term used to describe the mechanical response of materials which exhibit both the springiness associated with elastic solids and the viscous flow associated with fluids [53]. This phenomena is associated with long and short range rearrangements of long-chain molecules. Creep and stress relaxation are characteristic of viscoelastic behaviour. Polymers are viscoelastic and therefore deformation is dependent on strain rate as well as temperature.

For a sliding speed v and a corresponding frequency f, at which the adhesion term reaches its maximum value, the critical length involved in the sliding process (l = v/f) is 50 Å. This value is comparable with the length of a segment of molecules. Thus it appears that the adhesion process of friction occurs on a molecular scale and the time- and temperature dependent properties of friction are closely related to the viscoelastic properties of the polymer [54,55].

2.3.3 Mechanical Properties

Mechanical properties such as hardness, elastic modulus, Poisson's ratio, yield stress and elongation to break control the deformation of polymeric materials.

In adhesive wear, the frictional force is the product of the shear stress τ and the real area of contact. The real area of contact is largely governed by the mechanical properties of the polymer. There is evidence that it is the mechanical properties of the polymer that govern frictional losses in the consideration of the ploughing component of friction [56]. It is however important to note that although the mechanical properties of a polymer are an important factor in determining wear behaviour, a detailed knowledge of the mechanical properties does not allow an accurate prediction of the level of wear.

2.4 Wear of UHMWPE

2.4.1 Introduction

UHMWPE is a semicrystalline polymer which, as a result of its excellent wear properties is used in many varying applications. Very high molecular weight polyethylene is available as prepared by the Ziegler process. These materials have average molecular weights in the range 1-5 E6. They are processed in the rubbery phase because difficulties with decomposition are encountered in the molten state. They are linear molecules with densities of about 0.94g/cm^3. Difficulties with crystallisation of large molecules results in the yield strength and stiffness (which are dependent on the degree of crystallinity) being worse than those obtained for linear polyethylene of conventional weights. The high molecular weight materials have high abrasion resistance and impact strength as well as good stress crack resistance and low creep [36]. It is these properties that makes the high molecular weight variety of polyethylene useful for orthopaedic implants.

2.4.2 Wear Modes

Abrasive and adhesive wear are the principal wear modes found in water lubricated sliding wear of UHMWPE against metallic and ceramic counterfaces. On rough surfaces it is generally believed that abrasion is the principal mechanism while adhesion dominates on "smooth" surfaces [57]. Marcus et al. [43] found that for rough metallic surfaces (0.3μm R_a) microcutting and ploughing caused the initial material removal after which the wear fragments were laid down in the form of a transfer layer and adhesive wear became the dominant mechanism. This transfer film results in very low wear rates at low load and low speed conditions. On smoother surfaces, with R_a less than 0.05μm, no transfer layer is observed rather, polymer is transferred to the surface as thin discontinuous patches [43]. It has been postulated that these differences can be explained by considering the wear in terms of macroscopic and microscopic wear mechanisms [1]. Microscopic asperity wear is that which is likely to dominate the wear processes for rougher counterfaces. This (abrasive or adhesive) wear is associated with deformation of a nominally flat

polymer surface by repeated interactions with the microscopic asperities of the counterface. For macroscopic asperity wear the peaks of the polymer surface are typically up to 100 times larger than those of the asperities of smooth counterfaces. These peaks are deformed by the applied load and this deformation results in surface and subsurface stress concentrations as shown in Figure 2.8.

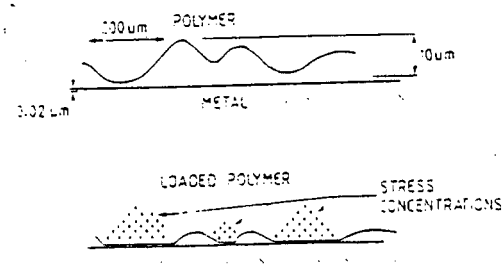

Figure 2.8 *a schematic of the proposed macroscopic asperity wear mechanism[1].*

It is likely that this deformation is built up gradually during continuous sliding until the plastic failure strain of the polymer is reached and the polymer peak is removed. When sliding occurs against rougher surfaces the polymer material is removed before significant subsurface strains can develop. Subsurface cracking has been observed in polymers after wear testing under constant load. This subsurface crack propagation may accelerate the removal of the polymer peaks and increase the macroscopic polymer wear. This type of subsurface fatigue may explain the high wear rates found in acetabular cups which articulated on smooth undamaged femoral heads [1]. Dowson and Harding found that the wear of UHMWPE against smooth high purity alumina ceramics surface roughness R_a of 0.02μm in distilled water yields a wear coefficient approximately 56% of that for UHMWPE against stainless steel in the same environment [58].

2.4.3 Counterface Roughness

The sliding wear behaviour of UHMWPE against metallic or ceramic counterfaces can be considered to be a combination of adhesive and abrasive wear. A variation in counterface roughness changes the dominant wear mechanism(s) and can determine the presence of a transfer layer. Generally rougher surfaces result in higher initial wear rates. The bedding-in period is characterised by microcutting and ploughing. Steady state wear (which is associated with a drop off in wear rates) is established once a coherent transfer layer is laid down on the counterface surface [43]. The wear

of rough surfaces is considered to be a microscopic wear mechanism whereby the asperity peaks of the counterface are up to 100 times larger than those of the polymer and act as cutting tools to cause polymer loss [1].

Smoother surfaces are thought to be characterised by adhesive wear [57]. There is no coherent build up of transfer film on smooth metallic or ceramic surfaces [44,58]. Smooth metallic surfaces exhibit a small amount of lumpy transfer [43] while ceramic surfaces show no evidence of transfer [58]. The wear of smooth surfaces is considered to be a macroscopic wear mechanism whereby subsurface strains develop as a result of the deformation of polymer asperity peaks. This strain is built up during the sliding process until the plastic failure strain is reached and the polymer peak is removed [1].

Hollander and Lancaster showed that the wear rate decreases with increasing values of average asperity radius [59]. In addition to this the wear rate has been found to be directly proportional to the base angle of the cone of a hard indentor. Bahadur and Stiglich [57] have shown that the steady state wear rate increases rapidly with the wear particle size on rough surfaces varying from r.m.s values of 0.51μm to 24.1μm.

For rough surfaces, the wear particle size has been found to vary inversely with the number of asperity peaks per mm, and to be directly proportional to the asperity angle for water lubricated wear between UHMWPE and steel [57]. Rose et al found that for bovine serum lubricated wear of UHMWPE sliding against steel, wear debris from specimens with low wear rates tend to be wholly fibrous [51] while the debris from specimens with high wear rates is coarse and granular [60]. These results were confirmed by clinical retrieval studies [61].

2.4.4 Grinding Direction

Marcus et al. [43] found that wear on cross-ground surfaces are more sensitive to counterface roughness than those obtained on parallel ground surfaces. A uniform coherent film was found to form relatively quickly when sliding takes place perpendicular to the counterface grinding direction. This is believed to be because any material that is lost by shear can be accommodated in the valleys between the

asperities of the surface. Polymer transfer was found to be patchy when sliding parallel to the counterface grinding direction [43].

2.4.5 Morphology

When HDPE slides against steel in water, wear takes place on the crystallographic a-c plane i.e. normal to the b axis. The a-c plane is the boundary where the neighbouring crystals slip over each other and in this way wear debris separates from the crystal substrate. It is possible that water molecules may be absorbed on the a-c plane where they act as a lubricant [62].

2.5 Wear in Prosthetic Implants

2.5.1 Introduction

The number of artificial hips implanted world-wide exceeds 500 000 annually [1]. These surgical implants must be able to bear the forces of normal patient activity, while at the same time withstanding mechanical failure.

Most patients undergo total hip replacements (THR's) to combat some form of bone disease such as rheumatoid arthritis or osteoarthrosis. The ideal life span required of prostheses is of the order of 30 years. However, as hip replacements become more common among younger patients, the life span required of THR's is increasing. In addition to this, the stresses placed on the THR's by a younger more active person far exceed those of older patients. The poor durability of prosthetic hip implants leads surgeons to consider alternatives wherever possible for younger patients [62].

The materials used in THR's must therefore be able to withstand the physiological environment as well as the substantial loads imposed on the hip joint. The 30 year life requirement of the THR's implies that the materials need to be fatigue resistant within the physiological environment. This means maintaining their properties at temperatures of 37°C and in the presence of synovial fluid or blood plasma. They must be biocompatible, i.e. they must not produce inflammatory reactions in the body [63]. In addition to this, prosthesis materials must withstand loading without any substantial dimension changes and without brittle failure. Furthermore, creep, fatigue and stress corrosion should be minimal [63].

In general the materials used in THR's are biostable and exhibit minimal degradation. Sliding of the two components against one another causes wear and this produces wear debris. It is this wear debris which is a commonly the cause of failure in THR's [1-12]. Particles of the UHMWPE wear debris are transported to the hard and soft tissue adjacent to the implant. These particles activate inflammatory cells (macrophages). The activated macrophages stimulate osteoclasts to cause local bone resorption or bone thinning around the implant.

Thus the choice of materials is critical to the success of the implant. Other factors to consider once the materials have been chosen are: surface finish of the materials, cleaning and sterilisation techniques and fabrication routes and their effect on biostability and service life [64].

2.5.2 Materials in Use

Artificial hip joints consist of a femoral component which attaches to the femur. The femoral head articulates in the acetabular component which in turn attaches to the acetabulum. The femoral component bears the load on the hip joint and the material of this component needs to be able to sustain loading without brittle failure. The articulation of the femoral head in the acetabular cup demands a bearing couple with very good tribological properties and superb fatigue resistance.

The materials initially used for low friction prostheses were a combination of 316L stainless steel for the femoral components and ultra high molecular weight polyethylene (UHMWPE) for the acetabular components. Steel was used because of its load-bearing capacity and corrosion resistance. The UHMWPE was used for its good tribological properties and its creep resistance when compared to other biomedical polymers. However, by the late 60's these THR's started to show limits in life expectancy. This was largely due to the high loosening rates of metal-on-metal systems and the high wear rates of the metal-on-plastic systems [65].

Advances on the materials front have introduced Co-Cr-Mo alloys, Ti-6Al-4V alloys and "commercially pure" titanium. These are less susceptible to corrosion and wear in the physiological environment than stainless steels that has been used in the past [66]. However, recent research has shown that titanium alloys have high rates of premature failure [67-72].

Alumina ceramics were introduced as joint replacement materials in the early 1970's. They are biocompatible and have low wear rates and good friction characteristics [73]. Alumina is most commonly used in THR's in conjunction with UHMWPE. This is because alumina ceramics are less dependent on the exact nature of the lubricant than the metallic materials mentioned. In addition to this, the superior wettability of ceramics when compared to metals results in good wear resistance [66].

Concern over the production of UHMWPE particles and their effect on macrophage response led to the production of ceramic:ceramic THR's. Alumina on alumina

systems have excellent wear rates and can have up to 4 000 times less wear debris than the equivalent metal on UHMWPE design. This combination is shown to have the greatest wear resistance, the least wear debris and the longest life. This is however dependent on several factors. These are :

- the size of the femoral head must not be too small or it may break.
- articular surfaces must be accurately designed with a clearance of 15 - 40μm between the two components.
- the surgeon must not hammer the acetabular cup as this may result in stress raisers.
- the cup must not be positioned too vertically because this may result in a point load which will dramatically increase wear [74].

Alumina prostheses are therefore difficult to position surgically and adjustments are very difficult to make. Generally the pair is manufactured as "matched". That is, the implant has specially paired components with tighter dimensional tolerances. In addition to this, these implants are more costly [74] and are also susceptible to so-called marginal loosening situations such as neck-cup impingement and impact forces. The high stiffness of the alumina has a tendency to cause bone shearing and subsequent failure of the implant at the bone-implant interface [74].

Further advances in THR surgery have led to the production of femoral components with modular stems. Modular stems enable the variation of the neck length and the head size of the femoral component and also allow a mixed alloy system [75].
One particularly favoured combination is the titanium alloy stem with the Co-Cr-Mo head. The Ti alloy is chosen for porous coated uncemented stems because of its relatively low elastic modulus, while Co-Cr-Mo is favoured for the head because of its superior wear characteristics. There is however a certain amount of galvanic and crevice corrosion resulting from coupling these two metals in the physiological medium. This corrosion results in the production of debris and a reduction in mechanical properties of the implants [75].

Modular systems have been used with Co-Cr-Mo stems and alumina heads [77]. This eliminates the corrosion while providing good wear properties at the articulating surfaces.

More recently partially stabilised zirconia (PSZ) ceramics have been considered as an alternative to alumina. PSZ is tougher than alumina and has a finer grain size which allows the production of a finer surface finish. Preliminary tests have shown zirconia to be biostable.

Thus it would appear that the best compromise of wear and mechanical properties at this stage is the ceramic:UHMWPE system. Wear debris remains a significant problem resulting in more failures than any one factor. Reducing the production of wear debris would significantly increase the life of total hip replacements (THR's). Investigating the wear behaviour of the ceramic:UHMWPE system by testing alumina and zirconia against UHMWPE may provide important information regarding the nature of this wear process.

2.5.3 UHMWPE Wear in Implants

The maximum principal stress in UHMWPE caused by normal walking is usually less than 10MPa in total hip replacements (THR's). Thus the maximum shear stress occurs at the surface of the UHMWPE component. Studies of retrieved UHMWPE components [1] have revealed the existence of large amounts of residual plastic strain within the surface region of the acetabular components. In the acetabular/femoral head contact, only the microscopic asperities are deformed plastically, while the nominal contact is elastic. Wang et al. [78] postulated that, during walking every contact asperity on the UHMWPE will experience repeated cyclic deformation by the passing asperities on the femoral head. In this way an incremental residual plastic strain $\delta\varepsilon$ is built into each contact spot with every interaction of this kind. Failure will therefore occur when the ductility of the material within each contact spot has been exhausted. Thus by assuming ε_c as the critical strain for UHMWPE under these conditions, a wear particle may be produced when the accumulated plastic strain after n_c asperity encounters reaches ε_c so $\delta\varepsilon n_c = \varepsilon_c$

Assuming a fully plastic asperity situation and a uniform distribution of N asperities with equal height and equal tip radius. From the random walk theory [79], there will be N contact spots at any given moment and $N^{1/2}$ passes sweeping through the same spot per walking cycle. By relating this to the true area of contact and the volume of the wear particles, Wang et al. [78] found $\Delta V \propto P^{3/2} R_a^{3/2} 1/(\sigma_u^{3/2}\varepsilon_u)$.

where V is the total volume of wear particles produced

P is the average applied load per contact cycle

R_a is the centre-line-average roughness of the femoral head

σ_u is the ultimate tensile strength

ε_u is the elongation at break

$\sigma_u\varepsilon_u$ is representative of the strain energy at break in a tensile test.

It was concluded that the tensile rupture energy or toughness is the most important property determining volumetric wear rate [78].

2.5.4 Wear Debris Effects

The major concern relating to the long-term clinical performance of implants is the tissue reactions which are caused by UHMWPE debris. Fine UHMWPE particles that are transported to the hard and soft tissue surrounding the joint cause chronic inflammation reactions [80] around the joint and result in bone resorption [7]. UHMWPE particles activate macrophages (inflammatory cells) which stimulate osteoclasts to cause local bone resorption [1]. In 9 revision operations documented by W J Maloney et al. [81], in which the joints had failed as a result of osteolysis or bone loss, the osteolytic regions were covered by a fibrous membrane. Analysis of the histological sections revealed sheets of macrophages within this fibrous membrane. Intracellular polyethylene particles ranging from submicron size to about 3 μm were identified. Larger particles of polyethylene were seen in association with multinucleated giant cells. The reactions to the wear debris are dependent on the size and morphology of the wear debris. Particle size determines the type of response to the wear debris. As the particle size decreases, the relative surfaces area available for physical and chemical reactions increases. This results in an increased potential for detrimental reactions [82]. The composition [83], rate of production [84], particle size [85], shape [86] and surface characteristics [87] affect the biological response of the

implant. Component loosening and tissue reaction to wear debris are two of the most common causes of implant failure [88].

Osteolysis or bone loss as a result of local bone resorption is a common complication of total hip replacements. Maloney et al. [89] reported femoral osteolysis in radiographically stable uncemented THR's. Biopsy material demonstrated particulate metal and polyethylene (PE) debris with focal aggregates and macrophages. W J Maloney et al. reported that in investigating 15 hips with considerable pelvic osteolysis, loss of the femur was most commonly seen in the region of the greater or lesser trochanter. In 9 of the revision operations the osteolytic area was covered by a fibrous-tissue membrane. Sheets of macrophages were found within the fibrous membrane. There were more PE particles than metallic particles [90].

Particulate debris can be generated at the hip articulation and at other locations. This debris has the potential to gain access to the effective joint space (effective joint space is the entire bone-implant interface which is accessible to joint fluid, [91]) and stimulating osteolysis. The ease with which wear debris gains access to the interface between the implant and the bone is determined in part by the integrity of the bone-implant interface [90]. Osteolysis rarely results in pain and substantial bone loss can occur before the fixation of the implant is substantially compromised. Lee et al. found that metallic debris found in periarticular tissues of failed, non-infected cemented hip joints ranged in size from 0.8 to 1.0μm in the short dimension and 1.5 to 1.8μm in the long direction. Polymer debris for the same samples was found to vary from 2 to 4 μm in the short dimension and 8 to 13 μm in the long dimension. Shanbag et al. found that most PE and mineral particles present in interfacial tissue are submicron size. Fragments larger than 7 μm are generally assumed to be too large to be phagocytosed by macrophages [92] and contribute minimally if at all to the biological responses leading to osteolysis [93,94]. Finer particles are believed to stimulate macrophages [93-95].

2.6 Lubrication

2.6.1 Introduction

Lubrication is a common method used to reduce wear. The lubricating medium separates the two interacting surfaces and assists the sliding of the respective surfaces by reducing the friction between them. A good lubricant should therefore prevent solid-solid contact and should have a low shear strength to ensure low friction. A liquid is the best lubricant because it can be sheared an infinite number of times without failing from wear or fatigue [96]. There are various types of lubricating conditions and these are determined by the nature of the wear process.

2.6.2 Hydrodynamic Lubrication

Hydrodynamic lubrication occurs when the mating surfaces are separated by a viscous liquid which is thicker than the surface roughness (R_a) of the surfaces. Hydrodynamic lubrication occurs when the viscosity of the lubricant and the geometry of the two surfaces may be used to generate sufficient pressure to prevent solid contact. At this point the minimum resistance to sliding is reached [97]. Hydrodynamic lubrication can be described by the Reynolds equation as

$$dp/dx = 12\eta((U_1 + U_2)/2)((h - h^*)/h^3)$$

where p = pressure

x = co-ordinate along the longitudinal axis

η = absolute viscosity

U = velocity in the tangential direction

h = film thickness

h*= film thickness at the point of maximum pressure

This assumes that the fluid is incompressible, the fluid properties remain constant, inertia and turbulence effects are negligible, the solid bodies remain rigid and that h is sufficiently small so that fluid pressure can be considered constant [98].

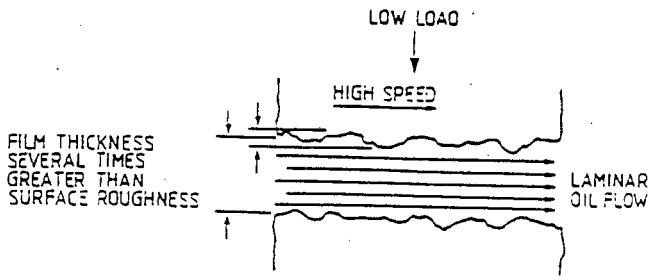

Figure 2.9 *Hydrodynamic lubrication[99]*

2.6.3 Elastohydrodyamic Lubrication

In elastohydrodynamic lubrication, surfaces are separated by a viscous fluid with a thickness greater than that of the R_a of the surfaces. Elastohydrodynamic lubrication differs from hydrodynamic lubrication in that it applies to 'highly loaded' contacts where loads act over relatively small contact areas. The high pressures affect lubricant behaviour by changing the viscosity of the lubricant as well as resulting in elastic deformation which changes the geometry of the bodies bounding the lubricant film. The film thickness is determined by the conditions in the inlet region for both rolling, mixed rolling and sliding conditions. Frictional resistance is then due to the internal viscosity of the lubricant. The lambda ratio is defined as :

Λ = (elastohydrodynamic film thickness)/(composite surface roughness) [100].

Composite roughness has been defined in various ways ranging from the mean of the values for the two surfaces to the square root of the sum of the of the squares of the individual roughnesses. For values of the lambda ratio of unity or less, the kinematics of the situation may promote local pressure generation associated with asperities. This tends to result in the flattening of the asperities causing pressure changes. In this case the lambda ratio becomes meaningless and effective fluid film lubrication can persist after the transition to mixed or boundary lubrication should have occurred. This applies especially to so-called 'soft' elastohydrodyanamic (EHL) applications and can be seen in the analysis of a synovial joint. The initial asperities cause a small ripple on the smooth surface pressure profile which results in the flattening of asperities to a substantial extent. This in turn results in a larger effective lambda ratio and, the effective fluid film is preserved for longer than initial calculations would suggest. Dowson defines this as 'micro-elastohydrodynamic lubrication' [101].

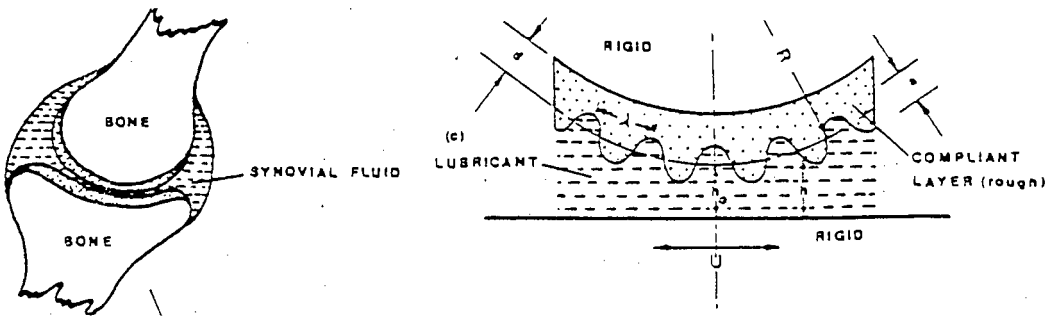

Figure 2.10 model of a synovial joint[101]

2.6.4 Thin Film or Mixed Lubrication

In thin film lubrication, surface asperities penetrate and disturb the laminar conditions of flow. This results in the load being shared by the hydrodynamic forces of the lubricant and the contacting surfaces of the asperities. For thin film lubrication, the friction resistance is due to a combination of the shearing of the lubricant film and asperity interaction [99].

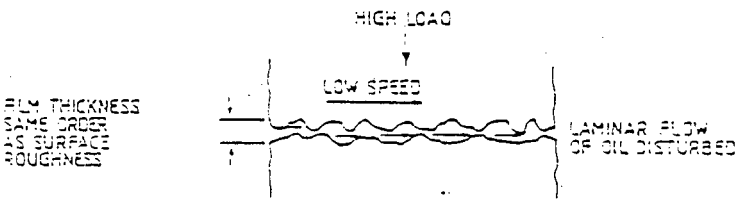

Figure 2.11 Thin film lubrication[99]

2.6.5 Boundary Lubrication

Boundary lubrication occurs when contact pressures are sufficiently high and sliding velocities are sufficiently low so that hydrodynamic effects are completely absent. The entire load is then carried by a multi-molecular layer of boundary lubricant a few Angstroms thick.

The main purpose of a boundary lubricant is to reduce the amount direct solid-solid interaction. Good boundary lubrication is best provided by an interfacial film of long

chain molecules with a strong attraction between chains to resist the penetration of surface asperities and low shear strength so that it can be easily sheared. Boundary lubrication is complex and is therefore difficult to quantify [102].

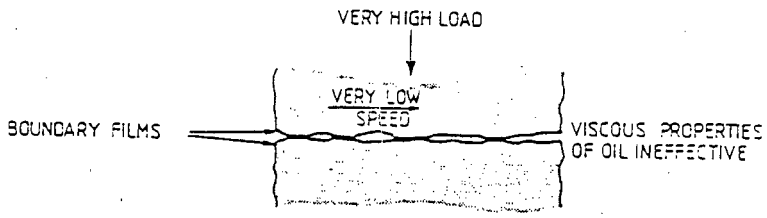

Figure 2.12 Boundary lubrication [99].

2.7 Lubrication of Implants

2.7.1 Introduction

In human skeletons, the limb segments articulate on one another or on the trunk segments by means of synovial joints. In synovial joints, bone ends are hollow and enlarged with a shell of approximately 0.5mm-1.0mm thick supported on a system of braced struts. The two shapes are more or less congruent and are spherical, cylindrical or saddle in form. The bone ends are covered with sufficient articular cartilage to ensure that articular cartilage articulates on articular cartilage. Articular cartilage varies over a thickness of 3-4mm and is seldom covitant over the joint surface [103].

In the absence of load, the gap between the cartilage surfaces depends on the forms of the underlying bones, the thickness of the cartilage layers and the relative positions of the bone segments [103].

The ends of the bones are surrounded by a capsule or bursa which functions to keep the synovial fluid in and the other fluids out. This capsule is lined with cells which produce hyaluronic acid (the characteristic component of synovial fluid) [103].
The loads on hips and knees during walking vary in such a way that high loads combine with low surface entrainment velocities, while low loads combine with higher entraining velocities. When the femoral head first encounters the acetabular socket, a thick film of fluid separates the two surfaces. Friction is inversely related to film thickness, so friction is low at this point. As the film is squeezed down under the effect of heavy loading, the friction will increase. So for high loads/low velocities, the only possible mechanism for supporting a film of fluid will be a squeeze film action [104,105].

2.7.2 Articular Cartilage

Articular cartilage is a collagen fibre mesh in a gel of mucopolysaccharides attached to proteins. Mucopolysaccharides are also known as glucosaminoglycans (GAG). The protein core with GAG attached at several sites and branching out sideways from

the core is known as proteoglycan. Articular cartilage contains by weight approximately 68 - 75 % water, 2 - 8 % GAG, 15 - 20 % collagen and 1 - 2 % protein. GAG molecules contain carboxyl and sulphate groups which are negatively charged. Electrical properties therefore affect the mechanical and transport properties of the cartilage. Swelling pressure associated with water inside and adjacent to the cartilage can also affect these properties. Collagen fibres are strong in tension and weak in compression and are maintained in tension by the swelling pressure generated by the aqueous gel of the proteoglycan [103].

Articular cartilage has two functions. Firstly, to distribute joint forces over the underlying cartilage and secondly, to provide a bearing surface. For the first function, the articular cartilage should have a minimum thickness and a stiffness between zero and that of the bone. For the second function, low friction and low wear rates are required. The repeated stresses on the joint must not cause irreparable mechanical breakdown. There is a possibility that incipient fatigue failure excites a healing response [103].

2.7.3 Synovial Fluid

The lubrication of synovial joints is complex and not easily understood. There are several mechanisms of lubrication available to the synovial joint. Current models of synovial fluid lubrication implement hydrodynamic lubrication assisted by the secretion of synovial fluid from the cartilage into the space between interacting cartilage surfaces. Synovial fluid causes either a thin layer of hyaluronic acid-protein to be absorbed on the cartilage, or a concentrated gel to form in the loaded region (this gel persists as a squeeze film) [103]. Hyaluronic acid is an alternating copolymer which is largely responsible for the lubricating effect of the synovial joint [106]. Proteoglycans which form the matrix of the cartilage are chemically closely related to the hyaluronic acid and protein in the synovial fluid. Proteolglycan is a protein core with glycosaminoglycans (mucopolysaccharides) attached at several sites and branching sideways from the core. These mucopolysaccharides also contain negatively charged carboxyl and sulphate groups. It is likely that this protein core is

made up of glycoproteins [103]. The most extensively investigated glycoproteins are low molecular weight proteins known as α- globulins [106].

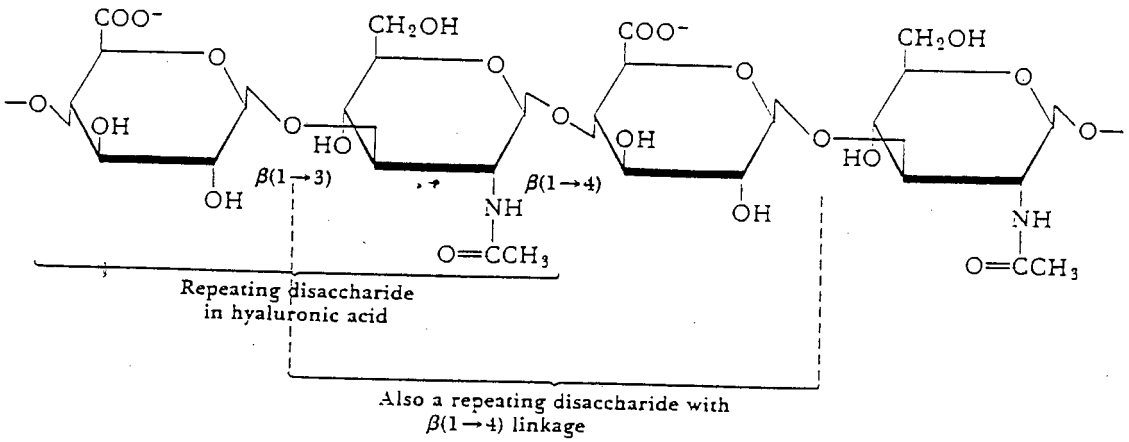

Figure 2.13 Hyaluronic acid, an alternating copolymer largely responsible for implant lubrication [107].

α_1 - Acid Glycoprotein (orosomucoid)

This is one of the most soluble proteins encountered in human plasma [106]. The composition of the carbohydrate and protein portions of orosomucoid is shown in Table 2.1. α_2 -Glycoproteins can be resolved into Ba- and Zn- α_2 proteins [106]. The composition of the Zn- α_2- proteins is shown in Table 2.2. Ba- α_2- glycoproteins have a molecular weight of about 49 000. They contain 80% protein, 6% hexose (galactose and mannose), 5% hexosamine (essentially glucosamine), 5% sialic acid and 0.3% fucose [106].

Table 2.1 Amino Acid Composition of Orosomucoid [106]

	Grams of amino acid* per 100 gram of orosomucoid	Grams of amino acid residue
Arginine	3.65	3.27
Aspartic acid	7.44	6.43
Cystine	0.60	0.52
Glutamic acid	10.73	9.42
Glycine	0.82	0.62
Histidine	1.31	1.16
Isoleucine	3.15	2.72
Leucine	5.21	4.50
Lysine	5.03	4.21
Methionine	0.65	0.57
Phenylalanine	3.91	3.43
Proline	2.37	2.00
Serine	2.51	2.06
Threonine	4.80	4.07
Tryptophan	1.25	1.11
Tyrosine	1.99	1.79
Valine	2.82	2.39
Total of amino acid residues		50.56
Total of carbohydrate residues		37.30
Deficit		12.14
		100.00

* Grams of amino acid recovered from the hydrolysate of 100 g dry and ash-free orosomucoid.

Table 2.2 Chemical Composition of Zn-α_2-Glycoprotein [106]

	Grams/100 g glycoprotein*	Moles/41,000
Galactose	2.3	6
Mannose	4.2	10
Fucose	0.2	1
Glucosamine	4.0	10
Sialic acid	7.0	10
Alanine	3.65	17
Arginine	4.53	11
Aspartic acid	8.65	27
½ Cystine	0.96	3
Glutamic acid	13.09	36
Glycine	2.70	15
Histidine	2.48	7
Isoleucine	2.62	8
Leucine	5.90	18
Lysine	7.02	20
Methionine	1.04	3
Phenylalanine	3.30	8
Proline	4.60	16
Serine	3.68	14
Threonine	2.86	10
Tryptophan		10
Tyrosine	6.88	15
Valine	5.51	19

* Figures are not corrected for water taken up during hydrolysis.

2.7.4 Lubrication Action of Joints

Synovial fluid is generally clear or yellowish and viscous and can be described as a dialysate of blood plasma. It contains 1/3 the protein concentration of plasma. The synovial fluid mucins are polymers of high molecular weight, sometimes as high as several million. Chemically, synovial fluid is hyaluronic acid which is bonded more or less firmly with various amounts of protein [108]. Sinha et al. [109] suggested that synovial fluid may be considered as a micropolar fluid containing long-chain hyaluronic acid molecules. Synovial fluid can thus be characterised by three physical constants, μ, χ and γ (as opposed to Newtonian fluids which are characterised by one constant, μ) which are obtained from lubrication theory [110] and are related as follows:

$$dp/dx = 1/2(2\mu + \chi)\delta^2 u/\delta y^2 + \delta v/\delta y$$

where p = hydrodynamic pressure

u = velocity

v = microrotational velocity

μ = Newtonian viscosity

χ,γ = viscosity coefficients characteristic of synovial fluid, the exact values of which are still unknown

2.7.5 The Effect of Proteins on the Lubricating Function of Synovial Fluid

Linn and Radin [111] digested synovial fluid with hyaluronidase so that its viscosity was reduced by breaking the chains of the hyaluronic acid which normally acts as a viscosity raiser in synovial fluid. The digestion process resulted in a reduced viscosity, but the coefficient of friction was found to be the same. Tryptic digestion which breaks down proteins with minimal effect on viscosity was found to cause the frictional coefficient to double from 0.0028 to 0.0054 (typically). It was concluded that synovial fluid was acting as a boundary lubricant under conditions of constant heavy loading. The same experiments were carried out by O'Kelly et al. [112] under dynamic loading conditions. It was found that hyaluronic acid digestion reduced the viscosity and increased the friction. From this it was concluded that under normal walking dynamic cycles, fluid film lubrication of joints dominates, while under static heavy loads, mixed lubrication prevails with boundary lubrication dominating [102].

CHAPTER 3

EXPERIMENTAL METHODS

3.1 Test Materials

The materials used were

1. UHMWPE which is processed for use in prostheses. (*Chirulen* supplied by Solidur Poly-hi Meditek) This material is purer than the conventional industrial product. Special precautions are taken during processing and production so as to ensure that the ash content is very low and that the titanium and aluminium concentrations are below 20 and 40 ppm respectively. The powdery raw material is carefully plasticised in a compression moulding press and then heated to 200°C to melt it. The powder which is evenly distributed in the mould is cold compressed under a pressure of approximately 100 bar. This temperature is maintained at a pressure of 50 bar to ensure the complete plastification of the powder. It is then cooled and the pressure slowly raised to 100 bar. The material is therefore considered to be isotropic [113]. Physical, thermal and electrical properties of the *Chirulen* as supplied by the manufacturers can be obtained from appendix E.
2. Counterfaces of yttria partially stabilised zirconia (YPSZ) and alumina both of which were supplied polished by Astromet USA.

The wear pins were cut from the bulk polymeric material in the form of square pins 10mm x 10mm x 25mm. One end was then milled round to provide a cross sectional area of $10mm^2$. These were then radiused at the change in section to prevent large stress concentrations at this point which could result in the failure at this junction during reciprocating sliding wear testing. See Figure 3.1.

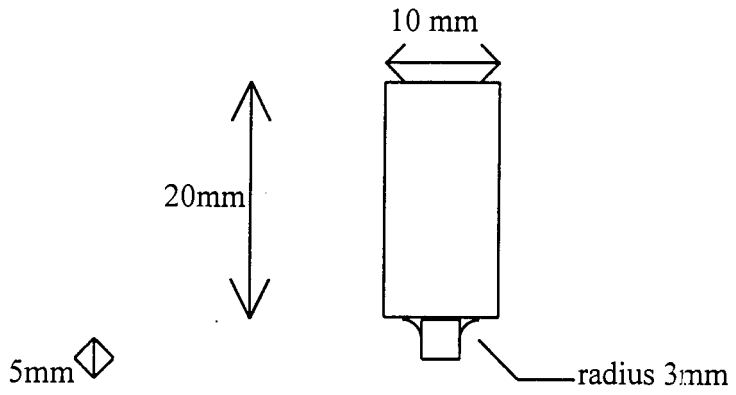

Figure 3.1 *Geometry of wear pins.*

The YPSZ and alumina counterfaces were bars of 50mm x 12mm x 10mm. These were sintered from powdered form into the required shape (see Figure 3.2.). PSZ samples were initially polished by the supplier to an average surface finish of $R_a \approx$ 0.01μm. In order to investigate the sensitivity of the wear rates to counterface roughness, these were then polished using an automatic polisher to give a surface finish R_a of 0.06μm. Alumina samples were polished by the supplier to an average surface finish Ra ≈ 0.04μm. The reason for the discrepancy between the surface finish of the two ceramics was that similar polishing methods only allow for a surface finish of 0.04μm for the alumina ceramics before grain pullout becomes significant and can affect the wear process. The geometry of the pins and the counterfaces was determined by the wear rig and the sizes of the samples were dictated by the ease with which they could be loaded into the test apparatus.

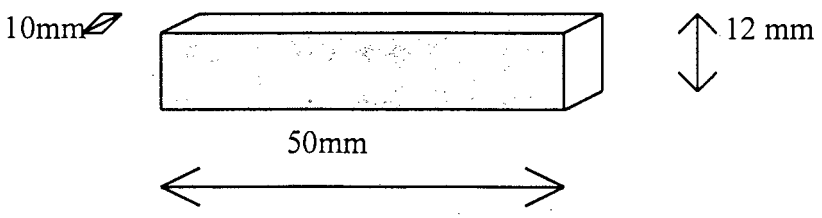

Figure 3.2 *Geometry of ceramic counterfaces.*

All the test materials were subjected to a similar cleaning procedure. They were rinsed in distilled water and then ultrasonically cleaned in absolute alcohol for 2 minutes prior to wear testing and at each interval of 5 km or 10 km during testing. Conditioning tests were conducted on unworn UHMWPE pins in order to determine whether any of the water, saline or albumen solutions were adsorbed onto the polymer surface. These tests indicated that there was little adsorption into the surface and that the mass of the polymer pins remained constant (within the range of the mass balance) over the soaking intervals which corresponded to testing intervals.

The tests were conducted on a reciprocating pin-on-plate wear rig. The ceramic counterfaces were fastened onto a reciprocating shuttle and the counterfaces reciprocated against a fixed wear pin. A schematic of this apparatus can be seen in Figure 3.3.

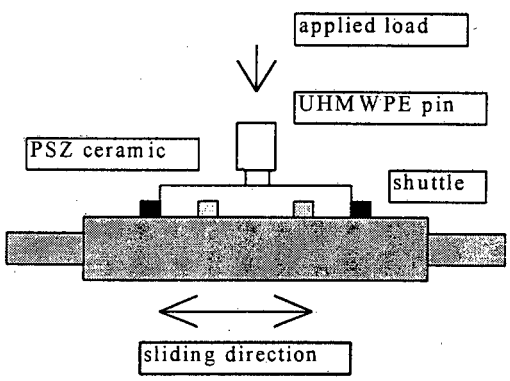

Figure 3.3 *A schematic representation of the reciprocating pin-on-plate wear apparatus.*

Pins were loaded in a specimen holder and compression loaded by a spring designed to give a linear response. The load was transmitted via a load cell to a give a reading in mV. This was calibrated and converted to a reading in N and was monitored throughout the testing.

3.2 Test Apparatus

Photographs of the test apparatus can be seen in Figures 3.4, 3.5 and 3.6 and consists of the following:

1. the backing disc is the central component and all the test cell components for specimen mounting, testing and monitoring are mounted to its one face.
2. the rig is driven by a 1.5kW/220V dc motor which is rigidly mounted on a fixed plate (not shown).
3. the driven and the driving pulleys are connected by a fabric belt and are ratioed 1:2.1 (not shown)
4. the rectangular lower base plate holds two parallel shafts on which the shuttle reciprocates horizontally by means of two support brackets.
5. the shuttle and support brackets were originally high strength aluminium alloy (7017) which has good corrosion properties. This was altered to 316L stainless steel to combat corrosion from the saline solution.
6. a mounting plate of stainless steel is screwed on the top face of the shuttle.
7. the upper base plate is held in a horizontal position above the lower base plate during testing.
8. two support brackets are bolted to the bottom face of the upper base plate. These retain two parallel shafts which run in a polymer bearing. The shafts are housed in the friction plate.
9. the upper base plate assembly is able to swing through 90° about a hinge pivot.
10. when in the horizontal or testing position the bottom face of the upper base plate rests on the support block.
11. the base plate can be tightened against this block by means of the thumbscrew.
12. the base plate is flush with the support only when it is horizontal.

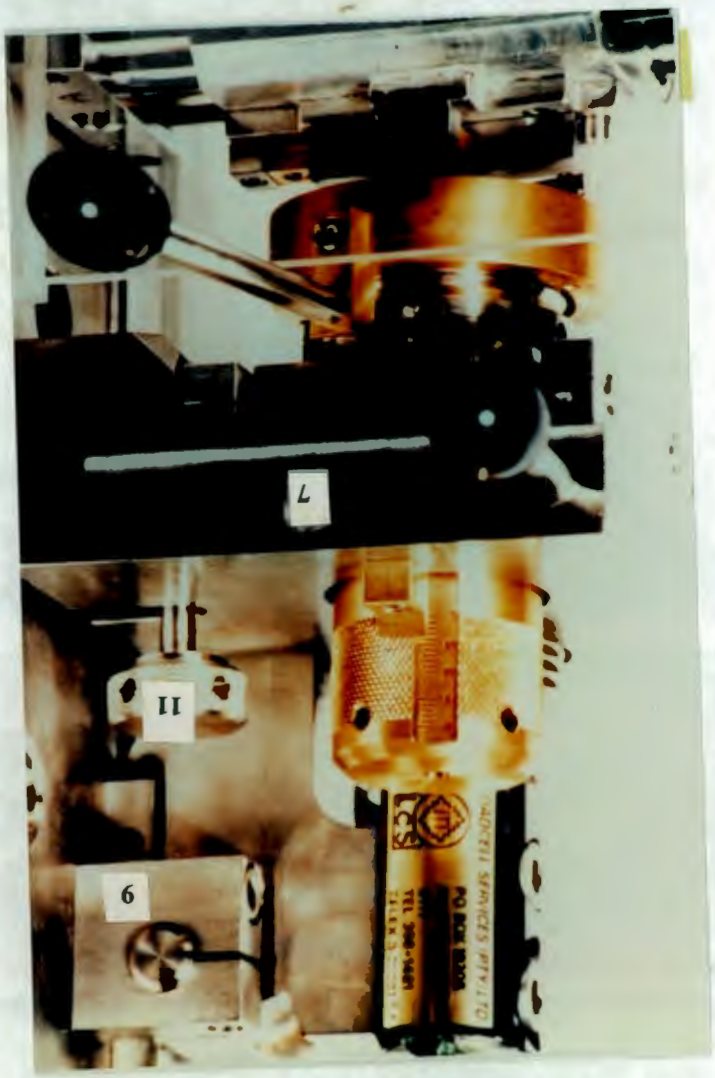

Figure 3.4 Test rig I in loaded position

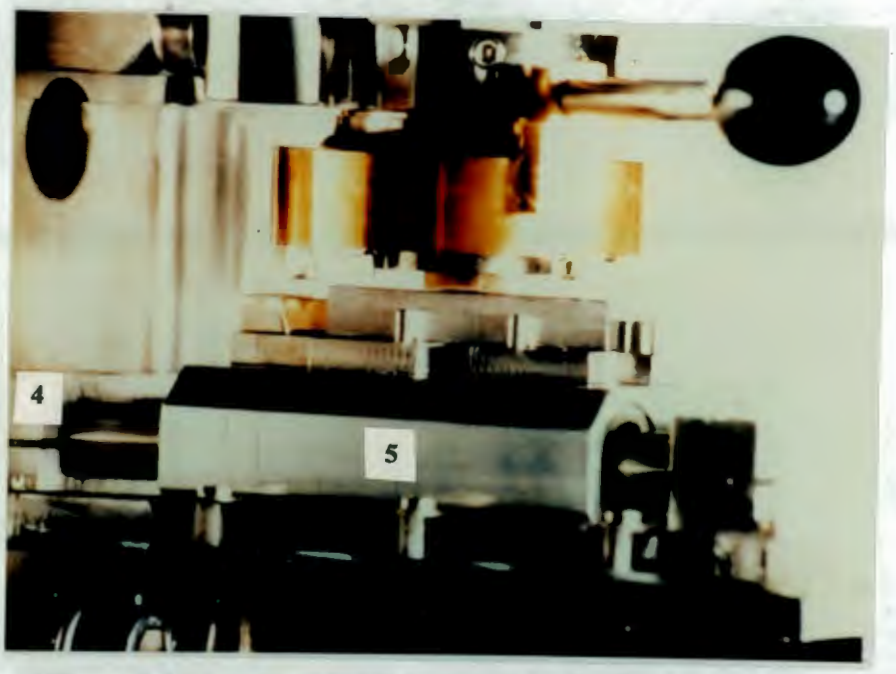

Figure 3.5 Specimens loaded against each other

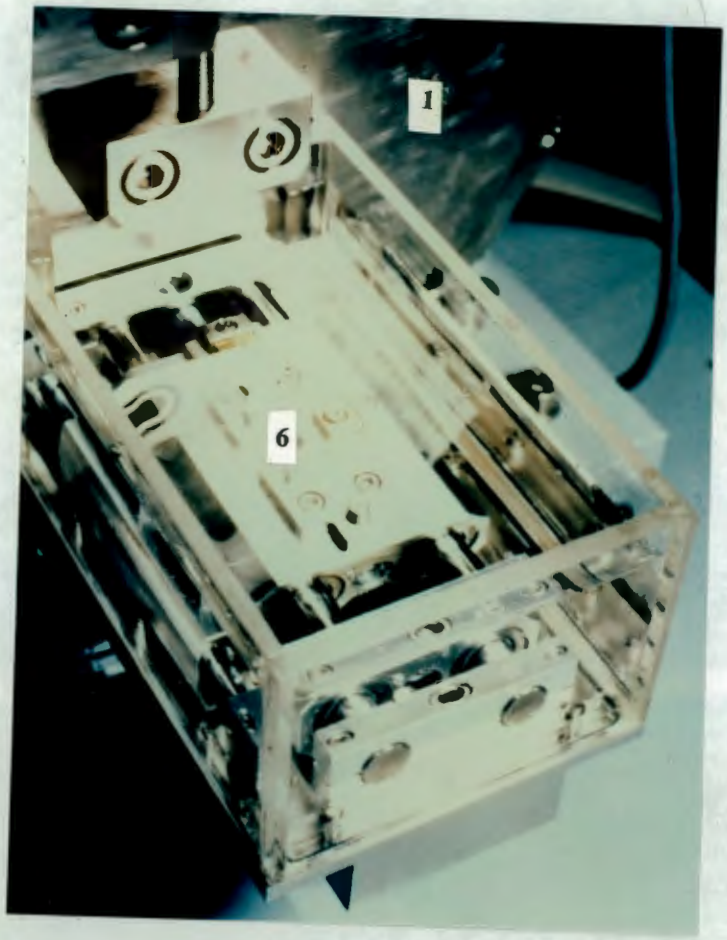

Figure 3.6 Reciprocating shuttle in bath

3.2.1. Specimen Location

- the stationary specimen is held in position by a chuck consisting of two phosphor bronze jaws, one fixed, the other adjustable.
- the reciprocating specimen is placed on the flat surface of the specimen mounting plate.
- the long axis of the specimen mounting plate is positioned in line with the reciprocating axis by means of three locating pins.
- tightening the wedge blocks forces the specimen against the pins.
- the specimen holder fits into the load assembly housing.
- two diametrically opposed slots are machined along the outer face of the holder allowing it to fit over the two hold fingers as it is inserted.
- rotation of the specimen in the housing is prevented by two holes of different diameters. These couple up with two matching pins protruding from the plunger. This allows axial movement but prevents rotation.

3.2.2 The Loading Mechanism

- loading of the specimen is achieved by a compression load spring designed to give a linear response of 0 - 100N.
- the spring force is adjusted by turning the screw cap which has linear graduations of 5N on its outer face.
- a needle roller bearing is fitted to the load plunger to prevent the spring from rotating while it is compressed.

3.2.3 The Coolant Bath

- a perspex enclosure is fitted to the lower base plate. This consists of three sides and an open end with a small perspex cover to prevent fluid from splashing out of the bath. The volume of the coolant bath was 250 mm^3.

3.3 Test Parameters

1. Sliding Velocity

Sliding velocity is sinusoidal with a maximum value of 0.4 m/s and with a constant average speed of 0.25m/s. Frictional heating at 0.25m/s is considered to be minimal. The speed was set at a constant 0.25m/s as it has been found experimentally [114] that at this is close to the maximum velocity at which wear tests can be conducted which yield results similar to those for orthopaedic implants, thus allowing tests to be completed faster.

2. Pressure

This was set at 10 MPa in order to be within the physiological range for THR's This value remained constant throughout the testing. The pressure was set using a compression load spring which was adjusted by turning a screw cap and force readings were displayed and monitored on a LED. The pressure was adjusted throughout the test in order to avoid the effects of creep.

3. Counterface Roughness

It has been found that increasing the counterface roughness increases the wear rate dramatically [115]. Initially the counterface value was kept within a constant range (the polishing process eliminates the possibility of a completely static value). The average value for the alumina was 0.04μm. The average value for the PSZ was 0.01μm. However, counterface roughness values were later changed in order to determine the effect of the protein solution on this variable.

Table 3.1 Surface Roughness Values for Various Counterfaces

Counterface Material	Surface Roughness	R_a
PSZ	0.01μm	0.06μm
Alumina	0.04μm	

4. Lubricant

Several lubricants were used in order to determine the effects of the addition of a protein into the lubricant. It has been contended in the past that the proteins in synovial fluid affect the wear process [118]. For this reason two different protein solutions were used and distilled water and saline solution used as controls. Firstly synovial fluid was used. Human synovial fluid was obtained from patients undergoing knee replacement operations for osteoarthritis. Synovial fluid produced in reaction to this joint disease is similar in composition to healthy fluid and is produced in larger quantities than those found in healthy joints. The synovial fluid had to be diluted because of its scarcity. Fluid had to be changed every 5 km to avoid as far as possible any denaturing of the proteins. It was chosen not to add antibiotics to extend the lifespan of the proteins as it is still not clear as to how the antibiotics affect the wear process. The lubricant was drained after 5 or 10 km tests. The synovial fluid was diluted with physiological saline.

The saline solution used had the following composition

- 9g sodium chloride (NaCl)/1000 ml
- 154mmol sodium ion
- 154mmol chloride ion
- pH approximately 5.5
- sterile and pyrogen free

This was chosen because it is known to be stable in the physiological environment and because some proteins are only soluble in a saline environment.

Various attempts were made to ensure sufficient synovial fluid from either human or bovine origin for testing purposes. This was unsuccessful and an alternative source of protein lubrication was sought to replace that of the synovial fluid in the test apparatus. As the investigation was concerned with the effect of a viscous protein lubricant on sliding wear, albumen was selected. It was available in large quantities and was observed to behave physically in a similar manner to synovial fluid. A single synovial fluid test was conducted and then used as a basis for comparison for both the albumen solutions and distilled water.

Albumen contains the chief reserves of water and of certain nutrients (protein and mineral salts) for the developing embryo [113].

Albumen contains the following proteins :

Table 3.1 *Table of the Proteins found in Albumen [112]*

Protein	Percentage of total
Ovalbumin	69.7%
Ovomucoid	12.7%
Ovoconalbumin	9.0%
Ovoglobulin	6.7%
Lysozyme and ovomucin	1.9%

These proteins are made up of various proportions of amino acids (see appendix). The elemental composition of some of these proteins as a percentage of dry weight is shown as follows:

Table 3.2 *The Elemental Composition of Some Proteins found in Albumen as a Percentage of Dry Weight [114]*

	C	H	N	S	P
ovalbumin	52.8%	7.1%	15.5%	1.66%	0.12%
ovo-conalbumin	52.5%	7.0%	16.6%	1.83%	0.00%
α-ovomucoid	49.0%	6.9%	13.1%	2.20%	0.0%
lysozyme	48.7%	6.4%	18.6%	2.53%	0.0%

Ovalbumin is representative of glycoproteins with a low proportion of carbohydrate. Ovalbumin has a molecular weight of about 45 000 and contains per molecule a single prosthetic group consisting of 5 mannose residues, 3 glucosamine residues and 3

acetyl groups. The molecular weight of the prosthetic group is about 1440 so there is 3.2g carbohydrate per 100g ovalbumin [107].

The molecular weight of conalbumin is approximately 87 000. One alanine is terminal. Conalbumin binds 2 atoms of ferric iron per molecule. Copper and zinc are bound much less strongly. The binding of the ferric or cupric ions requires the presence of HCO_3^- and the reaction is facilitated by small polybasic anions complexing the metal. The interaction with the ferric ions sets free 3 and interaction with the cupric ions sets free hydrogen ions [107].

Thus the following lubricants were used:

Lubricant	Percentage protein	Percentage saline soln
distilled water	0	0
saline solution	0	100
synovial fluid	5	95
albumen	5	95
albumen	10	90
albumen	15	85

5. Sliding Distance

Mass loss measurements were taken of the UHWMPE pins and surface roughness (R_a) measurements were taken of the ceramic counterfaces at 5km intervals corresponding to the change in lubricant over a variety of total sliding distances. Friction measurements were also taken . Several sliding distances were selected. These were dictated by several factors. Firstly there was sufficient synovial fluid for one test to reach a sliding distance of 35km. Thus the albumen and distilled water tests were run to 35km for the basis of comparison. Further tests were run to 50 and 100 km. In a prosthetic hip joint a sliding distance of 10 to 50 km a year is covered [119] and these results were taken as an indication of the extent of wear that one could expect over that period of time.

3.4 Experimental Measurements

3.4.1. Measurement of Specific Wear Rate

The UHMWPE mass loss was monitored using a Sartorious Research mass balance with an accuracy of 0.01mg. Polymer mass loss was converted to a volume loss (V) which was plotted against the sliding distance (S). This eliminated the necessity for measuring dimensional changes and was done to reduce the experimental error introduced by polymer creep (although loading was continually monitored and creep was considered to have minimal effect on the loading of the UHMWPE specimen). The specific wear rate (K_0) was obtained from the slope of the graph divided by the normal load P which gave the specific wear rate $K_0 = V/PS$

3.4.2. Measurement of Counterface Roughness

Counterface roughness tests were conducted using a Taylor-Hobson Surtronic 3P talysurf. These were taken to coincide with the polymer mass loss measurements. Roughness traces were taken to give an indication of the way in which the wear track was forming and if there was any significant surface layer. The error readings of the roughness measurements also gives an indication of the variation of the transfer layer. i.e. large error readings indicate substantial changes across the wear track. However there was a certain amount of penetration of the stylus into the polymer transfer layer so were taken to establish any trends rather than considering the exact values that were obtained.

3.4.3 Measurement of Frictional Forces

The sliding wear rig in use did not allow for accurate friction measurements because the length of the deflection beam prohibited this. Therefore, in order to monitor the coefficient of friction of these samples, a different experimental apparatus was used. This was also a conventional sliding wear rig. It was used only to monitor friction measurements and therefore no other readings i.e. mass loss and surface roughness were taken. Figure 3.6 shows a schematic representation of the transducer used to measure the friction force at the sliding interface. The lower specimen holder is

mounted on several rows of stainless steel ball bearings in the direction of sliding. These are placed in parallel machined grooves and are constrained to move. This is considered to be a frictionless trolley. The trolley is connected via a rigid steel beam to a vertically mounted bending beam load cell. When a frictional force is generated at the sliding interface, it produces an horizontal displacement. This displacement is transmitted directly to the load cell. The signal is then amplified and displayed on the screen of an oscilloscope. The coefficient of friction is calculated by dividing the horizontal friction force by the applied normal load.

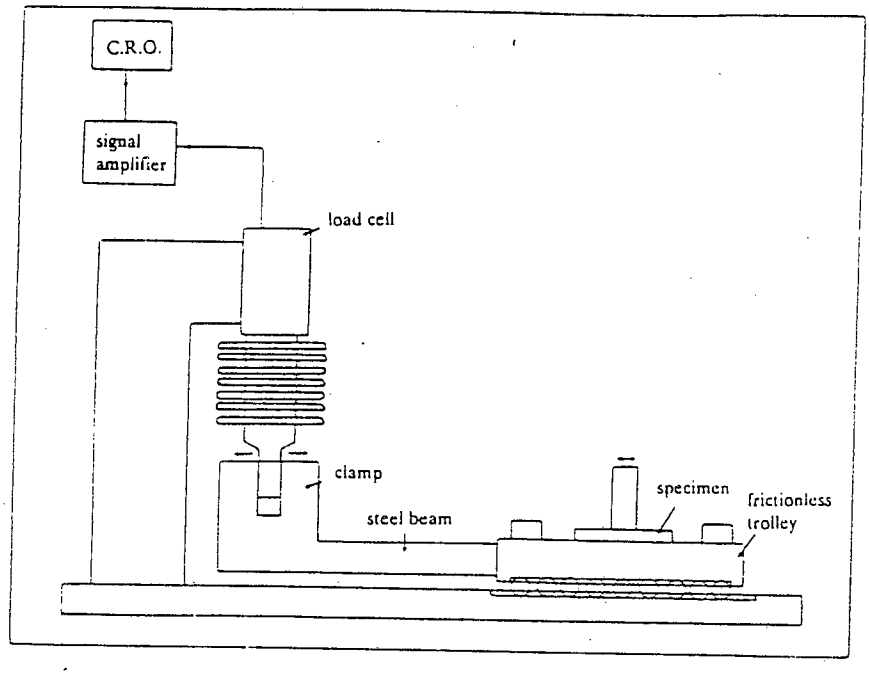

Figure 3.6 *Schematic of the force transducer for the friction measurements*

A typical variation of the friction force vs. time curve during reciprocating wear is shown in Figure 3.7. This is typical of a water lubricated test and shows how the friction coefficients are derived.

Samples were all loaded to 10 Mpa and tests conducetd at an average velocity was 250mm/s. As a result of the fact that the lubricant bath volume was too large, about 25l, synovial fluid solution was not used as a lubricant. The design of the lubricant bath and the fact that some of the submerged parts were mild steel prohibited the use of any protein solution for lubrication. This was because this system was difficult to

control and because the corrosion of the mild steel parts would affect the wear process.

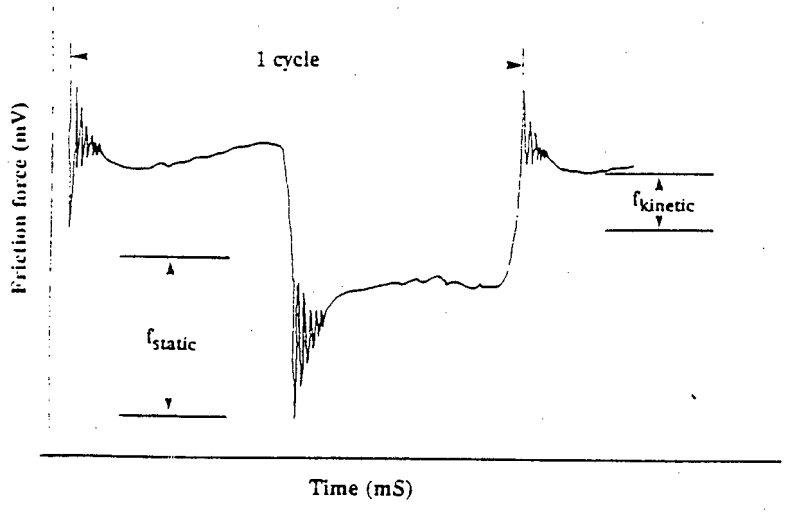

Figure 3.7 Schematic of a friction force vs. time curve for reciprocating contact.

3.4.4 Collection of Wear Debris

Wear debris was small and difficult to see with the naked eye. Two methods were used to collect the debris generated in order to examine it.

1. For tests conducted in rig 1

- the lubricant was drained every 5 or 10 km
- the drained lubricant was filtered using Whatman qualitative filter paper
- the filter paper was dried and cut into sections for viewing in the scanning electron microscope (SEM)

2. For tests conducted in rig 2

- the larger surface area of the wear pin allows more wear debris to be generated
- tests were conducted continuously for 100km
- debris was collected by cleaning the coolant bath with a rubber surface
- this was then sectioned and viewed in the SEM in order to view debris that has adhered to the surface.

3.4.5 Test Reproducibility

The test reproducibility of the rig was determined by running a series of tests under the same conditions. The tests were run in 5 % albumen by volume, at an average velocity of 0.25m/s and under a constant load of 10MPa. There was little volume loss recorded and so the sensitivity of the mass loss measurements must be considered to be a limitation in the accurate reproducibility of these tests. Variability in the wear rates can largely be ascribed to small changes in counterface roughness as the polishing process does not allow for the accurate reproduction of counterface roughness. Figure 3.8 shows the variation of the wear rates over four tests. From these tests, the reproducibility of the rig was deemed acceptable.

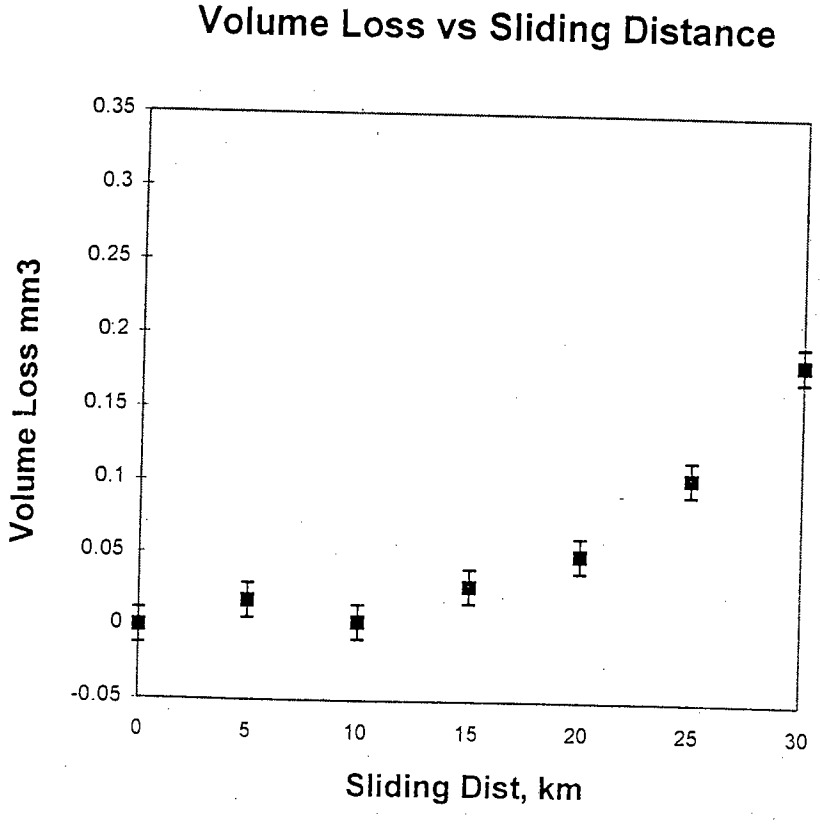

Figure 3.8 Variation of measurements for wear rig

3.5 Polymer Characterisation

3.5.1 Scanning Electron Microscopy

After the completion of a test the polymer pins and ceramic counterfaces were ultrasonically cleaned in alcohol and then in isopropanol. The pins and counterfaces were then gold-palladium coated using a Polaron E5100 Series II 'Cool' Sputter Coater. This was done to ensure that the specimen was conducting and that it did not charge in the beam. Filter paper and rubber sections were also gold-palladium coated. Samples were then mounted on aluminium stubs using carbon dag. Samples were then viewed in the Cambridge S200 Stereoscan scanning electron microscope (SEM). An accelerating voltage of 15 or 20 kV was used. These were chosen as the best micrographs could be obtained at these accelerating voltages. In addition to this, the UHMWPE is beam sensitive and tended to crack when exposed to beams of high accelerating voltages.

3.5.2 Energy Dispersive Spectroscopy (EDS)

It was not possible to use EDS to obtain a semi-quantitative composition of the wear debris or the transfer layers on the ceramic counterfaces. This is because carbon and hydrogen are the principal elements in both the polymer and the proteins and these elements cannot be analysed using the EDS system. EDS was used to check for foreign particles such as rust that may have been generated during testing. The Tracor Northern TN 5400 energy dispersive X-ray microanalyser attached to the SEM was used for this purpose.

3.5.3 Optical Microscopy

A Reichart projection microscope was used to obtain images of microtomed UHMWPE films under polarised light. Polymer chains are highly anisotropic with respect to their dimensions and thus pollarisability parallel to the chain will differ from that perpendicular to it. The refractive index of the light wave with an electric vector parallel to the chain will therefore differ from that of a wave with its electric

vector perpendicular to it. That is to say that polymer chains are intrinsically birefringent and orientation effects are manifested as a visible birefringence.

3.5.4 Scratch Tests

It appeared that the polymer surface was altering as a result of sliding wear. In order to investigate how the surface of the worn UHMWPE pins differed to that of the unworn pins, scratch tests were conducted on worn and unworn surfaces. The UHMWPE surfaces were scratched with a Rockwell C diamond indentor under a load of 50N [119]. These were then viewed optically and in the electron microscope.

3.6 Counterface Characterisation

3.6.1 Optical Microscopy

Optical photographs of the zirconia and alumina surfaces were taken at varying stages of the sliding wear process. For this purpose a Nikon Optishot optical microscope was used.

3.6.2 Scanning Electron Microscopy (SEM)

Zirconia and alumina worn ceramic surfaces were Au-Pd coated. Samples were then mounted on aluminium stubs using carbon dag. Samples were then viewed in the Cambridge S200 Stereoscan scanning electron microscope. An accelerating voltage of 15 or 20 kV was used. The material visible on the counterface was considered to be UHWMPE and because of its beam sensitivity relatively low accelerating voltages were chosen.

3.6.3 X-Ray Photoelectron Spectroscopy (XPS)

As the nature of the transfer layer was unclear from the micrographs, XPS was used in an attempt to analyse whether the protein solution was adsorbing onto the counterface surfaces. A VG Esaclab MkII was used. The samples were irradiated with X-Rays of 15kV and the binding energy of the emitted photoelectrons were determined in a hemispherical analyser. A semi-quantitative analysis of the surface can be calculated within a detection limit of 0.1at%.

3.6.4 Secondary Ion Mass Spectroscopy (SIMS)

SIMS was used in order to verify the results obtained for the XPS. A VG Escalab MkII fitted with a MIG 100 SIMS attachment was used. The atomic mass of sputtered ions is determined in a mass quadropole. The analysis depth is 10 Å and the detection limits vary from ppm to ppb

3.6.5 Auger Electron Spectroscopy (AES)

As only one test was run using synovial fluid, the sample on which the XPS and SIMS were conducted was Au-Pd coated for SEM viewing. Thus it was not clear if

the SIMS analysis was being conducted below the coating layer. AES was used to determine whether the results that were obtained for the XPS and SIMS analyses were a depiction of the transfer layer below the Au-Pd coating or that of the Au-Pd coating itself. A Phi 595 Scanning Electron Microbe was used and samples were irradiated at 3kV. The Auger electrons that are emitted from the surface are measured in a cylindrical mirror analyser. Semi-quantitative results can be calculated from the peak areas within a detection limit of 0.1%

3.7 Wear Debris Analysis

3.7.1 Scanning Electron Microscopy(SEM)

Filtered lubricating solution and collected debris was too fine to be viewed optically. Debris was collected on rubber surfaces or on filter paper. These were Au-Pd coated using a Polaron E1500 Series II "Cool" Sputter Coater. The debris was photographed and size fraction analyses were conducted.

3.7.2 Energy Dispersive Spectroscopy (EDS)

EDS analyses were conducted on the debris to determine whether it was UHMWPE. If scans for the debris particles were similar to the material adjacent to them, the debris was assumed to be UHMWPE. The Tracor Northern TN 5400 energy dispersive X-ray microanalyser attached to the SEM was used for this purpose.

Chapter 4

RESULTS

4.1 Introduction

This chapter presents an analysis of the wear behaviour of UHMWPE when sliding against a ceramic counterface in various lubricating media. The experimental results are divided into several sections as follows:

(1) Wear

(2) Friction

(3) Polymer Behaviour

(4) The Nature of the Wear Scar

(5) The Nature of the Wear Debris

4.2 Wear

The results of the wear testing of UHMWPE against different counterfaces in various lubricants are shown in figures 4.1, 4.2 and 4.3. and summarised in tables 4.1 - 4.6. The results are split into three sections. The first section 4.1 deals with the results obtained for wear tests conducted on zirconia counterfaces with an average R_a value of 0.01μm. The second section 4.2 deals with the results obtained for wear tests conducted on zirconia counterfaces with an average R_a value of 0.06μm in various lubricants. Finally in 4.2.3 the effect of varying the counterface is considered.

Table 4.1 *Table of Surface Roughness for Wear Tests Against Zirconia Counterfaces with Initial Surface Roughness (R_a) 0.01μm in Various Lubricants*

Sliding dist. (km)	Ave R_a (μm) for distilled water	Ave R_a (μm) for synovial fluid	Ave R_a (μm) for 5% albumen	Ave R_a (μm) for 10% albumen	Ave R_a (μm) for 15% albumen	Ave R_a (μm) for saline solution
0	0.01	0.01	0.01	0.01	0.015	0.01
5	0.028542	0.02	0.02433	0.027485	0.01665	0.042749
10	0.044333	0.035	0.03087	0.048465	0.024165	0.08333
15	0.046665	0.045	0.027222	0.030835	0.032665	0.12085
20	0.067075	0.035	0.0333	0.02165	0.02	0.128335
25	0.055416	0.08167	0.04332	0.04665	0.025835	0.185002
30	0.053749	0.08167	0.073867	0.083335	0.0925	0.197515
35	0.09389	0.08333	0.155	0.042485	0.058315	0.505
40	0.0625		0.0933	0.04	0.121667	0.085
50	0.03		0.15	0.1	0.07	0.0933

Table 4.2 *Table of Volume Loss for Wear Tests against Zirconia Counterfaces with Initial Surface Roughness (R_a) 0.01μm in Various Lubricants*

Sliding dist (km)	Vol. Loss (mm^3) for distilled H_2O	Vol. Loss (mm^3) for Synovial Fluid	Vol. Loss (mm^3) for 5% Albumen	Vol Loss (mm^3) for 10% Albumen	Vol. Loss (mm^3) for 15% Albumen	Vol. Loss (mm^3) for Saline Solution
0	0	0	0	0	0	0
5	0.06093	0.032258	0.017921	-0.0613	-0.0323	0.107528
10	0.039425	0.096774	0.003584	0.03123	0	0.876344
15	0.232975	0.139785	0.028674	-0.00538	-0.06989	1.58065
20	0.383846	0.11828	0.050179	0.24193	-0.0323	3.182788
25	0.365591	0.172043	0.103943	0.145161	-0.1667	4.672043
30	0.397849	0.16129	0.182796	0.274094	-0.1075	5.569893
35	0.532258	0.108568	0.387097	-0.02258	-0.17204	
40	0.650538		0.612903	0.63441	-0.24713	7.784946
50	0.72043		0.902689	0.75269	0	8.215055

4.4 Polymer Behaviour

4.4.1 SEM Examination of Worn Polymer Pin Surfaces

The surface of the polymer pins was examined using the electron microscope for evidence of wear mechanisms. UHMWPE pins were machined and then subjected to wear testing. Initially all the pins had a similar appearance to that seen in Figure 4.5 (a). Thereafter the effect of the sliding wear was to alter the surface characteristics in various ways. There was an orientation of the surface polymer into the direction of sliding in addition to which the different lubricants resulted in different behaviour on the surface of the polymer pins which can be observed in the micrographs which follow.

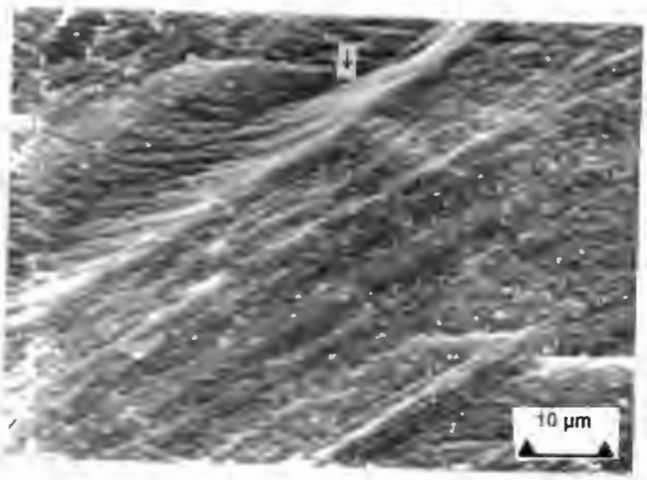

Figure 4.5 (a) Unworn Pin Surface

Figure 4.5(a) shows an unworn pin surface. Flow lines from machining of the pin surface can be seen. The pin surface was nominally flat with variations in the surface roughness resulting from the machining process with an R_a value of 0.3µm.

There was some concern that corrosion of the wear apparatus in the presence of a saline environment was affecting the wear process through the production of iron oxide (rust) acting as a third body abrasive. Large scale production of rust, using pure saline solution as a lubricant resulted in high wear rates and cutting of the polymer surface was observed. However, tests run in the protein lubricating and distilled water lubricating solutions showed no evidence of abrasive wear with the exception of one test. Some ploughing was found on the UHMWPE surface of a pin that was run in 15% albumen lubricant for 35 km. This was believed to be a result of the presence of

iron oxide residue from the previous test. For the albumen lubricated tests where the coolant bath was clean, it was concluded that the conalbumin content of the albumen was bonding to any Fe^{3+} ions that were produced, and reducing the ability of these ions to form rust. Discoloration of the lubricant was taken as an indication that ferric ions were present in solution.

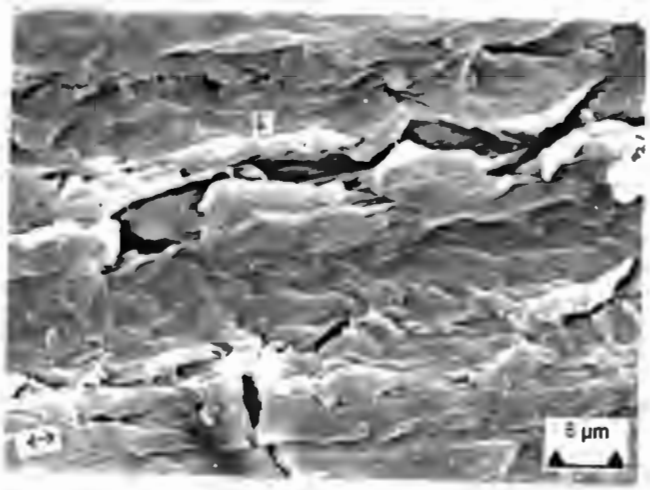

Figure4.5(b) UHMWPE pin run to 50km of sliding distance in saline solution

Iron Oxide or rust was produced as a result of the exposure of the wear apparatus to a saline environment. Hard iron oxide particles caused cutting, ploughing and tearing of the surface of the UHMWPE pin as shown.

Figure4.5 (c)UHMWPE pin run to 35 km, distilled water lubricant.

This micrograph shows that the surface of the UHMWPE pin has been completely altered by the sliding wear process. The surface has become oriented in the direction of sliding and there is evidence of back transfer. i.e. UHMWPE has been transferred from the surface of the pin to the counterface surface. This was then transferred back onto the pin surface as indicated in the micrograph..

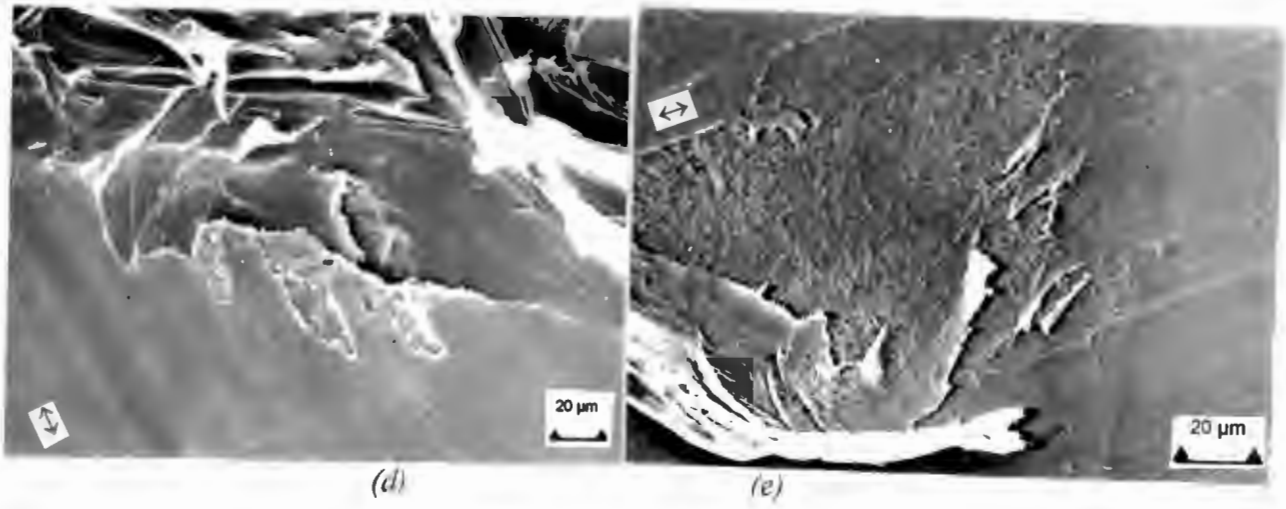

Figure 4.5 (d)UHMWPE pin run to 35 km in distilled water lubricant

Figure 4.5 (e)UHMWPE pin run to 100km in distilled water

From Figures 4.5 (d) and (e) it is can be seen that there is shear of the UHMWPE surface layers. The UHWMPE is oriented in the direction of sliding and shear takes place predominantly near the edges of the pin in Figure 4.5 (d) and in some of the more central regions in Figure 4.5 (e).

Part 2 5% Synovial Fluid Lubricant

Figure 4.5 (f) UHMWPE pin run to 35 km in synovial fluid

Figure 4.5 (g)UHMWPE pin run to 35 km in synovial fluid lubricant.

Shear is occurring from the more central regions of the pin in Figure 4.5 (f). UHMWPE stringers can be seen peeling from the surface. Note that the exposed area is uneven when compared to that of the adjacent regions. UHMWPE has been sheared from the surface in Figure 4.5 (g) and there is evidence that portions of a stringer have been removed while the remaining portion had readhered to the pin surface as indicated.

Part 3 5% Albumen Lubricant

Figure 4.5 (h)UHMWPE pin run to 35 km in 5% albumen solution

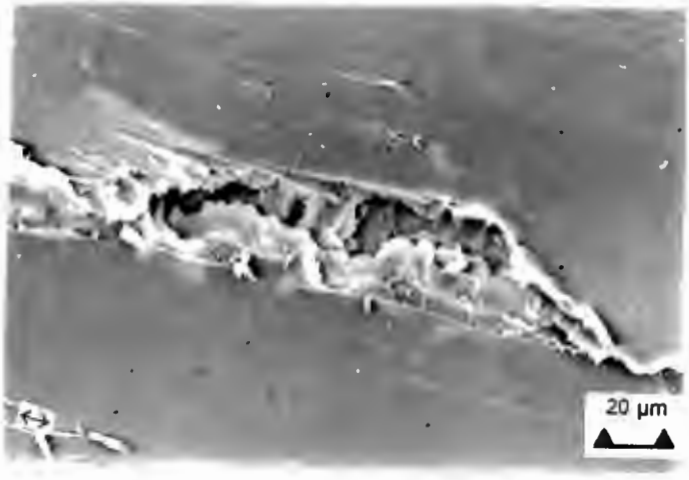

Figure 4.5 (i) UHMWPE pin run to 35 km in 5% albumen solution

The pin surface has been altered during sliding. Small areas have sheared from the pin surface in Figure 4.5 (h). There are numerous small stringers which can be seen to be peeling from the surface and then readhering to it. In Figure 4.5 (i) a deep crack can be observed, it is likely that this precedes the onset of shear from that area. Several of these cracks were observed on the surface of the albumen lubricated samples. The 5 % albumen lubricated samples had fewer deep cracks than those of the higher percentage albumen lubricated tests.

Part 4 10% Albumen Lubricant

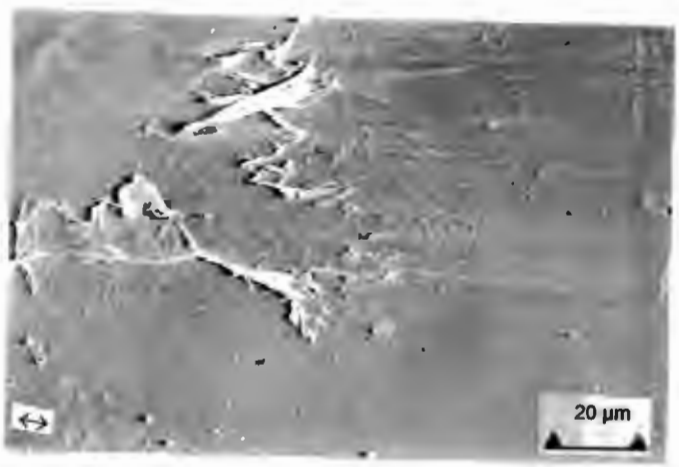

Figure 4.5 (j) UHMWPE run to 50 km in 10% albumen solution

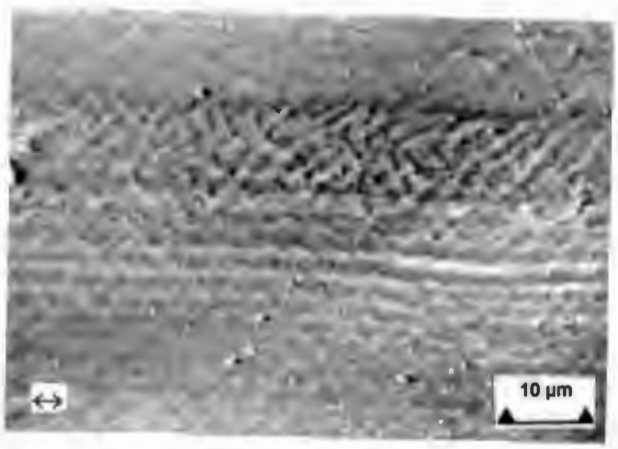

Figure 4.5 (k) UHMWPE run to 50 km in 10% albumen lubricant

These micrographs show two different types of surface characteristics on the surface of the 10 % albumen lubricated wear tests. Material has been sheared in small regions from the surface and some of these sheared areas can be seen to be readhering to the pin surface in (j). Note the microscale inter-ripple spacing seen in (k). These are evidenced in the areas underlying the sheared UHMWPE

Part 5 15% Albumen Lubricant

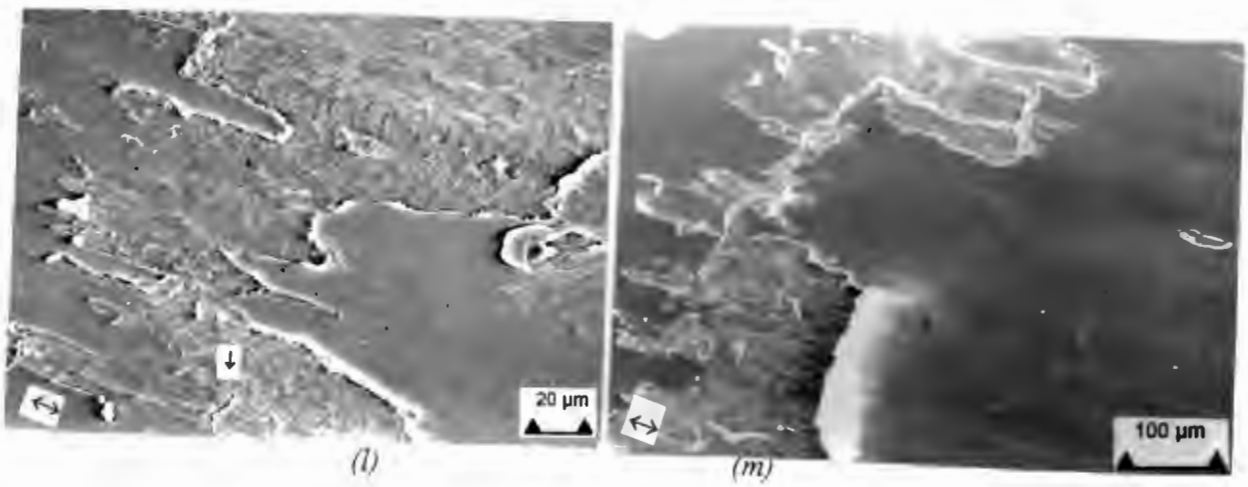

Figure 4.5(l)UHMWPE run to 35 km in 15% albumen solution

Figure 4.5(m)UHMWPE pin run in to 50 km in 15% albumen solution

Figures 4.5 (l) and (m) show that there is shear taking place on the surface of the UHMPWE pins which were lubricated in the 15 % albumen solution. Shear tended to take place close to the pin edges. The polymer material on the pin surface is even as a result of the sliding wear process. The region underlying the sheared area is irregular which is similar to that seen in Figure 4.5 (e) and (f) for the distilled water lubricated UHMPWE pins. The 15 % albumen lubricated pins differ from the distilled water lubricated pins in that there is evidence that the sheared regions appear to be readhering to the surface of the pin as indicated rather than being sheared from the pin surface. Some cracking of the underlying surface can be seen in figure 4.5 (l) as indicated.

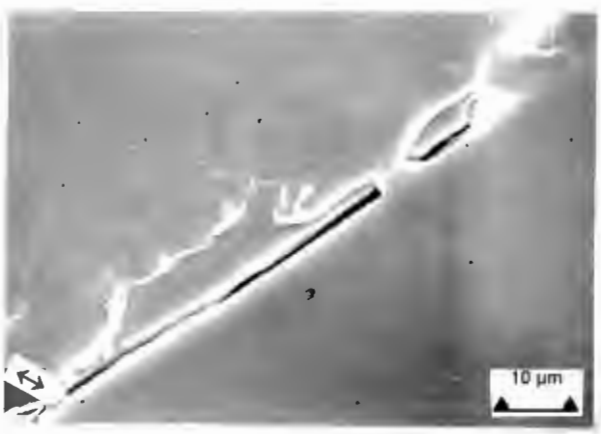

Figure 4.5 (m)UHMWPE pin run to 50 km in 15% albumen solution

Some cracking of the surface was seen to various degrees on the polymer surface as shown in Figure 4.5 (m). Cracks showed the polymer material separating from the surface. It is likely that this polymeric material shears from the surface in subsequent sliding. These cracks were more prevalent in the 15 % albumen lubricated solutions and were more frequent at the higher magnitudes of sliding distances.

Part 6 Distilled Water Lubricant against Rough (0.06μm) PSZ Counterface Surfaces

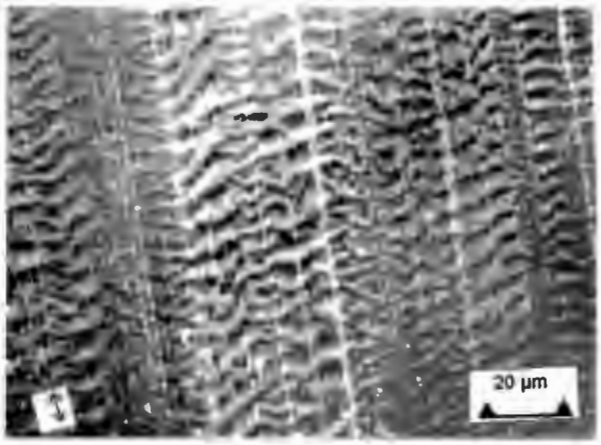

Figure 4.5 (n) UHMWPE run to 100km in distilled water against a zirconia counterface of R_a 0.06μm

This micrograph shows the surface of an UHMWPE pin run in distilled water against a zirconia counterface with a surface roughness of 0.06μm. On large sections of the pin surface, corrugations could be observed. It appears that intermittent shearing of the polymer surface layers is taking place.

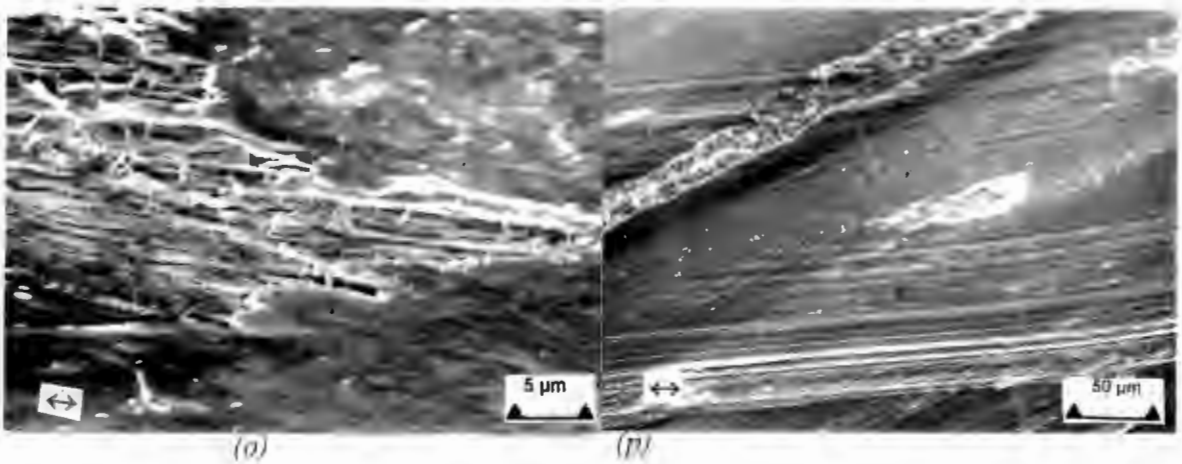

(o) (p)

Figure 4.5 (o) UHMWPE pin run to 50 km in 10% albumen solution against a zirconia counterface of R_a 0.06μm

Figure 4.5 (p)UHMWPE run to 50 km in 15% albumen against a zirconia counterface of R_a 0.06μm

In (o) a sheared area shows the fibrous structure of the material. This fibre structure was typical of the polymer surface characteristics found in the protein lubricating solutions. It can be seen that these fibres are being sheared off as small stringers. Some of the fibres are teased from the surface and these are likely to shear in subsequent sliding. Removal of smooth surface layers by shear results in the rough underlying areas observed in Figure 4.5 (p). There was large scale cracking across the surface of the pin in the regions that linked the sheared areas. This cracking ran transverse to the direction of sliding. The pin edges were flat and it appeared that no material was accumulating there. Removal of surface layers through shear processes could be seen in various regions across the pin surface.

Part 7 Alumina Counterfaces

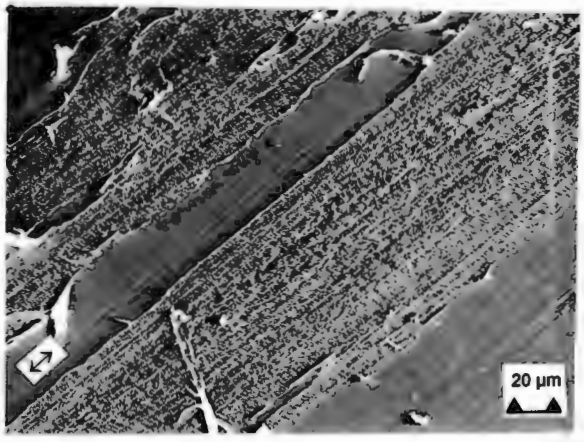

Figure 4.4.1(s) UHMWPE run to 100km in distilled water against an alumina counterface of R_a 0.04µm

Material was sheared from the UHMWPE surface over most of the pin surface. The uneven structure of the bulk material can be clearly seen.

4.4.2 Scratch Tests of UHMWPE Surfaces

Scratch tests were performed on UHMWPE surfaces using a diamond indentor. A load of 50N was applied and the tests were conducted at a velocity of 4mm/minute. Unworn pins and worn pin surfaces were scratched in an attempt to determine whether the sliding process was affecting the hardness of the surface of the UHMWPE pins. The worn pins had been subjected to sliding wear over a distance of 100km in distilled water lubricant. The scratches on the first worn pin could be seen while those on the second worn pin could not be located which indicates that the wear process is resulting in hardening of the UHMWPE pin surface.

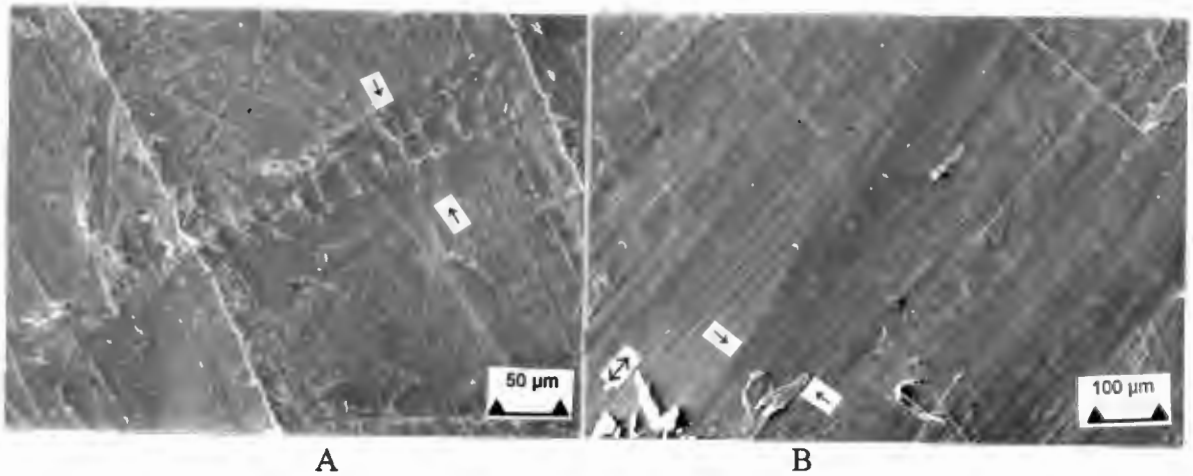

A B

Figure 4.6 - A Unworn UHMWPE surface with scratch shown

Figure 4.6 - B Scratch shown on worn UHMWPE surface

The scratches were barely visible and are highlighted as shown.

4.4.3 Investigation of the Subsurface Deformation of UHMWPE by Polarised Light

Thin sections (50 μm) thick were microtomed normal to the polymer pin surfaces. These were examined in polarised light to ascertain the effects of sliding wear on the surface layers of the UHMWPE pins in the various lubricating conditions.

It was found in Figure 4.7 (I) that there was evidence of subsurface deformation from the machining process as shown.

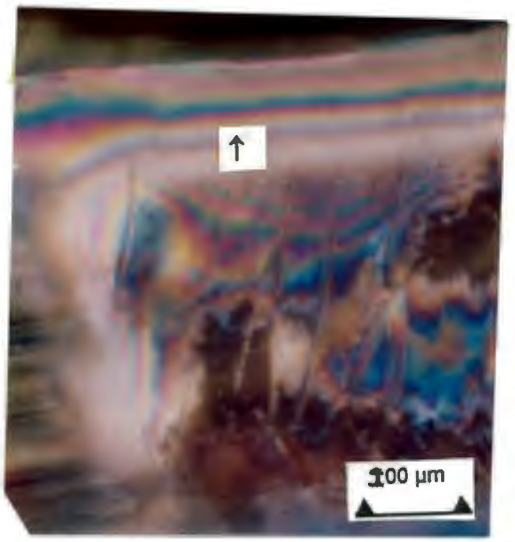

Figure 4.7 (I) Thin section of unworn UHMWPE pin seen in polarised light mode.

Figure 4.7 (II) shows that the nature of the UHMWPE surface has been altered by the sliding wear process and that there is strong evidence of subsurface deformation as indicated.

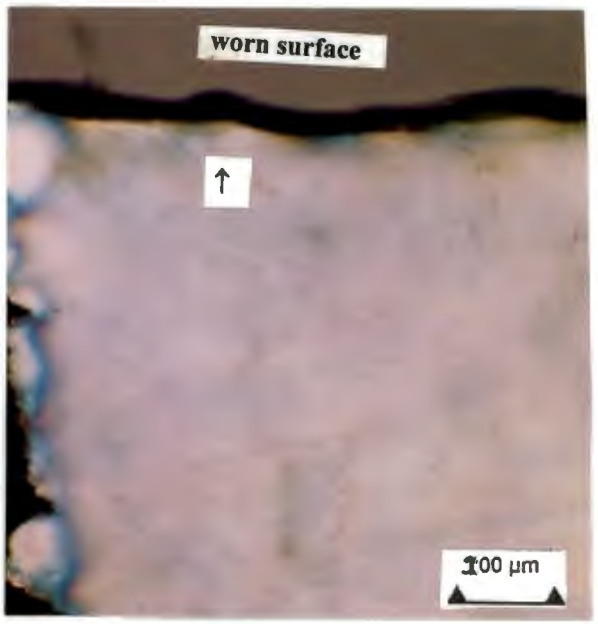

Figure 4.7 (II) Thin section of worn UHMWPE pin run to 35 km of sliding distance in distilled water lubricant.

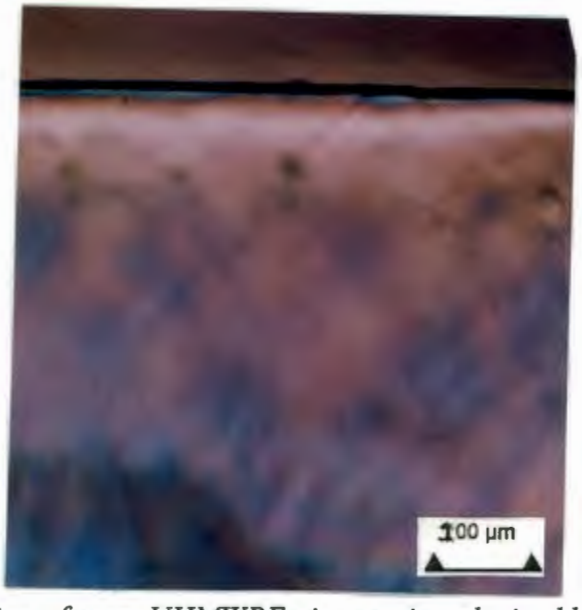

Figure 4.7 (III) Thin section of worn UHMWPE pin seen in polarised light mode. The pin was subjected to 35 km sliding distance in 5% albumen solution.

4.5 Nature of the Wear Scar

4.5.1 Optical Examination of the Wear Scar

Worn zirconia and alumina counterfaces were examined optically. It was clear that there was transfer of UHMWPE to the worn surface in an irregular manner .i.e. there was no evidence of a continuous transfer layer being laid down.

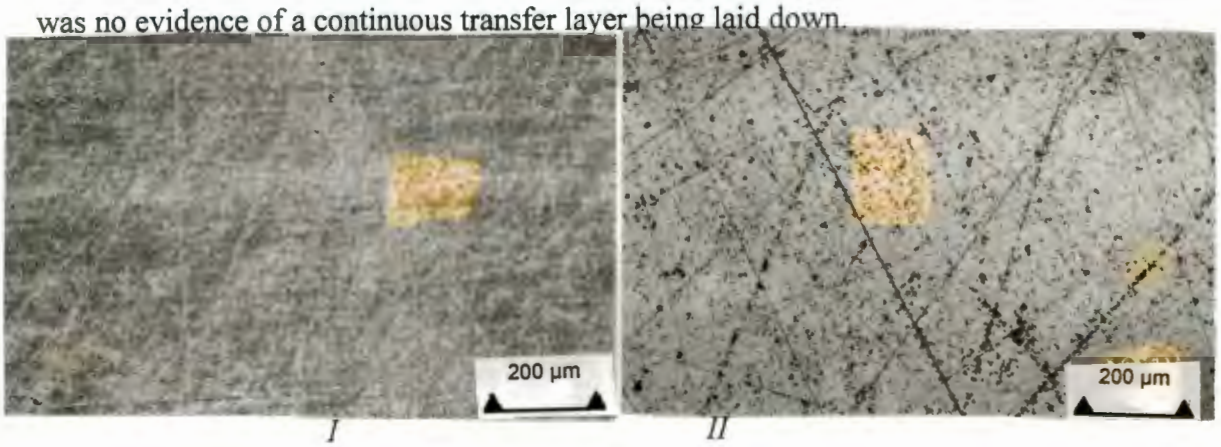

Figure 4.8 (I) Optical photograph of unworn zirconia surface-scratches are from polishing process

Figure 4.8 (II) Optical photograph of unworn alumina surface- porosity as a result of grain pull-out from the polishing process can be seen on the alumina surface

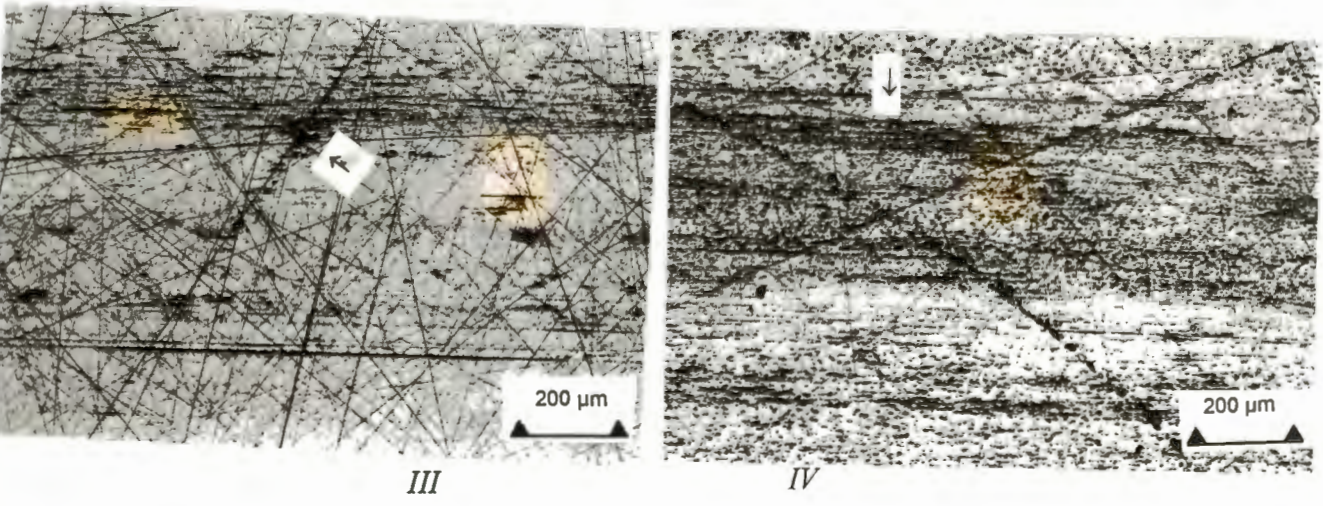

Figure 4.8 (III) Zirconia counterface run to 100km in distilled water

Figure 4.8 (IV) Zirconia counterface run to 100km in distilled water

In the Figures 4.8 (III) and (IV) it can be seen that the polishing scratches are acting as preferential sites for transfer of polymer to the counterface surface. The darker intermittent marks are UHMPWE which has been transferred to the pin surface. There is no evidence of a continuous transfer film on the surface, there is however a

certain amount of polymer transfer occurring as seen in III. The deeper polishing scratch (arrowed in Figure 4.8 (III)) which is running almost normal to the sliding direction is acting as a site to which polymer is adhering preferentially. It appears that adherent UHMWPE particles are acting as sites for further adhesion, as indicated. Figure 4.8 (IV) shows that the UHMWPE transfer varies across the wear track

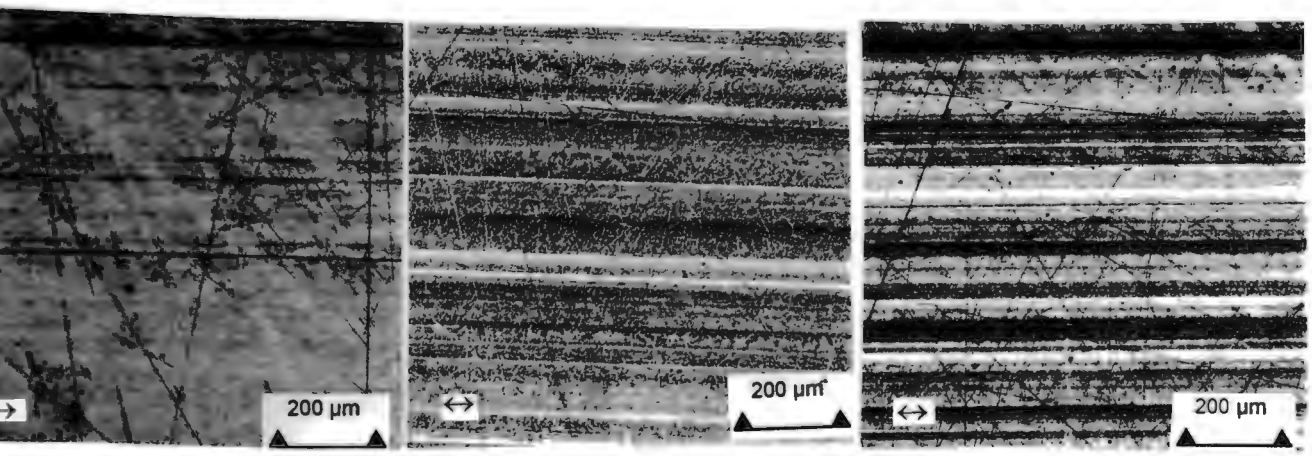

V *VI* *VII*

Figure 4.8 (V) Zirconia counterface run to 5km in synovial fluid solution

Figure 4.8 (VI) Zirconia counterface run to 20 km in synovial fluid solution

Figure 4.8 (VII) Zirconia counterface run to 35 km in synovial fluid solution

This series of micrographs (Figures 4.8 (V)-(VII)) is indicative of the change in the nature of the transferred layer as the sliding distance increases for a test conducted in 5% synovial fluid solution. In Figure 4.8 (V), after 5km of sliding distance, the darker, horizontal, parallel lines are an indication that there is some form of transfer to the zirconia counterface. In Figure 4.8 (VI), after 20km of sliding distance, these lines become more evenly spread across the wear scar. In Figure 4.8 (VII), after 35km of sliding distance, the lines are darker which is indicative of the fact that the transfer to the surface is becoming thicker. This transferred layer is very different to that seen in Figures 4.8 (III) and (IV). It is possible that there is some form of protein residue being laid down on the surface in addition to any UHMWPE transferred. Transferred material is a combination of protein and polymer. From this series of micrographs it is clear that there is increased adhesion to the surface as the sliding distance increases.

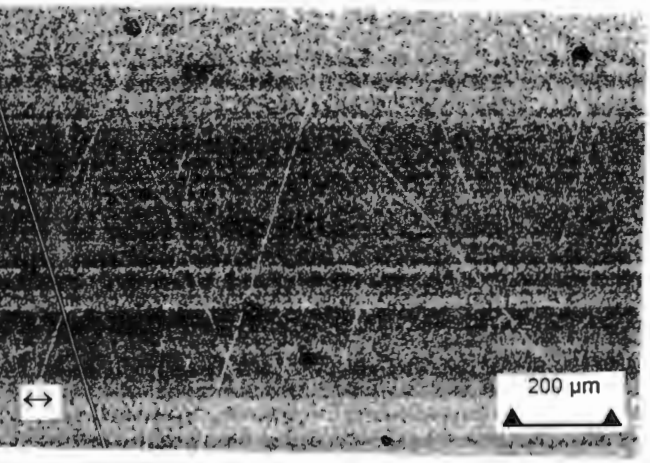

VIII

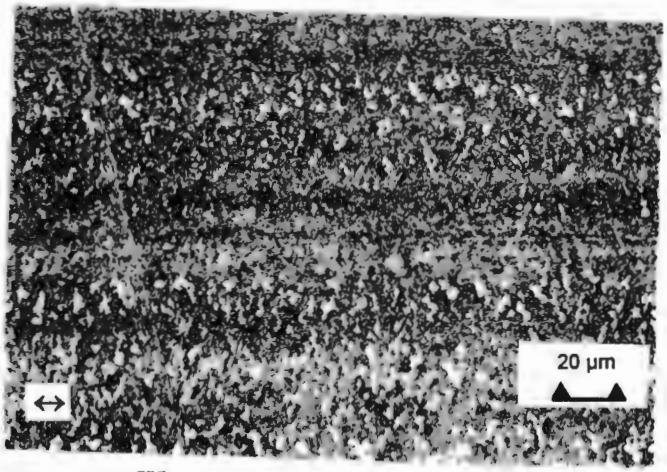

IX

Figure 4.8 (VIII) Zirconia counterface run to 30 km in 10% albumen lubricant

Figure 4.8 (IX) Zirconia counterface run to 30 km in 10% albumen lubricant - central region of the wear scar

Figures 4.8 (VIII) and (IX) show that there is transfer of polymer taking place onto the counterface surface. The counterface surface is different to the unworn counterface seen in Figure 4.8 (I). The parallel, horizontal marks on the surface of the counterface are an indication that some transfer is taking place. In Figure (IX) the bright particles on the surface of the counterface are polymer particles that have been transferred to the counterface surface. These bright particles seem to have become uniform in thickness during the sliding wear process taking place for a test conducted in 10% albumen solution.

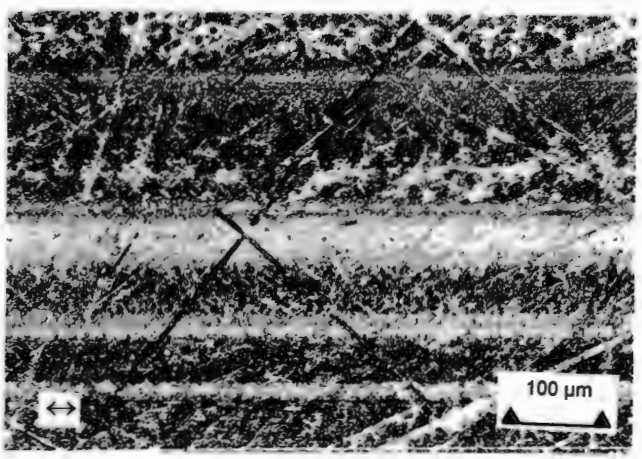

Figure 4.8 (X) Zirconia counterface of R_a 0.06µm run to 40 km in distilled water lubricant

Figure 4.8 (X) shows that there is transfer of polymer to the rougher counterface surface. This can be seen by the darker areas which are parallel to one another indicating that there is transfer occurring preferentially in the direction of sliding (the same direction as the parallel regions). However the transfer is discontinuous as can be seen by the lighter transfer smears. Furthermore the polishing scratches are acting as sites for polymer transfer. There is increased transfer of UHMWPE to the counterface surface when compared to that of the smoother surface in Figures 4.8 (III) and (IV) conducted in distilled water lubricant.

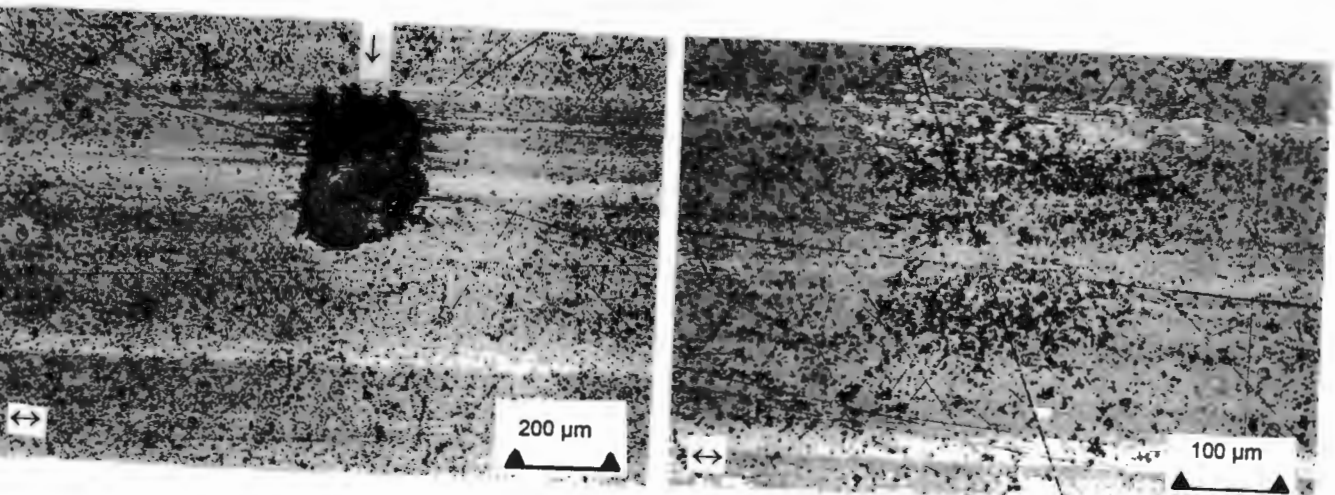

XI *XII*

Figure 4.8 (XI) Alumina counterface run to 100km in distilled water

Figure 4.8 (XII) Alumina counterface run to 100km in distilled water

Figures 4.8 (XI) and (XII) show that there is some polymer transfer to the surface of the alumina counterfaces. This can be seen by the darker regions on the surface of the alumina. Comparing the above two figures, UHMWPE transfer to the alumina surface can be seen to vary across the wear track. Transferred particles tend to act as sites for further adhesion as can be seen in Figure 4.8 (XI). There is evidence in Figure 4.8 (XII) that transferred particles are being flattened during the wear process. This can be seen in the form of bright particles on the alumina surface as indicated.

4.5.2 S.E.M Examination of Counterface Wear Tracks

Zirconia and alumina counterfaces were viewed at high magnification using the scanning electron microscope. The nature of the transferred material varied with the various lubricants. This behaviour mirrored that found in the optical investigation.

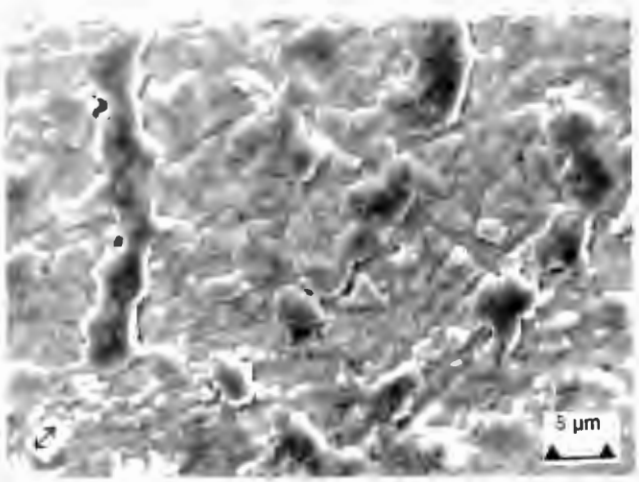

Figure 4.9 (I) Zirconia counterface run to 35 km in distilled water

Transferred material observed in the optical investigation was confirmed to be UHMWPE particles. UHMWPE of varying sizes can be seen to be adhering to the zirconia surface in Figure 4.9 (I).

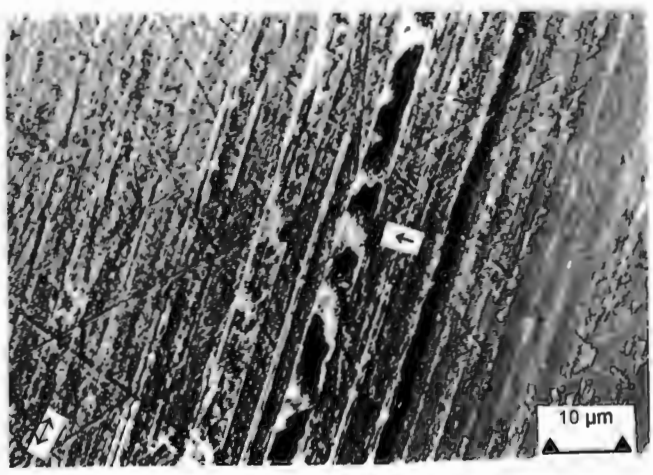

Figure 4.9 (II) Zirconia counterface run to 100km in distilled water

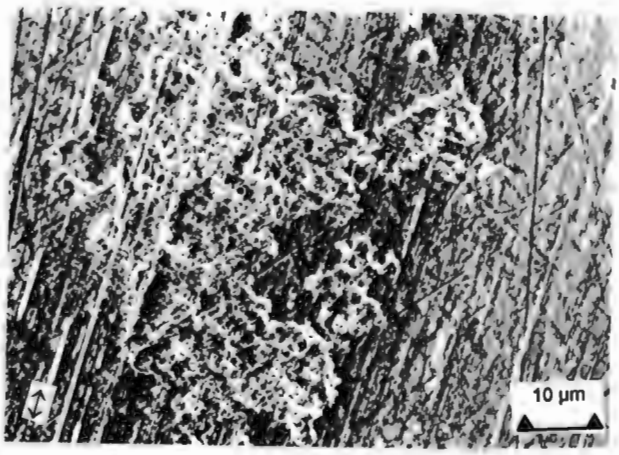

Figure 4.9 (III) Zirconia counterface run to 100km in distilled water

Comparing 4.9 (I) and 4.9 (II) it is clear that UHMWPE transfer varies across the wear scar. The transfer of the polymer material tends to be in the direction of sliding and varies over the counterface surface. In Figure 4.9 (II) there is evidence of stick-slip as arrowed in Figure 4.9 (II). In Figure 4.9 (III) it can be seen that UHMWPE has been transferred to the surface . This transferred material appears to be is acting as a preferential site for further transfer. This can be seen by the large amount of polymer transfer in the same region and the variation in thickness of the UHMWPE across this region.

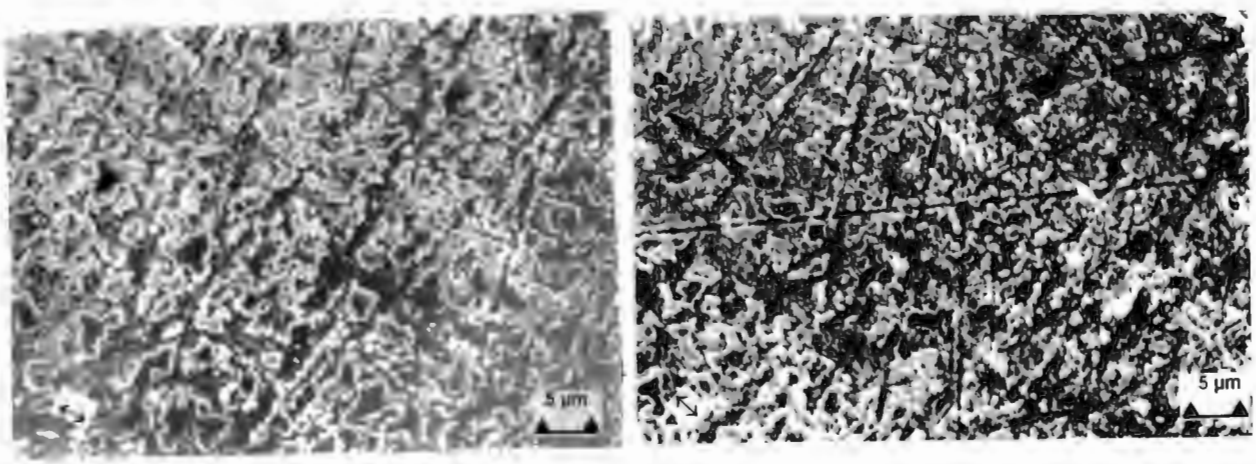

IV *V*

Figure 4.9 (IV) Zirconia counterface run to 35 km in synovial fluid solution

Figure 4.9 (V) Zirconia counterface run to 35 km in synovial fluid solution

What appears to be polymer particles of varying sizes can be seen on the zirconia surface in Figures 4.9 (IV) and (V). These are flattened in appearance and were likely less uniform originally and have been systematically depressed during sliding.

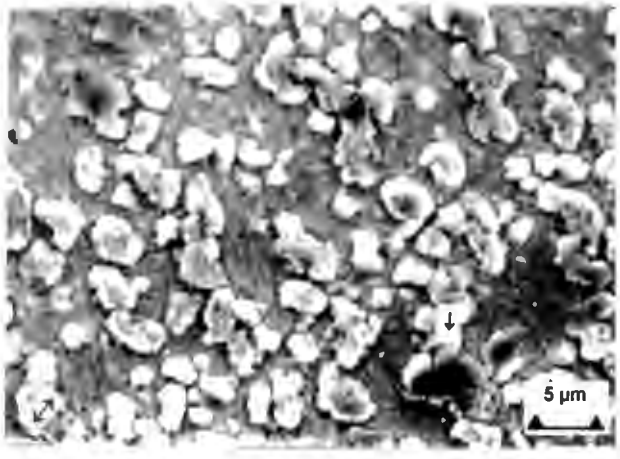

Figure 4.9 (VI) Zirconia counterface run to 35 km in 5% albumen solution

The particles visible on the surface in Figure 4.9 (VI) appear to be rolled up UHMWPE particles which were evident on the surface of the wear pins as short stringers. Note the flattened particle indicated. This is similar to the flattened particles in Figures 4.9 (IV) and (V). There is an absence of visible polishing scratches and it is possible that this is because the protein from the solution is being laid down onto the zirconia surface and acting as an adhesive allowing these polymer particles to become attached to the zirconia surface.

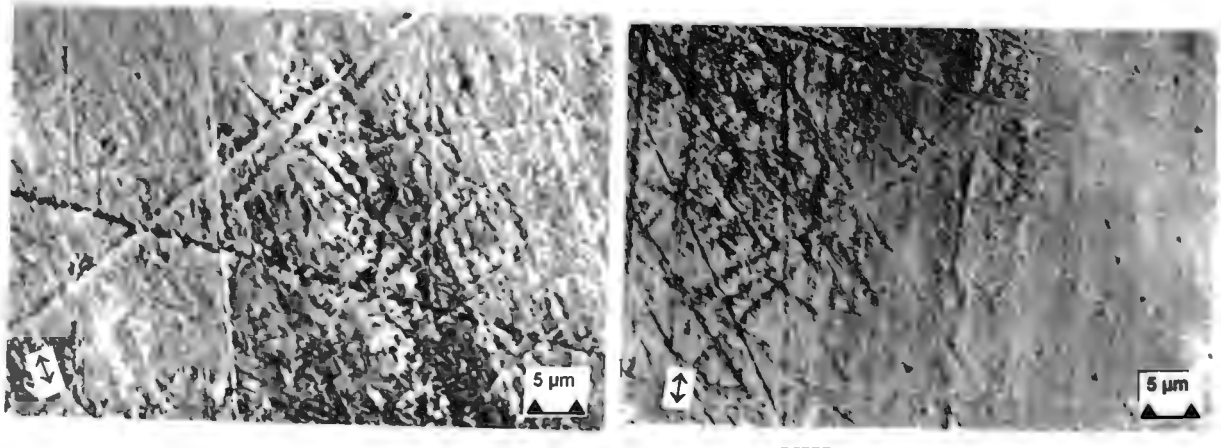

VII *VIII*

Figure 4.9 (VII) Zirconia counterface run to 35 km in 10% albumen solution

Figure 4.9 (VIII) Zirconia counterface run to 35 km in 15% albumen solution

There is some transfer of UHMWPE to the surface as indicated by the lighter section in Figure 4.9 (VII). These are small polymer particles which act as preferential sites for further transfer. These particles are very uniform in thickness. There was minimal transfer on the surface in Figure 4.9 (VIII). The region on the left shows that some transfer is occurring. The transferred material is very uniform.

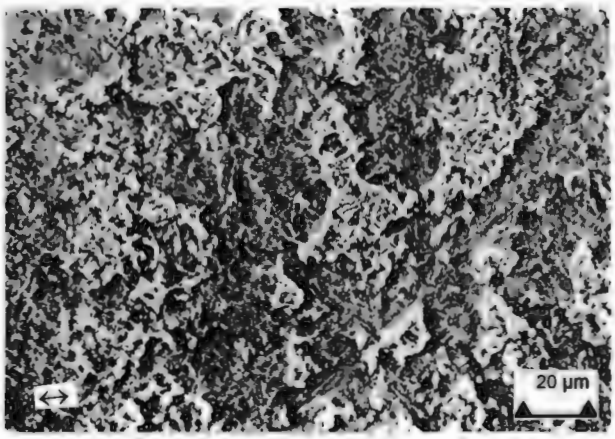

Figure 4.9 (IX) Zirconia counterface R_a 0.06µm run to 100km in distilled water lubricant.

Figure 4.9 (IX) shows polymer transfer to the counterface surface. Once again the transferred UHMWPE is acting as preferential sites for further transfer. Most of the raised agglomerates are made up of particles of approximately 1µm thick and up to 8µm in length

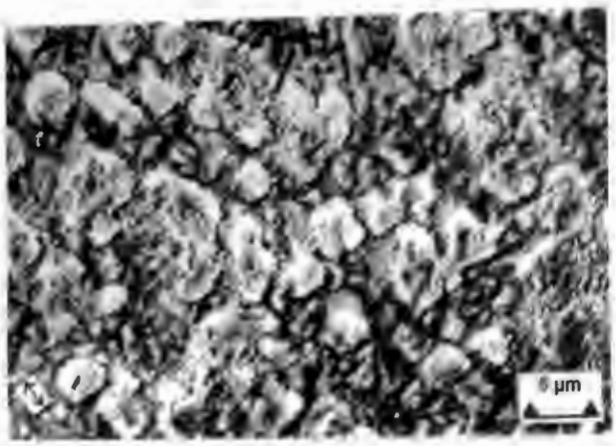

Figure 4.9 (X) Zirconia counterface Ra 0.06µm run to 50 km in 10% albumen solution

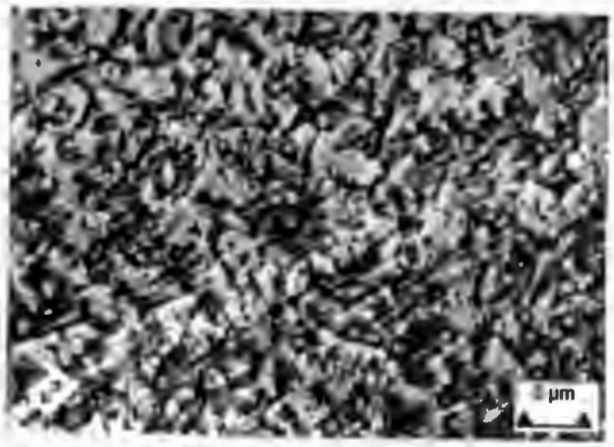

Figure 4.9 (XI) Zirconia counterface Ra 0.06µm run to 50 km in 15% albumen solution

Both samples run in the protein solutions against the rougher zirconia counterfaces also show agglomerated particles on the surface in Figures 4.9 (XI) and (X). These particles decrease in size for increasing protein content. The particles in Figure 4.9 (XI) are smaller and finer than those in Figure 4.9 (X).

4.5.3 Analysis of the Wear Scar

Transfer of material for the samples tested in the protein solutions differed to those tested in the distilled water. An attempt was therefore made to analyse the material on the counterface wear track to determine whether some protein residue was adsorbing onto the ceramic surfaces. SIMS, XPS and AES were used for this purpose. The results are shown in Tables 4.2 (I - IV) and Figures 4.10 (I) and (II).

Section 1 XPS Analysis of the Wear Scar

UHMWPE contains only hydrogen and carbon. In addition to this, one would expect to find adsorption of atmospheric oxygen, carbon and hydrogen onto the surface of any sample exposed to the atmosphere. The elements contained in the albumen solution that are characteristic of the proteins, apart from carbon and hydrogen, are sulphur, nitrogen and phosphorous and oxygen. In the synovial fluid, the characteristic elements, apart from carbon and hydrogen, are nitrogen and oxygen (which is present in the COOH group of all amino acids). In addition to this, higher atomic percentages of carbon when compared to that of distilled water can also be considered to be an indication of the presence of proteins.

Table 4.2 (I) XPS analysis of unworn zirconia ceramic soaked in 5% albumen solution for 48 hours

Element	Peak Position (eV)	Atomic %	Probable Compound
Al	74.0	3.3	$Al_2O_3/Al(OH)_3$
P	133.5	0.5	$H_xC_yO_zP$/Hydroxyapatite
Zr	183.0	8.6	ZrO_2
S	163.5	0.5	
C	285.0	51.2	CH/Adsorbed carbon
N	400.0	7.2	H_xC_yN/N with O,S
O	531.5	27.9	Al_2O_3/ZrO_2/O with N

Figure 4.2 (II) XPS analysis of zirconia ceramic run to 35 km in distilled water

Element	Peak Posn On W.S (eV)	Peak Posn Off W.S (eV)	At% On W.S	At % Off W.S	Probable Compound
Al	74.5	74.0	0.1	2.6	Al_2O_3
Si		102.0		1.8	
P	133.5	133.0	1.8	0.3	$H_xC_yO_zP$/Hyroxyapatite*
S		164.5		0.1	
Zr	183.0	182.5	5.2	5.3	ZrO_2
C	285.0	285.0	54.7	52.7	CH/adsorbed C
N	400.5	400.0	4.2	4.5	H_xC_yN/N with O,S
O	531.5	531.0	31.8	30.7	$Al_2O_3/Fe_2O_3/ZrO_2$
Fe	711.0	711.5	2.1	1.9	Fe_2O_3

Table 4.2 (III) XPS analysis of zirconia ceramic run to 35 km in 5% synovial fluid solution

Element	Peak Posn On W.S (eV)	Peak Posn Off W.S (eV)	At% On W.S	At % Off W.S	Probable Compound
Cl	199.5	199.0	1.4	1.1	NaCl
Zr	183.5	-	1.3	-	ZrO_2
C	285	285	60.7	68.4	CH/absorbed C
Pd	336	335.5	12.6	12.6	Pd
N_1	394	-	1.4		
N_2	399.0				H_xC_yN/N with O,S
N	394		0.4		
O	532	532	20.6	16.6	Fe_2O_3/ZrO_2
Fe	710	-	1.4	-	Fe_2O_3
Zn	1022	1021	0.6	0.8	ZnO

Table 4.2 (IV) XPS analysis of zirconia ceramic run to 35 km in 5% albumen solution

Element	Peak Posn On W.S (eV)	Peak Posn Off W.S (eV)	At % On W.S	At% Off W.S	Probable Compound
Al	74.5	74.5	0.1	2.1	$Al(OH)_3$
Si		102.0		0.2	
P	133	133.5	1.0	0.7	$H_xC_yO_zP$/ hydroxyapatite*
Zr	183.0	182.5	3.8	3.5	ZrO_2
Cl	198	199	1.7	0.4	NaCl
C	285	285	56	63.9	CH/ absorbed carbon
N	399.5	399.5	5.5	3.6	H_xC_yN/ N with O,S
O	530.9	531.5	25.2	20.6	$Al(OH)_3/ZrO_2$
Fe	710.0	710.0	6.7	5.0	Fe_2O_3

*for Hydroxyapatite a Ca peak should be detected. A peak is present at the position for Ca, but the Ca peak overlaps with the 3p Zr peak so it was not possible to identify the Ca peak unambiguously

Section I Analysis of XPS Results

In the albumen sample the elements that are present in the albumen and not in the polyethylene are N,S and P. S was not detected because the Zr peaks overlap with the S peaks. A higher N and P layer are detected on the wear track when compared to the unworn region and this suggests that there could be a layer of protein on the wear track. On the synovial fluid specimen a smaller N peak was detected , the presence of the Au-Pd coating on the surface of the sample probably affected the size of this peak. There is N present on the wear track of the synovial fluid specimen. This is can be resolved into two peaks and the binding energy of the "second" nitrogen peak suggests that this peak can originate from NH group bonded to C. This configuration corresponds to the N bonded in the synovial fluid and is taken as an indication that there is a layer of synovial fluid or synovial fluid residue on the ceramic surface.

4.5.3 Section II SIMS Analysis of Wear Scar

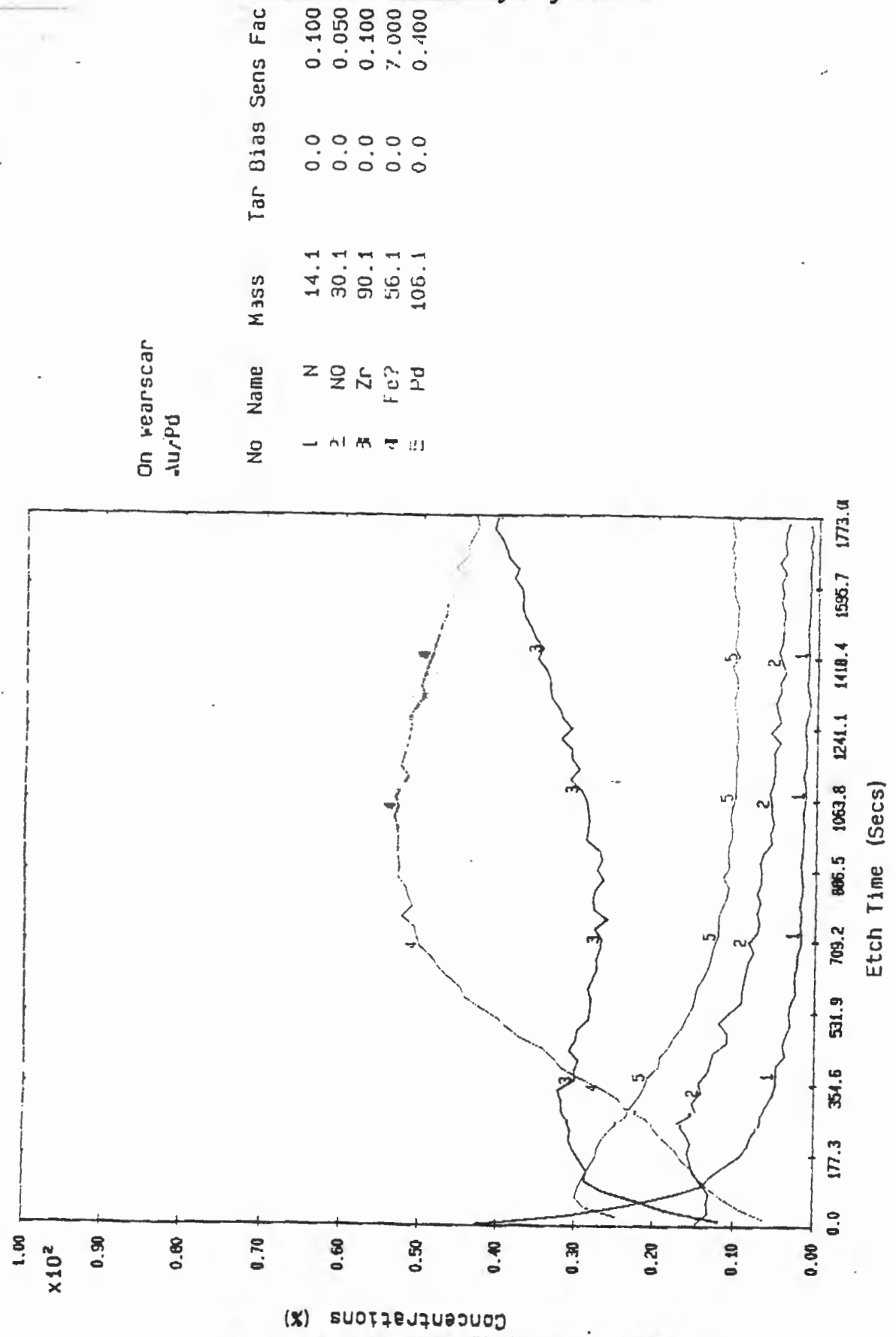

Figure 4.10 (I) SIMS Profile for Synovial Fluid

4.5.3 Section III AES Analysis of Wear Scar

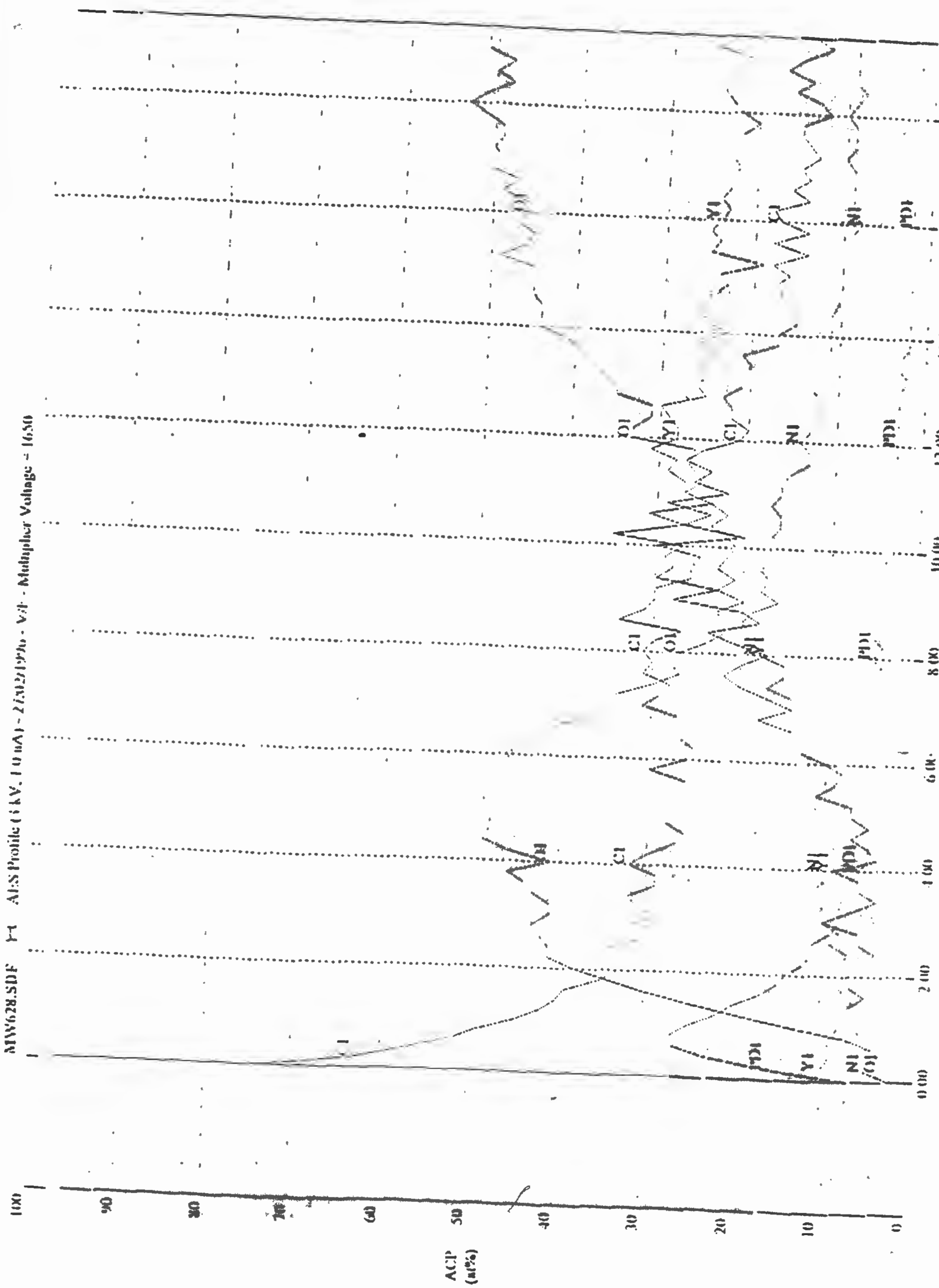

Figure 4.10 (II) AES Profile for Synovial Fluid

Section II Analysis of the SIMS Results

1. Albumen Sample

On the wear track , the ^{14}N (elemental) nitrogen peak is sputtered away within a minute or two. The NO peak was also monitored and indicates a layer is present underneath the adsorbed loosely bonded nitrogen. (This layer probably consists of adsorbed atmospheric contamination). This confirmed the XPS results and indicated that there was an adsorbed atmospheric contamination layer with C,N and O on the surface, with a layer containing bonded nitrogen beneath this layer.

2. Synovial Fluid Sample

The ^{14}N sputtered away within two or three minutes. A layer of NO was detected below this adsorbed nitrogen. It was not clear whether the Pd layer was sputtered away or if the nitrogen was detected in the Pd layer. So an auger depth profile was conducted on this sample.

Section III Analysis of AES Results

It was clear from Figure 4.10 (II) that the Pd was sputtered away after 2 minutes of sputtering time. Above this layer if C, N and O is detected on the surface of the sample indicating an adsorbed layer on the outer surface. The C,N and O are lower than the Pd layer. Beneath the Pd layer the O and N concentration increases. After 6 minutes sputtering time the nitrogen increases again and a nitrogen layer is detected. A depth profile was attempted away from the wear track. Once the Pd was sputtered away the sample became non-conducting and electronic charging occurred after two minutes of sputtering time. The wear track, as a result of some Fe present, remained conducting after this point. Therefore it was not possible to obtain a depth profile away from the wear track. There was however no indication of any nitrogen layer.

4.6 Nature of the Wear Debris

4.6.1 Morphology of Wear Debris

Lubricating solutions from the wear tests were filtered after each test and these were viewed using the scanning electron microscope.

p=4497 p=4922

Figure 4.11 (I) Debris from test run to 100km in distilled water lubricant

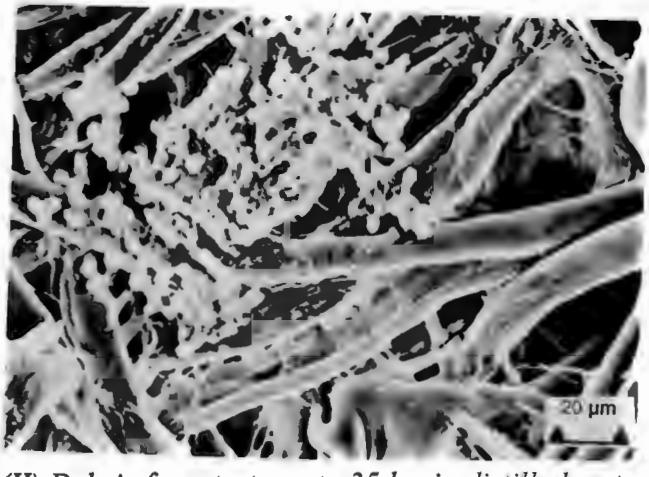

Figure 4.11 (II) Debris from test run to 35 km in distilled water lubricant

In Figure 4.11 (I) a large solid flake of UHMWPE debris is shown. This is characteristic of the larger UHMWPE particles which have visible surface corrugations. Figure 4.11 (II) is a micrograph of filter paper with UHMWPE debris trapped on the fibres of the filter paper. The larger fibres visible are fibres in the filter paper. The smaller agglomerated particles are UHMWPE debris from distilled water tests. The debris shown here was characteristic of the form in which UHMPWE debris was produced in the distilled water lubricated tests. i.e. that of large solid flakes with corrugations on the surface as seen in Figure 4.11 (I), and that of fine spherical particles that tend to agglomerate together as seen in Figure 4.11 (II).

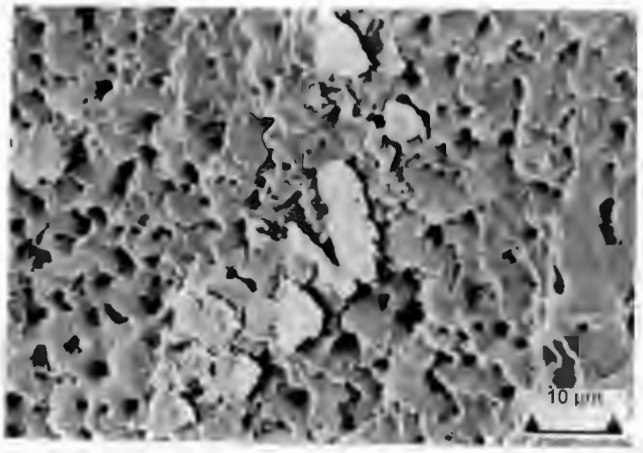

Figure 4.11 (III) Debris particles from test run to 35 km in 5% albumen solution

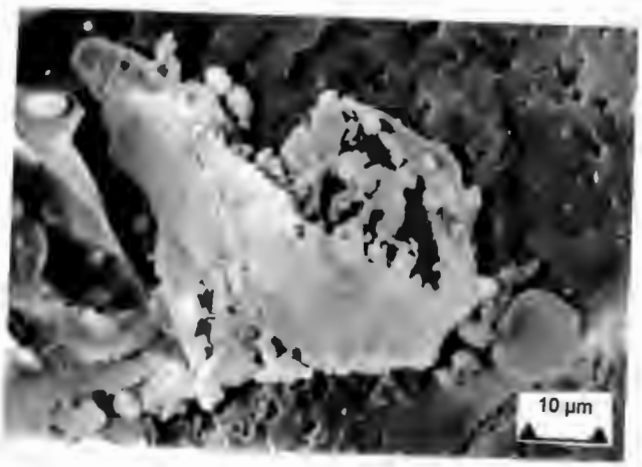

Figure 4.11 (IV) Debris particles from test run to 35 km in 5% albumen solution

Figures 4.11 (III) and (IV) show debris particles trapped on the protein residue after filtration. The size and shape of the debris from the albumen lubricant varied over a range of sizes. The particles were generally small and spherical or ellipsoid in shape as can be seen in Figure 4.11 (III) although there were several larger particles. One of these larger particles can be seen in Figure 4.11 (IV) as a folded flake with similar surface corrugations to those seen in Figure 4.11 (I) for distilled water.

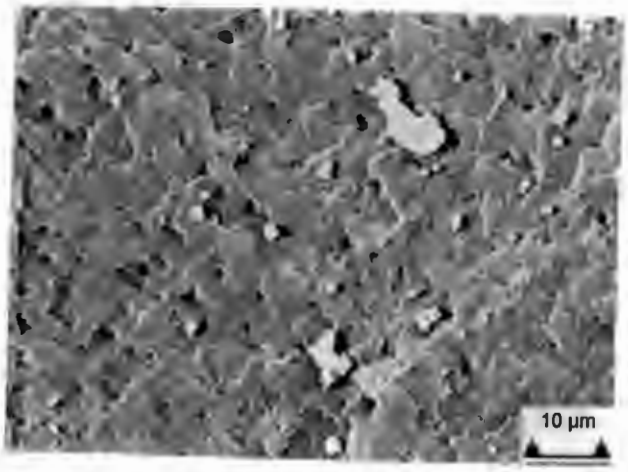

Figure 4.11 (V) Debris from test run to 35 km in 10% albumen solution

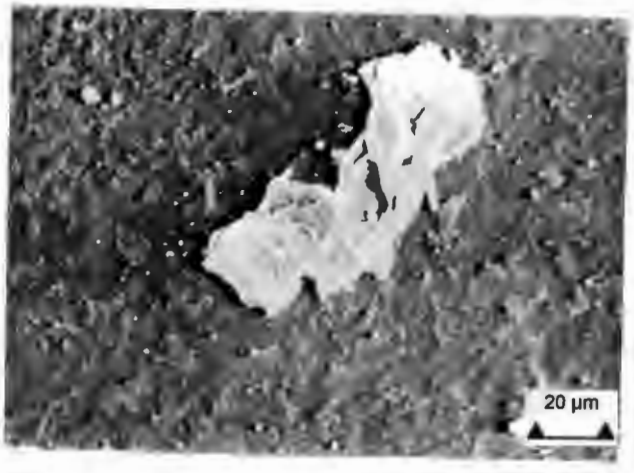

Figure 4.11 (VI) Debris from test run to 35 km in 10% albumen solution

Figures 4.11 (V) and (VI) show the debris particles formed in the 10% albumen solution that were trapped on the protein residue after filtration. Generally the debris particle size was small for the higher percentage protein lubricated tests. The small light particles are seen in Figure 4.11(V) are characteristic of the debris particles found for the 10 % albumen lubricated tests. However this is probably because the albumen solutions tended to lay down a residue layer on the filter paper which acted to trap the smaller particles on the surface of the filter paper so smaller particles were more found more frequently in the higher percentage albumen solutions. There were also some larger particles and these also had visible surface corrugations as in Figure 4.11 (VI). However generally the larger particles were not as large as those found in the distilled water lubricated tests.

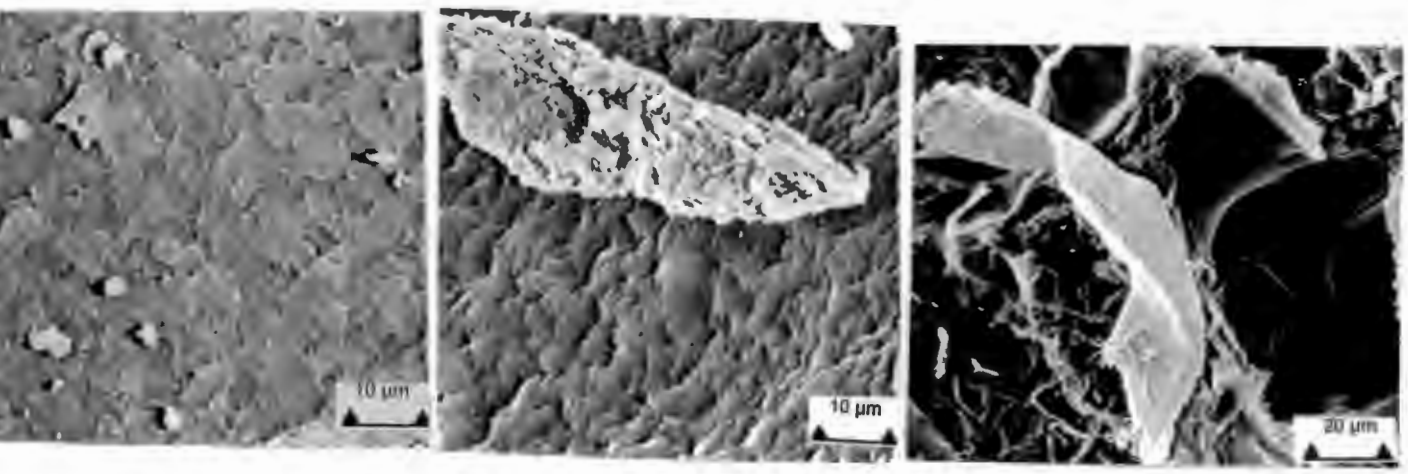

VII *VIII* *IX*

Figure 4.11 (VII) Debris from test run to 35 km in 15% albumen solution

Figure 4.11 (VIII) Debris from test run to 35 km in 15% albumen solution

Figure 4.11 (IX) Debris from test run to 35 km in 15% albumen solution

Figures 4.11 (VII) - (IX) are micrographs of debris particles from the 15% albumen solution that were trapped on the surface of the filter paper after filtration. The debris was principally small and spherical in shape as can be seen in Figure 4.11 (VII) . Larger particles were found and these were either agglomerates of smaller particles as in Figure 4.11 (VIII) or were solid flakes with surface corrugations as in Figure 4.11 (IX).

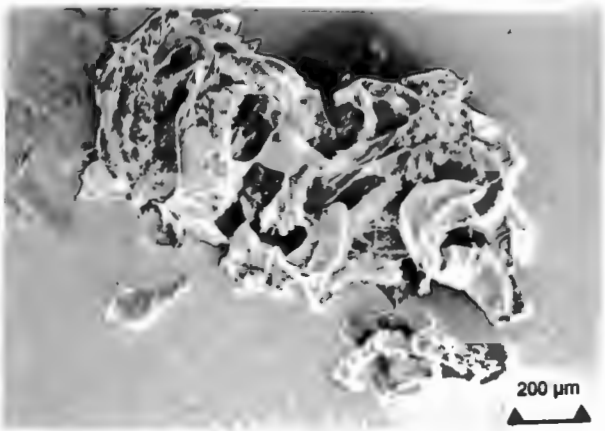

Figure 4.11 X Debris collected from test run to 100km in distilled water against zirconia Ra 0.06µm

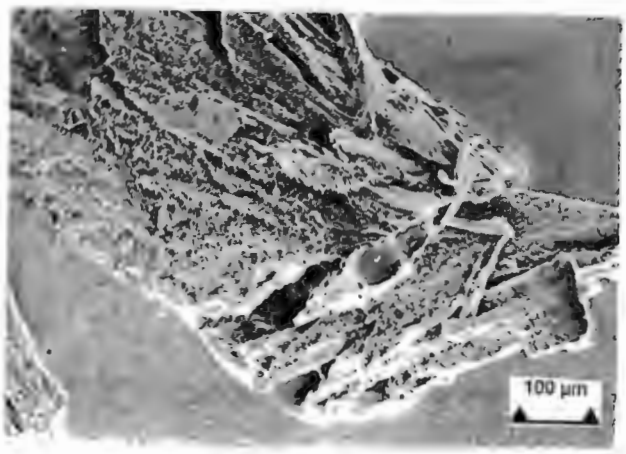

Figure 4.11 XI Debris collected from test run to 100km in distilled water against zirconia Ra 0.06µm

Debris from the tests against the rougher zirconia counterfaces run in distilled water came off the pin edges in large fragments these were collected and viewed using the SEM. Generally debris was large by comparison to the other material collected and was in stringer or agglomerate form as seen in Figure 4.11 (XI) or a combination of the two as seen in Figure 4.11 (X). It appears that the UHMWPE agglomerates at the pin edges until it is sufficiently large to break from the pin surface.

4.6.2 Morphology Analysis

Photographs of the UHMWPE debris from the protein solution samples were measured and classified according to morphology to give a breakdown of the shape and size of the debris particles. The particles were classified as spherical, ellipsoid or flake like. Lubricating solutions were drained every five km and filtered. Sections of the filter paper from various stages of each test were then selected at random. Typical regions from the selected sections were then photographed and the particles classified according to morphology and size. The number count of the particles was determined by the number if particles found within a certain area. For the 5 % albumen lubricated sample, 100 particles were counted, for the 10 % albumen lubricated sample, 400 particles were counted and for the 15 % albumen lubricated sample, 500 particles were counted. Debris particles from a distilled water lubricated test were also collected and counted. 100 of these particles were counted. However due to the nature of the filtration process, it is likely that many of the smaller particles were lost and as such could not be counted.

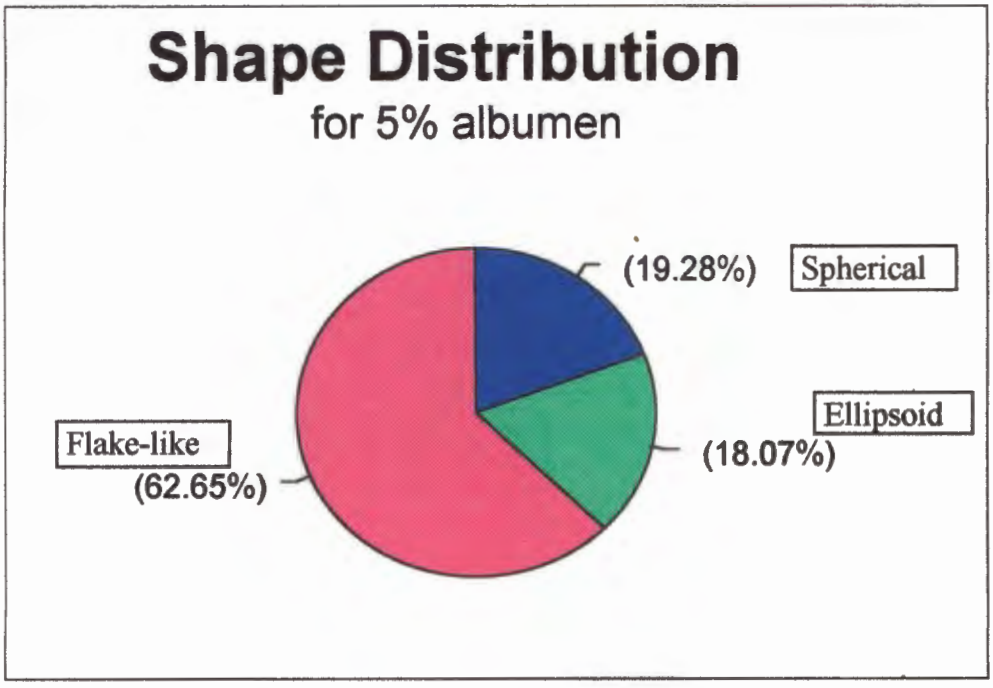

Figure 4.12 (I)

Most debris particles produced during sliding wear in 5 % albumen solution fell into the larger flake like category (63%). Smaller spherical particles could have been difficult to detect in the filter paper.

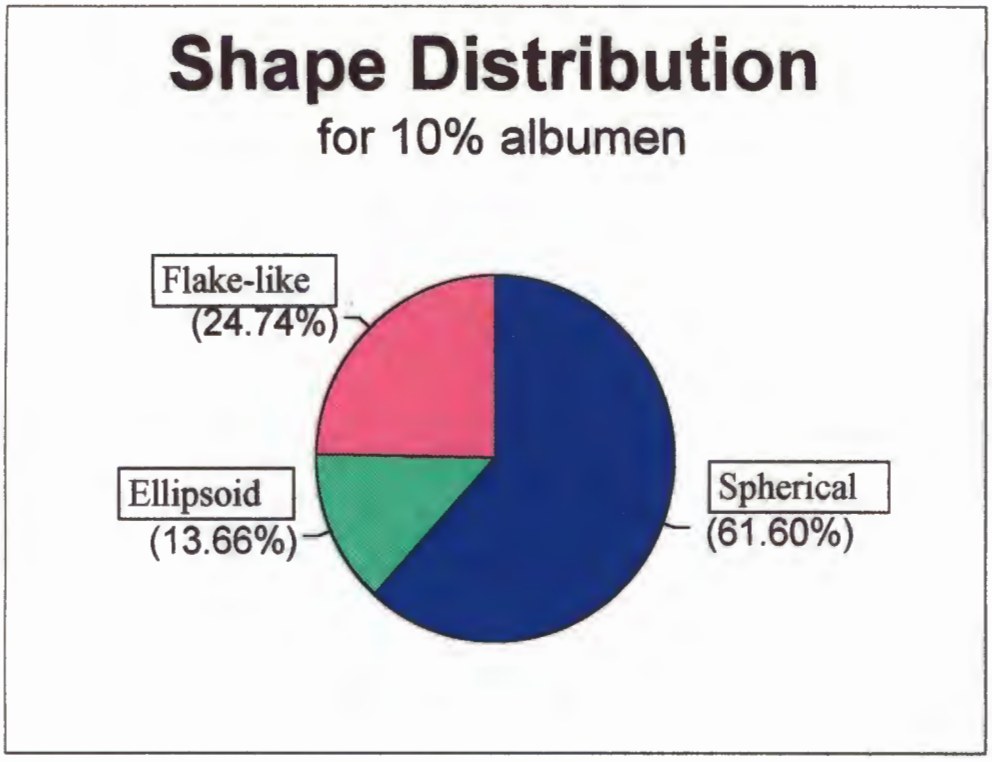

Figure 4.12 (II)

Most particles recovered from the 10% albumen solution were spherical in shape (62%) with a reduction in the number of flake-like particles to 25%.

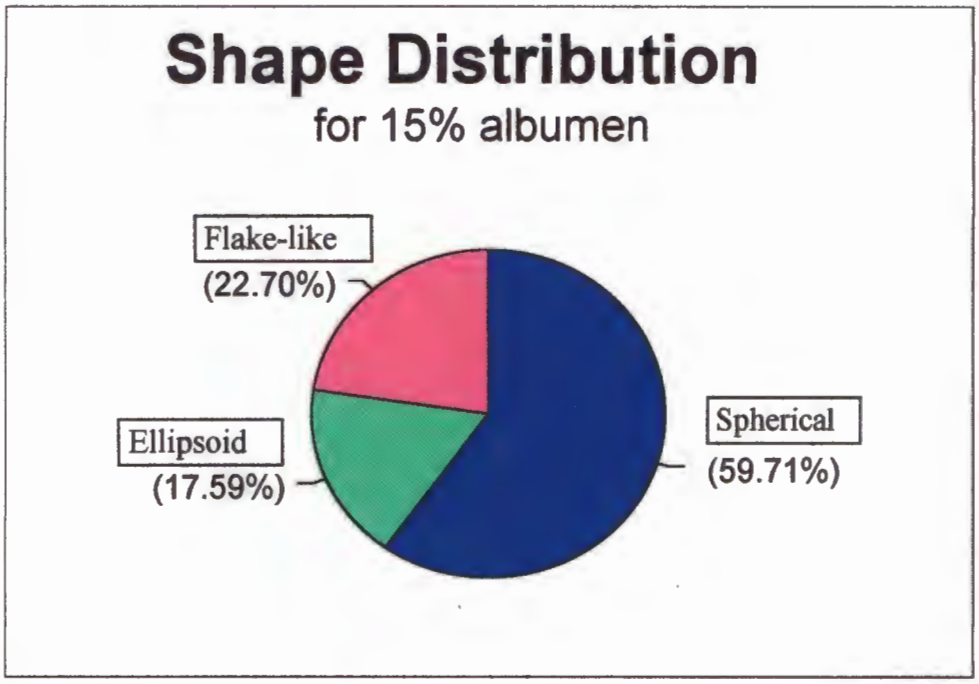

Figure 4.12 (III)

Most particles from the 15 % albumen solution were spherical in shape (60%), with the distribution for all particles being similar to that of the 10% albumen solution

4.6.3 Size Distribution Analysis of UHMWPE Wear Debris in Albumen Solutions

Particles photographed in the SEM were measured and plotted as pie charts in Figures 4.13 (I) - (X). The number of particles counted for each lubricating solution was determined by the area over which the particles were counted. For the distilled water lubricant 100 particles were counted, for the 5 % albumen solution 100 particles were counted, for the 10 % albumen 400 particles and for the 15 % albumen 500 particles.

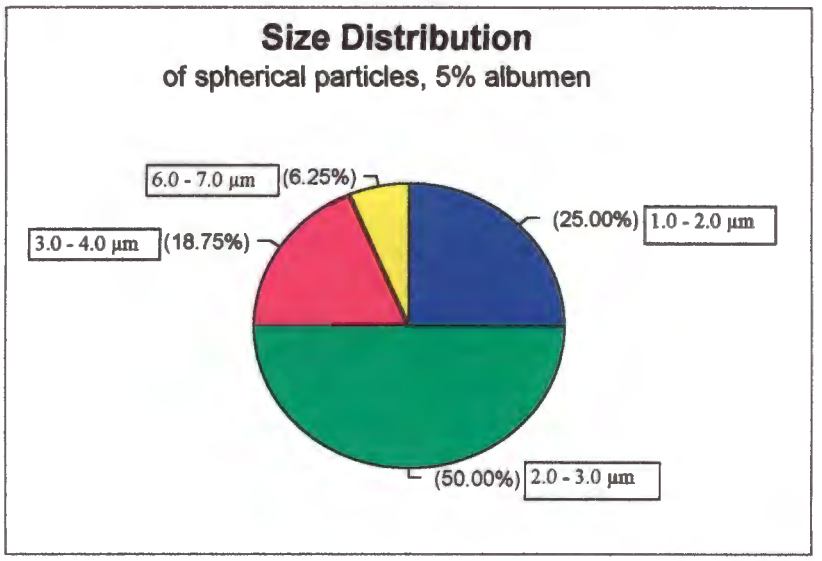

Figure 4.13 (I)

Figure 4.13 (I) illustrates that 75% of the spherical particles formed in the 5 % albumen solution fell between 1 and 3 µm

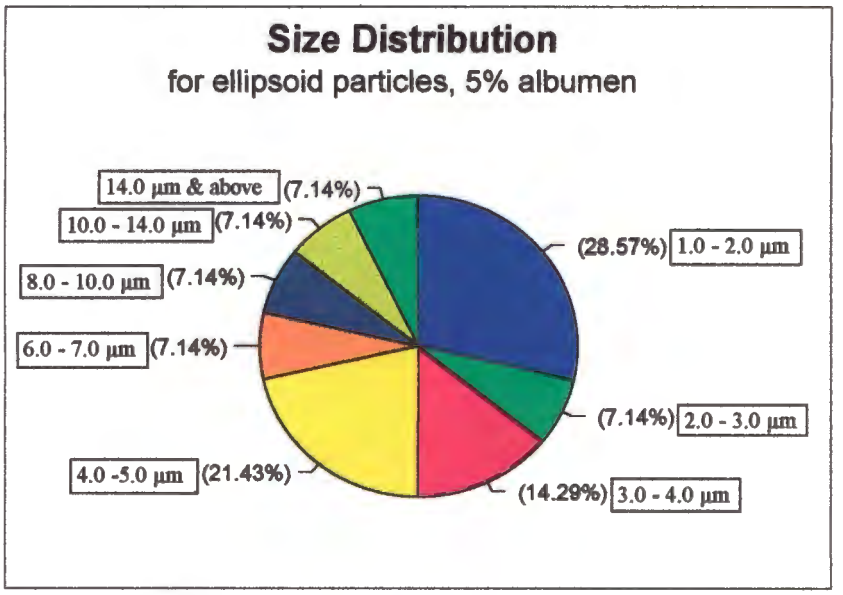

Figure 4.13 (II)

Figure 4.13 (II) shows that approximately 50% of the ellipsoid particles in the 5 % albumen solution fell below 4.0µm in size.

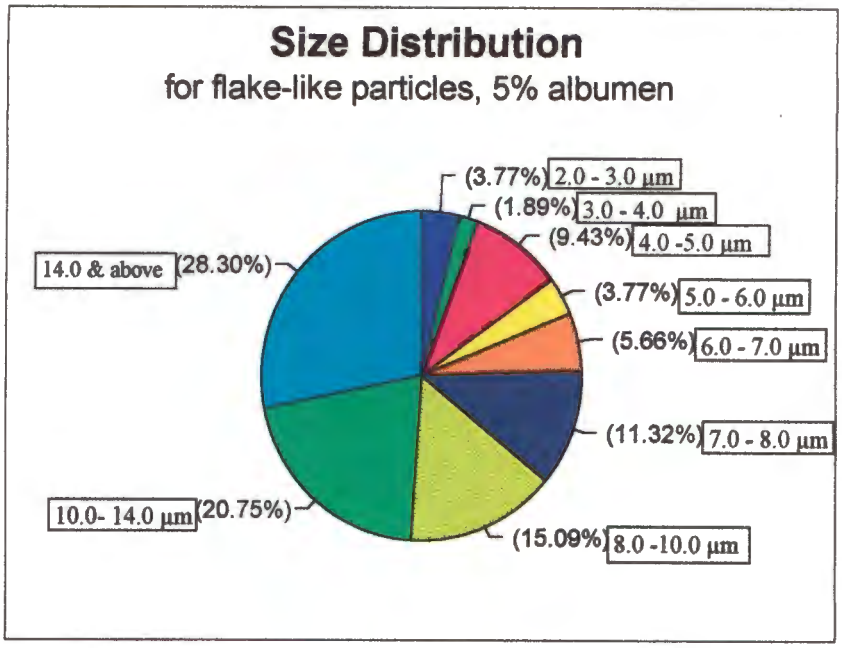

Figure 4.13 (III)

The flake-like particles were generally larger than those for the other shapes found in the 5 % albumen solution as seen in Figures 4.13 (I) and (II) A range of sizes was found with just over 50 % of the particles falling below 10µm.

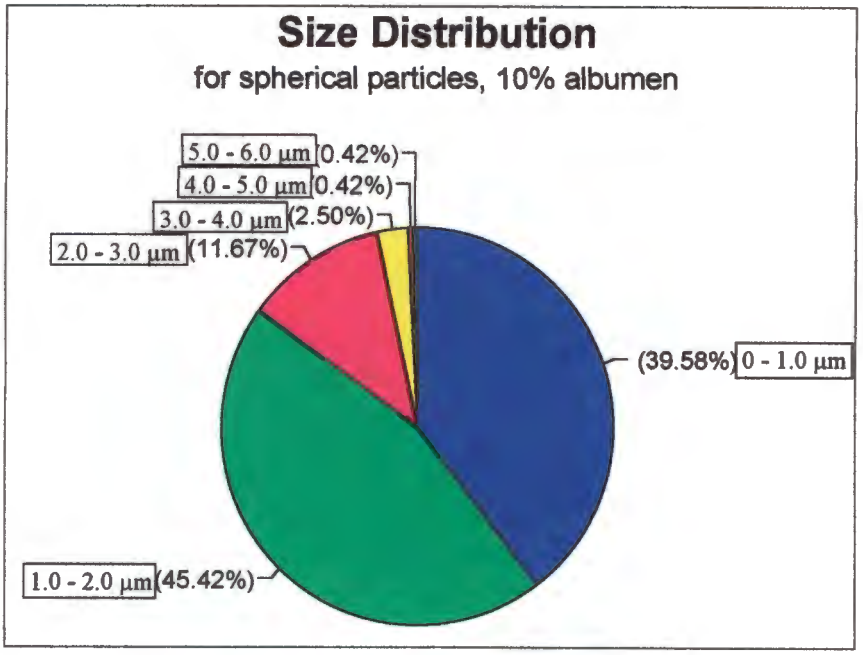

Figure 4.13 (IV)

From Figure 4.13 (IV) it can be seen that 85% of the spherical particles from tests conducted in 10 % albumen fell below 2.0µm in size.

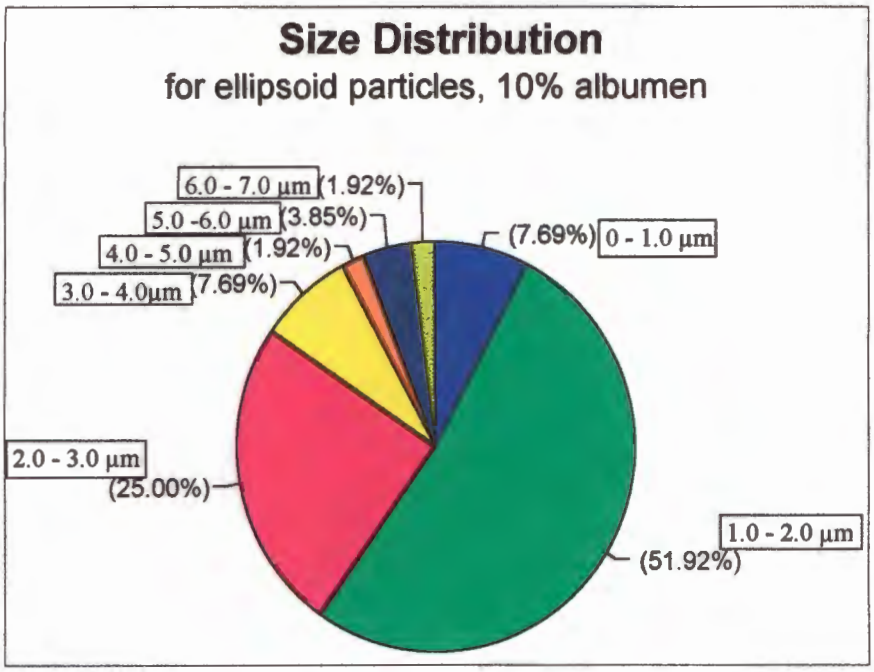

Figure 4.13 (V)

60% of the ellipsoid particles recovered from the 10 % albumen lubricated sliding wear tests fell below 2.0µm as seen in Figure 4.13 (V).

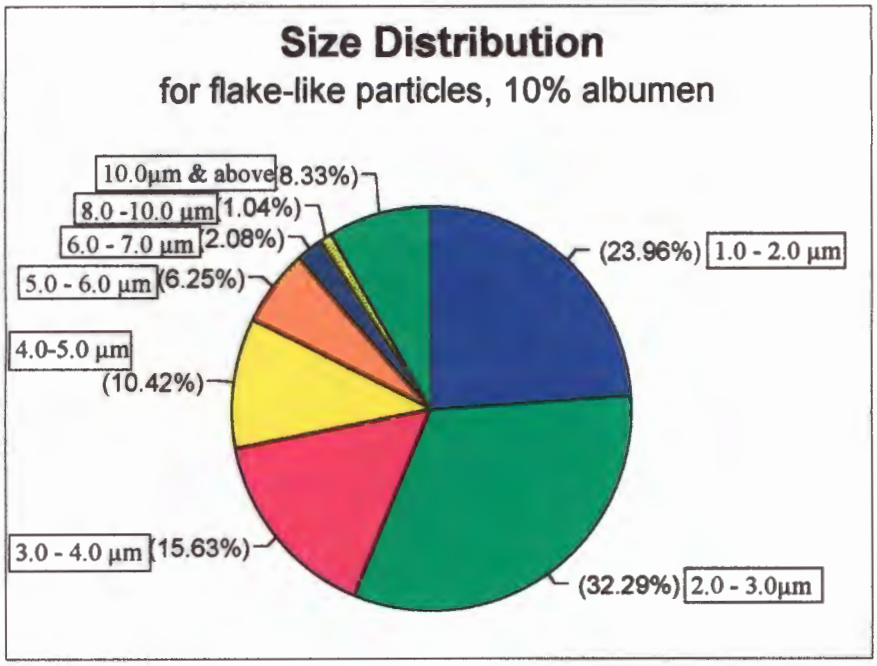

Figure 4.13 (VI)

From figure 4.13 (VI) it can be seen that for the 10 % albumen lubricated wear tests, 55% of the flake-like particles fell below 3.0µm

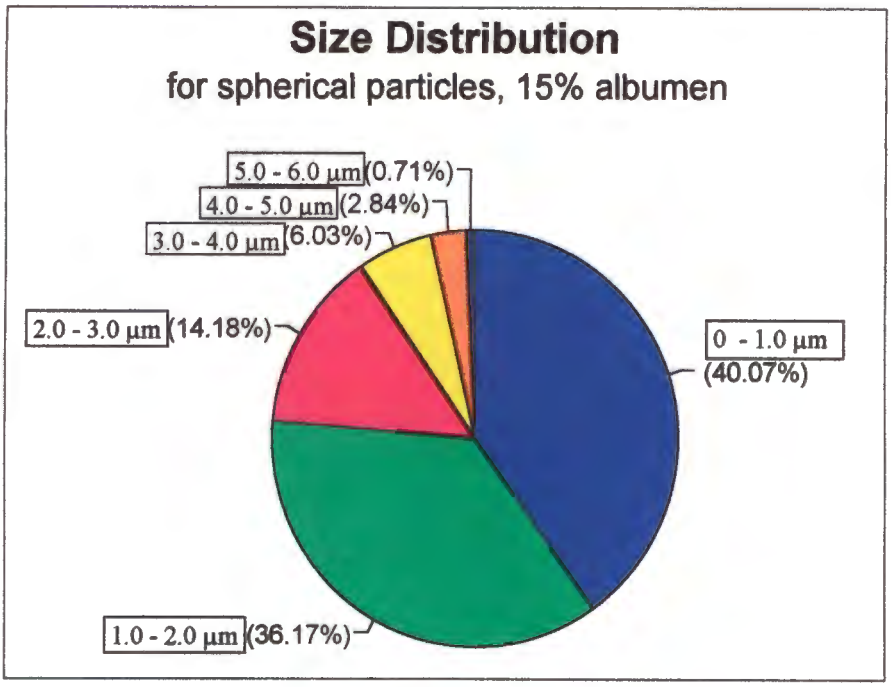

Figure 4.13 (VII)

76% of the spherical particles from the 15 % albumen tests fell below 2.0µm as shown in Figure 4.13 (VII).

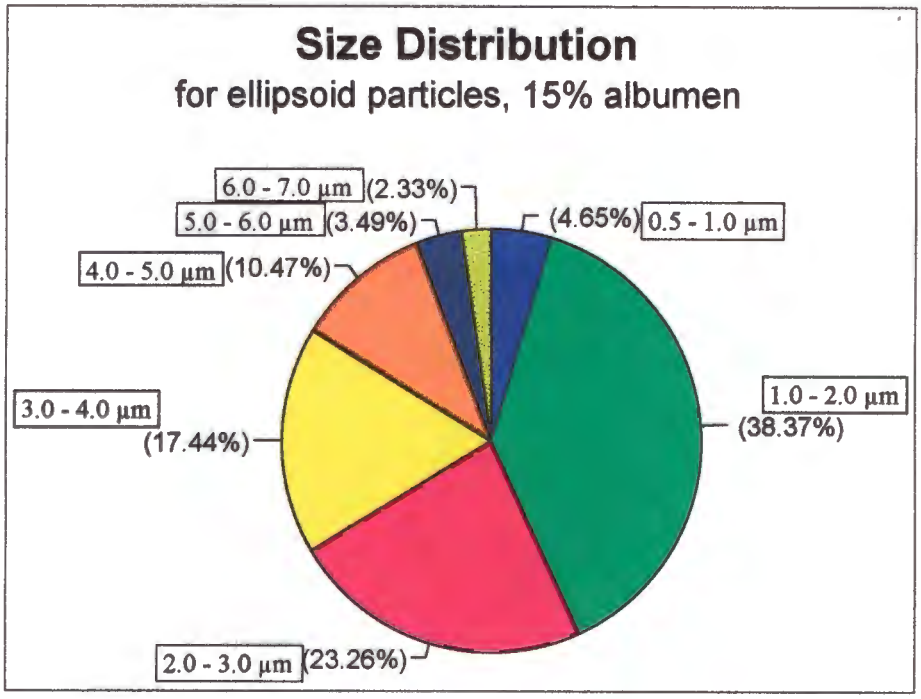

Figure 4.13 (VII)

66% of the debris ellipsoid particles fell below 3.0µm for testing in the 15 % albumen solution which is similar to that of 60% for the ellipsoid debris particles in the 10 % albumen solution.

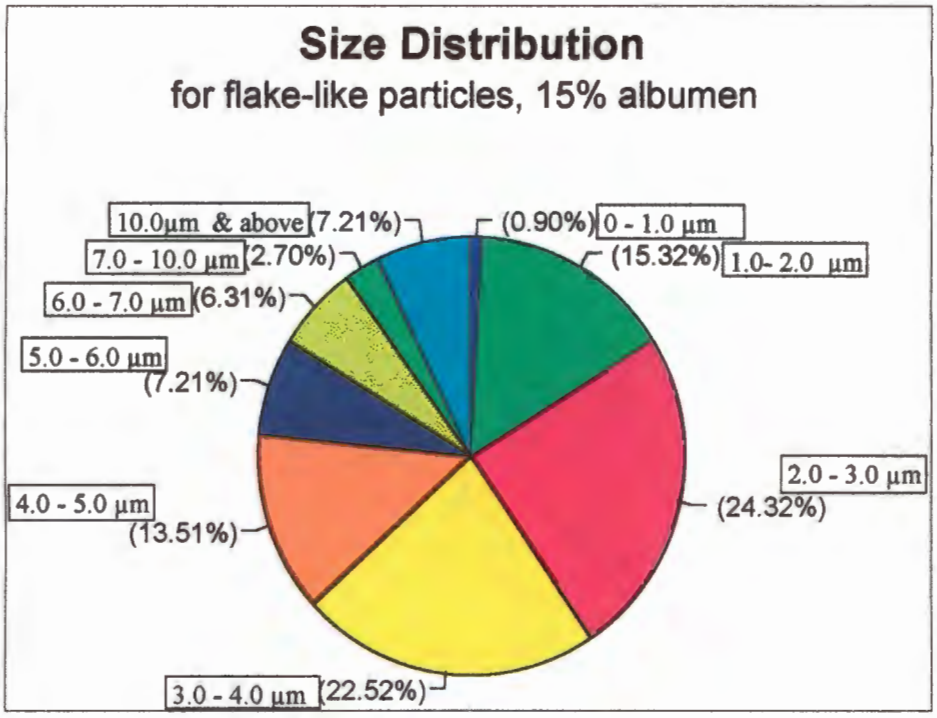

Figure 4.13 (IX)

62% of the flake-like particles produced during the sliding wear tests conducted in the 15 % albumen solution fell below 4.0µm as shown in Figure 4.13 (IX).

In the debris collected from the distilled water lubricated wear tests, the large majority of the particles were found to be flake-like in shape. The average particle size was generally much larger than those found for the protein lubricated wear tests. As the particles were larger, it was easier to discern the particle morphology.

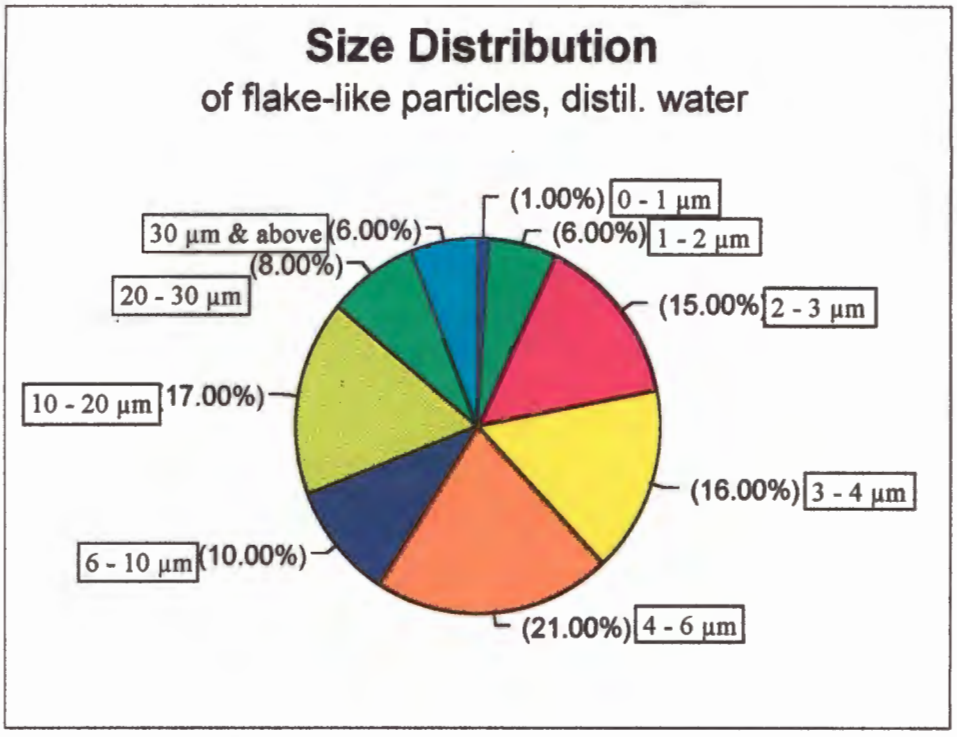

Figure 4.13 (X)

The debris particles collected from the distilled water lubricated tests were generally larger than those collected for the protein lubricated tests, with only 37% of the flake-like particles falling below 4µm compared with 62 % of the polygonal particles falling below 4µm for the 15 % albumen lubricated test.

CHAPTER 5

DISCUSSION

5.1 Introduction

The tribological behaviour of a wear system is influenced by various factors. These include the counterface roughness, the bearing pressure and the lubricating medium. The wear behaviour of prosthetic joints is also influenced by all these factors. In order to understand and accurately predict the wear behaviour of a prosthesis, it is necessary to generate test conditions which approximate those that the prosthesis will undergo in the body.

An attempt has been made in this work to simulate conditions similar to those in the physiological environment by conducting sliding wear tests of UHMWPE against ceramic counterfaces in lubricating media containing proteins. The wear behaviour of UHMWPE in these environments is compared to similar couples in alternative lubricating media.

5.2 Friction and Wear Behaviour of UHMWPE

5.2.1 Saline Lubricated Sliding Wear

Tests were conducted using UHMWPE sliding against zirconia counterfaces with a surface roughness (R_a) 0.01μm in a saline environment. There was an incubation period of about 5 km before any measurable wear took place. The wear rate then remained steady at 2.13 x 10^{-6} mm^3/Nm until approximately 40km at which point the wear rate decreased slightly. This initial wear rate was significantly higher than that for any of the other lubricants used. This was attributed to the fact that iron oxide (rust) was observed in the wear apparatus and which was thought to be acting as a third body, thereby increasing the volume loss of the UHMWPE. It is believed that the reduction in wear rate at 40km was a result of the formation of a polymer transfer film on the surface of the zirconia counterface. This transfer layer was observed to be coherent in most regions across the wear track.

The measured counterface roughness, R_a, was found to increase to a value of 0.2μm at 30 km after which there was a general reduction in R_a, albeit with some scatter of results. This scatter can be attributed to the fact that the transfer layer was not completely coherent across the surface and that shear of UHMWPE was occurring from parts of the surface of the transfer layer. As the wear process was clearly affected by the presence of the corrosion products, further analysis of the results of the saline solution lubricated tests was abandoned.

5.2.2 Water Lubricated Sliding Wear

Tests were conducted using UHMWPE sliding against zirconia ceramic surfaces with a counterface roughness, R_a of 0.01μm in a distilled water environment. The volume loss for the water lubricated wear tests showed an incubation period of 'no wear' for approximately 10 km after which the wear rate was steady at 1.85 x 10^{-7} mm^3/Nm. During the incubation period, when little or no polymer is lost from the UHMWPE surface, there is a build up of plastic strain and orientation of the polymer chains in the interfacial layers. This is associated with the formation of a fibrous structure [26] and a twinning process [31, 117]. The evidence of subsurface deformation seen in the

micrographs of sections of the UHMWPE pins viewed using polarised light (Figures 4.7) supports this. The scratch tests showed that the top layer on the UHMWPE surface had altered in nature and become harder as a result of the sliding wear process.

When the plastic limit of the polymer surface layers was reached, there was an onset of wear during which parts of the highly stressed, oriented surface layers are sheared and lost in the form of sheets which then exposed the underlying material. This sheared material was then lost in the form of debris, transferred to the ceramic surface or back transferred to other regions on the polymer surface. Most of the material sheared from the UHMWPE surfaces was eventually lost from the edges of the wear pins. Cooper et al. [1] contended that the wear mechanism for UHMWPE sliding against a smooth counterface is one of "macroscopic asperity wear". This wear mechanism occurs when the asperities on the surface of the polymer pin are up to 100 times larger than those on the counterface. When a load is applied the polymer asperities deform and surface and subsurface deformation is built up during continuous sliding as a result of the applied load. This process continues until the plastic limit of the polymer is reached and the flattened peak is removed. The incubation period followed by a period of wear taking place by shearing from the polymeric surface was considered to confirm that macroscopic asperity wear was taking place. Shear was taking place on the surface of the UHMWPE pins, which is in agreement with Wang et al. [78] who found that the maximum shear stress in total hip replacements (THR's) occurs at the surface of the UHMWPE component. This shearing of polymer material from the pin surfaces is likely to occur at highly stressed regions at the surface. There is evidence that, in addition to this mode of material removal, polymer material on the surface layer was removed by a gradual pulling apart of the highly oriented surface layer. This is illustrated in Figure 5.2.1 where it appears that fibrous UHMWPE material is pulled apart from the region indicated in the micrograph. This irregular material is then pushed together again on the reciprocal cycle. This occurs until such time as the polymer material shears from the deforming region.

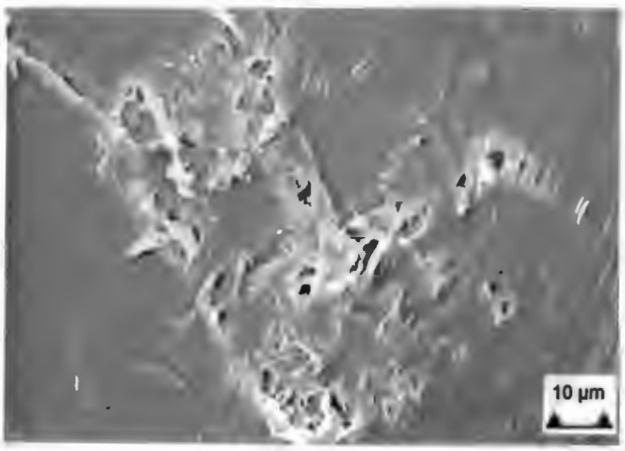

Figure 5.1 UHMWPE surface run to 100km in distilled water

It was clear that there was some transfer of UHMWPE to the ceramic counterfaces, but this transfer was not coherent across the surface. UHMWPE transferred to the zirconia surface in a very irregular manner which is a function of the roughness of the zirconia surface. That is, the smoother the counterface, the less able is the UHMWPE to adhere between the asperities on the counterface surface. For rougher counterfaces adhesion of UHMWPE to the ceramic surface results in a progressive build up of a transfer layer which was irregular in nature.

The transfer of UHMWPE to the surface of the ceramic is accompanied by an increase in counterface roughness from 0.01µm to 0.09µm. This was followed by a general decrease in counterface roughness (R_a) to 0.02µm at 50km of sliding distance. This decrease in counterface roughness can be attributed to the fact that the particles that were transferred to the ceramic surface become increasingly uniform in thickness as a result of the reciprocating sliding contact. The scatter that was observed for the surface roughness measurements is caused by the loss of polymer from the counterface which results in a less uniform surface layer.

5.2.2.1 The Effect of Changing the Counterface on Wear Rates

The average wear rate for UHMWPE sliding against zirconia and alumina ceramics in this work were found to be 1.85×10^{-7} mm^3/Nm and 2.67×10^{-7} mm^3/Nm respectively. compared to results obtained by Saikko [121] of $k = 2.6 \times 10^{-9}$ mm^3/Nm for UHMWPE sliding against zirconia (with an R_a value of 0.005 µm) and k

$= 3.3 \times 10^{-9}$ mm^3/Nm for UHMWPE sliding against alumina (with an R_a value of 0.005μm). The wear of UHMWPE against alumina and zirconia at similar R_a values (0.02μm on all counterfaces) has been investigated by Kumar et al. [122] and results were as follows

: for zirconia against UHMWPE in distilled water $k = 3.8 \times 10^{-8}$ mm^3/Nm

: for alumina against UHMPWE in distilled water $k = 6.8 \times 10^{-8}$ mm^3/Nm

In this work the improved wear behaviour of zirconia when compared to alumina can be attributed principally to the differences in surface roughness. Zirconia has a finer grain size than alumina which allows a better surface finish which has been shown to reduce wear [115]. Alumina is susceptible to grain pull-out during the polishing process and thus highly polished surfaces tend to be associated with porosity on the surface of the alumina ceramic as can be seen in Figure 4.9 (II). This porosity has an adverse effect on the wear process in that polymer tends to fill these pores. The porosity also effectively prevents a good surface finish equivalent to that of the zirconia from being achieved. In this work the best surface finish that was obtained on zirconia was 0.01μm whilst that on alumina was 0.04μm.

5.2.2.2 The Effect of Changing the Counterface on the Coefficient of Friction

For both the zirconia and the alumina counterfaces, the friction coefficient decreased as sliding distance increased and then stabilised at a sliding distance of 40 km. For the alumina ceramic the coefficient of friction varied from a high of 0.17 to a low of 0.07. The coefficient of friction of the zirconia ceramic varied from a high of 0.14 to a low of 0.03. These results are similar to those of Saikko [121] who obtained a high of 0.2 and a low of 0.06 for the alumina ceramic and a high of 0.2 and a low of 0.05 for the zirconia ceramic. It is likely that the reduction of coefficient of friction is a result of the flattening of any UHMWPE particles which have been transferred to the ceramic surface. Transferred particles are thought to be forced against the ceramic surface and smeared across the counterface during sliding and in so doing become more adherent to the surface. This effect can be seen in Figure 4.9 (II). Effectively the surface area over which sliding is being conducted is not only changed but is reduced, leading to a decrease in the coefficient of friction.

5.2.3 Protein Lubricated Sliding Wear

The addition of a protein containing lubricant was found to lower the wear rates of the UHMWPE sliding against zirconia ceramic surfaces compared to those obtained for both the saline and distilled water lubricated sliding wear. The average wear rates in mm^3/Nm for the various protein solutions are as follows:

Table 5.1 *Wear Rates if UHMWPE against PSZ (R_a = 0.01μm) in Various Lubricating Solutions*

Lubricant	Counterface Roughness , R_a (μm)	Wear Rate (initial) (mm^3/Nm)	Wear Rate (final) (mm^3/Nm)
Saline Solution	0.01	2.13×10^{-6}	3.2×10^{-7}
Distilled Water	0.01	1.85×10^{-7}	
5 % Synovial Fluid	0.01	8.3×10^{-8}	1.71×10^{-8}
5 % Albumen	0.01	3.2×10^{-8}	3.8×10^{-7}
10 % Albumen	0.01	6.0×10^{-8}	2.5×10^{-7}
15 % Albumen	0.01	-	-

These results can be compared with the results obtained by Kumar et al. [122] which were for alumina, zirconia and stainless steel with similar R_a values (0.02μm) lubricated by bovine serum and are as follows:

- zirconia in bovine serum $k = 5.6 \times 10^{-8}$ mm^3/Nm
- alumina in bovine serum $k = 1.01 \times 10^{-7}$ mm^3/Nm

Fisher et al [115] obtained a wear rate of 9×10^{-9} mm^3/Nm for UHMWPE sliding against stainless steel lubricated by bovine serum. Clearly the addition of a protein solution aids in lowering the wear rate of UHMWPE in reciprocating sliding contact.

5.2.3.1 Transfer Layer Formation

There was varying transfer of polymer to the ceramic counterface during the distilled water lubricated tests. Polymer transfer was irregular and transferred particles tended to act as sites for further adhesion. Furthermore, there was a progressive flattening of the polymer particles on the surface as can be seen in Figure 4.9 (XII). However it is

clear that the transfer of UHMPWE to the zirconia and alumina surfaces during the protein lubricated tests is different to that found in the distilled water lubricated tests as seen in Figure 4.9.

It seems likely that there was some transfer or adsorption of the protein onto the ceramic surface. The high nitrogen content obtained in the XPS analysis on the unworn soaked zirconia sample, when compared with that of the worn sample run in distilled water, is an indication that there is some protein being adsorbed onto the ceramic surface. For the unworn and the distilled water lubricated specimens no nitrogen double peak was detected. This nitrogen double peak was considered to be an indication that protein had been adsorbed onto the surface of the zirconia counterfaces. The absence of this double peak in the unworn soaked specimen indicates the possibility that the adsorbed protein on the ceramic surface undergoes some reaction under pressure which allows it to be adsorbed onto the zirconia surface. i.e. the high pressure on the protein lubricant may cause it to be more susceptible to adsorption onto the counterface surface. The high carbon content on the zirconia sample which was run in synovial fluid is an indication that both protein and polymer are being transferred to the ceramic surface. A high nitrogen content was not mirrored in the synovial fluid lubricated sample as there is less nitrogen in synovial fluid than there is present in albumen. Furthermore the nitrogen in the synovial fluid is part of an NH^{-} group and it is likely that this is the cause of the double peak observed in the XPS traces of the wear scar of the zirconia ceramic run in synovial fluid solution as reported in Table 4.2 (III) . Thus it is clear that there is some interaction with the protein and the ceramic counterface which results in the protein being laid down on the surface of the counterface.

The electron micrographs of the wear scars showed that the way in which the polymer was transferred to the surface in protein lubricated test differed to that shown in the distilled water lubricated tests. In the 5% albumen solution it appears that the polymer stringers visible in the fibrous sheared layers on the pin surfaces have been transferred and rolled up on the ceramic surface as is visible in Figure 4.9 (VI). It is likely that these particles then flatten to take on the morphology seen in Figure 4.9

(IV) for the synovial fluid lubricant. The flattened particles on the zirconia surfaces of the 5 % albumen lubricated samples were similar to those on the 5 % synovial fluid lubricated samples. There was very little transfer observed on the surface of the ceramic counterfaces that were lubricated in the 10% and 15% albumen solutions. Furthermore the material that was transferred to the surface of these ceramics was generally smaller and finer than that observed for the 5% albumen and the 5 % synovial fluid solutions. There is thus an indication that increasing the protein content of the lubricating solution decreases the size of the particles that are transferred to the surface.

5.2.3.2 UHMWPE Behaviour

UHMWPE pins that were subjected to reciprocating sliding wear in protein solutions, when observed in the SEM showed a change in behaviour to those pins that were worn in distilled water. Two types of behaviour were observed. Firstly material loss by shear from the pin surface in manner similar to that observed for distilled water lubricated tests. Prolonged sliding causes deformation of the polymer asperities resulting in a uniformity of surface. The deformation of asperities results in a build up of surface and subsurface strained regions by means of a strain accumulation process. The top surface of the pins is uniform and observed to have undergone an orientation change due to sliding in that the polymer chains are oriented in the direction of sliding. Shear thus occurs at the interface of the strained and unstrained regions.

The polymer materials subjected to protein solution lubrication were associated with a second type of behaviour. Protein lubrication affected the way in which the UHMWPE was removed from the pin surfaces. Small individual stringers could be observed on all the UHMWPE pins surfaces for the protein lubricated tests. There appears to be some form of molecular breakdown of the UHMWPE surface when interacting with the protein solutions. Noinville et al. [37] reported that the nonuniform distribution of charged amino acids in the three-dimensional structure will produce patches that will control the adsorption behaviour of proteins onto synthetic polymeric surfaces. It is therefore possible that in these regions adsorption of proteins occurs into the UHMWPE surface which is resulting in some form of

localised attack thereby resulting in weakening of the surface layers, cracking and the preferential removal of regions of the UHMWPE surface. It is also possible that the presence of voids in the amorphous regions as observed in oriented HDPE films assists this process. This theory is supported by the fact that cracking and ridging as seen in Figure 5.2 have been observed in retrieved worn acetabular cups as seen in Figures 5.3 and 5.4

Figure 5.2 SEM micrograph of UHMWPE surface run to 35 km in 5% albumen

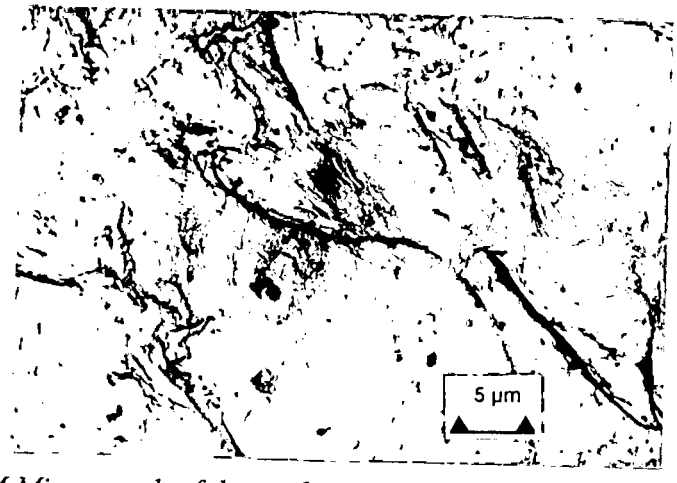

Figure 5.3 TEM Micrograph of the surface of a worn acetabular cup [after 124]

Figure 5.4 TEM Micrograph of a worn acetabular cup (different patient to 5.3.2) [after 124]

Another feature of the protein lubricated tests was the fact that the stringers and sheared areas appear to remain adherent on the UHMWPE pin surface. Material sheared from the pins run in distilled water was generally lost from the pin surfaces. In addition to this, back transfer of polymer from the counterface surfaces to the pin surfaces was observed only in the distilled water lubricated tests. It can therefore be concluded that the presence of proteins causes an alteration in the way in which the polymer wears. This occurs in two ways, by affecting the operative wear mechanisms and by reducing the likelihood of a sheared polymer layer being removed immediately. At increased sliding distances, the UHMWPE that sheared from the surface of the polymer pins run in the protein solutions and readhered to the pin surface is eventually removed as the strain accumulation process overcomes the adhesive effect of the proteins and removes these sheared regions. Furthermore the onset of cracking is observed at these increased sliding distances. This cracking is a result of the polymer surface interacting with the proteins in solution and is most prevalent at sliding distances in excess of 30km and the cracking effect is more widespread for increasing albumen contents. Cracking of the polymer surface also contributes to the increase in wear as it precedes shear from the pin surface. Thus for increased cracking of the surface one would expect increased shear from the surface. This would then be associated with increased polymer loss and an increase in wear rates.

5.2.3.3 The Effect of Changing Counterface Roughness

The wear rates of the UHMWPE pins sliding against counterface surfaces with R_a values of 0.06μm tested in the 10 and 15 % albumen solutions were low and remained relatively constant. These wear rates were comparable with those obtained for distilled water lubricated tests with counterface roughness values R_a of 0.01μm and also with the final wear rates obtained for the UHMWPE pins tested in the albumen solutions against counterfaces with surface roughness values of 0.01μm.

Increasing the counterface roughness for the distilled water , 10% and 15% albumen lubricated wear tests increased the wear rates (given in mm^3/Nm) as follows:

Table 5.2 Wear Rates if UHMWPE against PSZ of R_a 0.01μm and 0.06μm

Lubricant	Counterface Roughness , R_a (μm)	Wear Rate (initial) (mm^3/Nm)	Wear Rate (final) (mm^3/Nm)
Saline Solution	0.01	2.13×10^{-6}	3.2×10^{-7}
Distilled Water	0.06	6.25×10^{-7}	
10 % Albumen	0.06	2.0×10^{-7}	
15 % Albumen	0.06	5×10^{-8}	
Distilled Water	0.01	1.85×10^{-7}	
5 % Synovial Fluid	0.01	8.3×10^{-8}	1.71×10^{-8}
5 % Albumen	0.01	3.2×10^{-8}	3.8×10^{-7}
10 % Albumen	0.01	6.0×10^{-8}	2.5×10^{-7}
15 % Albumen	0.01	-	-

Increasing the counterface roughness had a significant effect on the manner in which polymer material was transferred to the ceramic counterface surfaces. Layered regions of UHMWPE were transferred to the counterfaces and the coarser particles were found to agglomerate and crack during the distilled water lubricated tests. The particles on the counterfaces run in the protein solutions resembled those run against smoother counterfaces in 5% albumen solution. These transferred particles were smaller and more uniform in thickness as shown for the 15% albumen lubricated sample seen in Figure 4.9 (XI). It is likely that the asperities on the rougher counterfaces trap the smaller UHMWPE particles and that these are then compressed against the counterface as a result of the ongoing sliding process. It is important to note that once again the transferred material in the tests lubricated by the 15% albumen solution was smaller and finer than that of the 10% albumen and the distilled water lubricated tests. This is an indication that increasing the protein content of the lubricating solution decreased the size of the polymer wear debris.

5.3 Production of Wear Debris

Wear debris particles generally came in two forms, that of large particles in excess of 10μm in size with visible surface corrugations, and that of smaller particles which were generally spherical or oval in shape. It is likely that the larger particles are directly lost by shear from the surface. The repeated reciprocating sliding against these shear areas results in a push-pull action against the shearing material which gives rise to the surface corrugations visible on the surface. The more prevalent smaller particles were probably produced by two sources. The larger debris particles may break down in the lubricating solution and the smaller sheared sections (particularly those present in the protein lubricated tests) removed from the polymer surface do not adhere to the counterface surfaces and are removed into the lubricating solutions.

It seems probable that the lack of smaller spherical particles in the distilled water and 5% albumen solutions, when compared to those that were found in the solutions of higher protein contents, can in part be attributed to the following: Firstly the nature of the protein lubricant tends to assist the filtration of the smaller particles. This is because viscous albumen, when filtered leaves a residue on the surface of the filter paper. Increasing the albumen content of the lubricant effectively increases the residue on the filter paper. This residue then acts to trap the smaller debris particles on the surface of the filter paper. Furthermore the debris removed from the UHMWPE surface in the 5% albumen lubricated test, was observed deposited on the ceramic surface.

The debris from the distilled water lubricated tests tended to be the larger corrugated particle type. This observation supports the view that different wear mechanisms occur in the protein lubricated systems and that the protein affects the size of the wear debris.

Generally the wear debris retrieved from the protein solutions was small with most particles falling between 0 and 7 μm in dimension. This supports the findings of Shanbhag et al. [3] for 11 failed Ti alloy THR's in which the polyethylene debris

particles were found to be generally spheroid in shape and varied from 0.1 to 2μm in mean dimension. Clusters of smaller particles were found varying from 0.2 to 0.3 μm wide and 10μm in length. These particles tended to be agglomerated in a mesh structure which varied from 50 to 80μm. Larger particles which resembled rolled plates were observed to be 20 to 200μm in length. Most of the debris particles were smaller than 1μm.

Lee et al. [82] observed that polymer debris from 30 cases of failed THR's were as follows:

	Dimension (μm)	
	Short	**Long**
Titanium alloy	41.±3.2	12.8±11.0
Co-Cr alloy	2.7±1.4	8.1±5.2
Stainless Steel	3.1±3.3	8.4±7.5

While Mckellop et al. [125] reported that most of the debris ranged from 0.2 - 8μm in size with the average being close to 1 or 2μm.

Thus the results obtained for the size distribution for the 10 and 15% albumen samples correlates quite well with those observed in the tissue surrounding failed THR's with particle size ranges from 0.5 to 14 μm and the average size falling between 1 and 2 μm. Differences between the average particle size *in vivo* and that obtained for the 5 % albumen lubricated test can largely be ascribed to the ineffectiveness of the 5% albumen solution so assist filtration of the lubricant. This resulted in smaller debris particles being far more difficult to identify on the filter paper surface. Furthermore it is interesting to note that the transferred UHMWPE particles on the zirconia counterface for the 5 % albumen lubricating solution are similar in morphology to those observed by Shanbhag et al.[3].

The higher albumen content in the lubricant tended to result in smaller wear debris. This is significant as it is the smaller debris particles (less than 7 μm) [92] which result in the bone resorption reaction in the tissue surrounding the prosthetic joint.

Increasing the protein content of the lubricating solution results in a greater tendency for molecular attack of the polymer surfaces, rather than material only being lost soley by shear as has been observed for the distilled water lubricated tests. The low wear rates for the increased protein content can be attributed to the fact that fibres, stringers and sheared regions tend to readhere to the polymer pin rather than being lost. The particles that are lost tend to be small (less than 2 μm) and large in number. It is clear that the presence of a protein in the lubricating media does affect the wear of UHMWPE.

It would appear that albumen can be used as a substitute lubricating solution for the investigation of prosthetic joint materials. The behaviour of the albumen was similar to that of synovial fluid and the wear rates obtained using the albumen solution were similar to that of the synovial fluid specimen. It should be noted that the albumen is different in composition to the synovial fluid and therefore results should be treated only as an approximation to the type of wear behaviour that can be expected in prosthetic limbs. Furthermore the load was static, a situation which is unlikely *in vivo*, and in this investigation the geometry of the hip joint has not been taken into account in this investigation.

CHAPTER 6

CONCLUSIONS

From the results obtained during this investigation the following general conclusions can be drawn:

Water Lubricated Sliding Wear

1. The wear mechanism which dominates water lubricated sliding wear of UHMWPE against a smooth ceramic surface is one of macroscopic asperity wear. During this process asperities on the surface of the UHMWPE pins are initially flattened during sliding resulting in a build up sub-surface deformation which is followed by shear of the UHMWPE surface layers when the plastic limit of the asperity peaks is reached.
2. The wear behaviour of UHMWPE sliding against ceramics is superior to that of UHMWPE sliding against metals and this can be attributed to the superior wettability of the ceramic surfaces which facilitates boundary lubrication.
3. The wear behaviour of zirconia is superior to that of alumina because the zirconia counterface has a lower surface roughness than that of the alumina samples.
4. The friction coefficient of the UHMWPE when sliding against alumina and zirconia materials decreases during sliding and stabilises at a low value. This behaviour is due to the presence of transferred material on the ceramic surfaces.
5. Increasing the surface roughness of the ceramic counterfaces results in an increase in wear due to the larger asperities on the ceramic counterface acting as cutting tools and removing larger amounts UHMWPE from the surface of the wear pin

Protein Lubricated Sliding Wear

1. Two mechanisms were found to contribute to polymer wear. Macroscopic asperity wear which results in similar behaviour to that observed in the distilled water lubricated wear, and that of chemical attack of the surface of the UHMWPE

which results in cracking and assists the removal of UHMWPE in the form of fine stringers which are fibrous in structure

2. Increasing the content of albumen in the lubricating solution resulted in a decrease in wear rate and an increase in the cracking of the pin surfaces. Increasing the protein content in the lubricant resulted in less transfer of polymer to the counterface surfaces. Furthermore, little UHMWPE debris was observed on the counterfaces for the samples run in the 10% and 15% albumen lubricant against counterfaces with R_a values of 0.01μm.
3. Increasing the counterface roughness resulted in higher wear rates, and UHMPWE particles were visible on the counterfaces for the 10% and 15% albumen lubricated tests. This can be attributed to the fact that the increased asperity height on the counterfaces causes UHMWPE debris to mechanically adhere to the surfaces. The size of the debris particles visible on the counterface was seen to be decreasing with increasing protein content.

Wear Debris

1. Increasing the protein content of the albumen solution leads to an decrease in the size of the debris generated and this debris does not adhere readily to the ceramic counterfaces for the 10% and 15% albumen solutions.
2. The difference in the average size and shape of the debris when comparing protein lubrication to that of distilled water, can be explained by the difference in the way in which polymer material is lost from the UHMWPE pin surfaces for the protein lubricated and distilled water lubricated testing.

Albumen Lubrication

1. It can be concluded that albumen can be used as a substitute for synovial fluid as a lubricating medium for the laboratory investigation of the behaviour of prosthetic implant material. However further research is necessary to establish the differences in behaviour of these two lubricants

APPENDIX A

OTHER MATERIALS USED FOR IMPLANTS

Prosthetic hip joints have been in use for about four decades. During this time substantial changes have taken place with regard to the materials used. The production of metal debris in metal on metal systems and the fairly high wear rates of the metal-UHMWPE systems has led to the use of new materials and combinations thereof. Alumina femoral heads articulating on UHMWPE acetabular cups show better wear behaviour than the original stainless steel implant systems but the production of UHMWPE wear debris is still a problem [75]. Alumina on alumina systems have excellent wear and tribological characteristics, but their high stiffness and brittle behaviour limits their usefulness [75]. Further advances have seen the development of commercially pure titanium (Ti), Co-Cr-Mo alloys and Ti-6Al-4V materials [75]. These systems are not perfect and exhibit one or more of the following: stress corrosion, production of wear debris, stress shearing of cortical bone and creep deformation. These all eventually result in the failure of the implant, although it may take many years to fail.

It is because of the limitations of the present systems that new materials have been developed. Many try to mimic the behaviour of cortical bone and most are ceramic based.

A.1 Particle Filled Materials

Particles usually behave isotropically and as they have a random distribution in the matrix of the particle filled materials, composites in this form usually behave isotropically. Particle filled composites are considered to be the most significant of the new composite materials and are beyond the experimental stages and are widely used in practice. Generally matrices of polyethylene with either hyroxyapatite (HA) or calcium phosphate fillers are used for bone substitution applications [121].

A.2 Fibre Reinforced Materials

Fibres in contrast to particles are anisotropic in nature and a composite will behave anisotropically if fibres are oriented in its matrix. The degree to which the composite

will be anisotropic is dependent on the degree of orientation and fibre length. Medically, carbon fibre reinforced polymers are most common. This can be attributed to their high strength and good biocompatibility [121].

(i) Short Fibres

The addition of short fobres produces a strengthening effect which is significant, but is insufficient for high load bearing applications. In joint replacement surgery these materials are used for sliding components. The matrix is either UHMWPE or Triazen (a special cynate resin) with carbon fibres. This type of material is especially useful for acetabular cups. The stiffer cup may improve the biomechanical situation while the slower creep will extend the lifetime. A reduction in wear may also result from the lubricating effect of the carbon . The principal disadvantage of these materials is that changes in shape can only be made by machining. This is overcome using thermoplastics such as polysulphone (PSU), polyethersulphone (PES) and polyimid (PI) which have already been shown to be biocompatible. These thermoplastics can be deformed by heating (this is useful during surgery) [121].

Table A.1 Table of the Applications of Short Fibre Reinforced Composites[121]

Application	Fibre	Matrix	Aim
Bone cement	Glass or carbon	PMMA	Increase in strength; reduction of creep
Dental	Glass Carbon	PMMA Epoxy	Same as above ; reduction of shrinkage
Joint replacements (sliding parts)	Carbon Carbon	UHMWPE or Triazin PSU , PES or PI	Increase in stiffness; reduction of wear and creep Increase in strength and stiffness

(ii) Long Fibres

These composites are important for high load bearing applications such as those required of orthopaedic implants. Generally carbon fibres are used to reinforce various polymers. Using composites allows for a variation in stiffness by altering fibre density and orientation. The resulting composite is similar in nature to cortical bone. Whether this is advantageous for prostheses is not yet clear. These materials do however exhibit distinct fatigue under cyclic loads and the thermosetting matrix polymers are susceptible to water sorption and ageing. (Thermoplastics mentioned do not appear to be sensitive to these problems)

Table A.2 Table of Applications of Long Fibre Reinforced Composites [121]

Application	Fibre	Matrix	Aim
Dental Implants	Carbon	Epoxy, PSU or PMMA	Increase in strength; "biomedical adaptation"
Joint Replacement	Carbon (glass)	Epoxy, PSU, PMMA or Triazin	Same as above
Fracture Stabilization	Carbon	Epoxy, PSU or other	Same as above

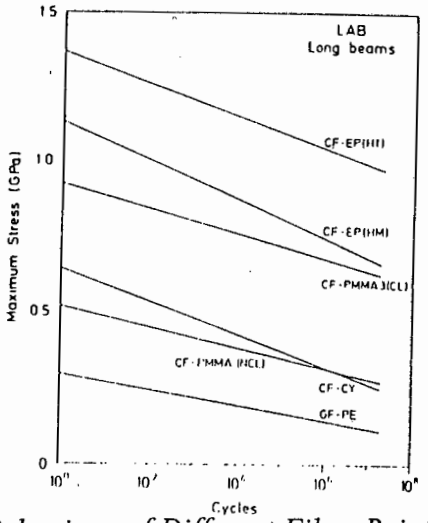

Figure A.3 *Fatigue Behaviour of Different Fibre-Reinforced Polymers "CF": carbon fibre, "EP":epoxy, "GF":glass fibre, "PMMA":acrylate, "CY":cyanate, "PE":polyethylene* [121].

A.3 Ceramic Fibre Reinforced Ceramics

At present only carbon-carbon materials are used in the medical field because of their excellent biocompatibility. Other structural ceramics include alumina and silicon carbide reinforced by carbon or silicon carbide fibres. This results in a less anisotropic material than their carbon-carbon counterparts.

All these materials are still widely experimental and biostability and biocompatibility as well as long term behaviour are not well estabiished.

A.4 Hydroxyapatite-reinforced Polyethylene

None of the materials in currently in use for prosthetic joints mimic the behaviour of cortical bone, as a result there are often problems with stress transfer across the tissue-implant interface. In the case of stiff materials such as alumina this often leads to stress shielding of the cortical bone. The hydroxyapatite (HA) reinforced PE (developed at Queen Mary College in collaboration with Brunnel University) seeks to overcome this problem [63]. Mature cortical bone has a stiffness of 7-25GPa, a critical stress intensity K_{IC} of 2-12 $MNm^{-3/2}$ and a critical strain intensity of 600-5 000 Jm^{-2}. The bone is a biological composite of HA reinforced collagen (of which HA constitutes the osteonal lamellae and provides a brittle ceramic filler - about 0.5 volume fraction) dispersed in a compliant matrix [63]. Polyethylene has been extensively used as a biomaterial and has been established as biostable. HA is calcined bone ash and as such is also biocompatible. No coupling agents are used and thus this composite was expected to be biostable. The HA-reinforced polyethylene showed zero response to cytotoxicity tests in human embryonic lung tissue and, implanted in adult rabbits for up to 6 months showed no adverse results. Furthermore a secure bond between the natural tissue and the synthetic material was created and this ensured a more stable implant. However further laboratory and clinical trails are necessary to determine whether the HA coating will be replaced by bone or fibrous tissue and if the enhancement coating (HA) may become a source of particulate debris itself [63].

Hydroxyapatite Volume Fraction	Young's Modulus (GNm^{-2})	Strain to Fracture (%)	Fracture Mode	Bioactivity[a]
0	1.3 ± 0.2	> 90	Ductile	x
10	1.4 ± 0.2	79 ± 10	Ductile	?
20	2.0 ± 0.1	50 ± 4	Ductile	?
25	2.5 ± 0.2	43 ± 3	Ductile	?
30	3.0 ± 0.2	34 ± 5	Ductile	?
35	3.7 ± 0.4	32 ± 8	Ductile	?
40	4.4 ± 0.7	29 ± 5	Ductile	√
45	5.9 ± 0.5	7 ± 3	Brittle[b]	?
50	7.7 ± 1.3	3 ± 1	Brittle[c]	√

[a]Bone apposition around implant.
[b]K_{IC} = 2.9 ± 0.3 $MNm^{-3/2}$
[c]K_{IC} = 2.4 ± 0.2 $MNm^{-3/2}$

Figure A.4 *The Effect of Varying the Volume Fraction of HA* [63]

A.5 Carbon Composite Ceramics

Carbon fibre (CF) reinforced silicon carbide (SiC) is under investigation for hip joint replacement materials due to its biological and mechanical stability. Materials are made with CF reinforcement infiltrated with silicon resulting in SiC deposition. Lab tests have shown low wear rates and coefficients of friction in the range of 0.1. Using hip and knee joint simulators it was determined that the CFSiC-CFSiC bearing components are unsuitable because of high wear rates. CFSiC appears to be acceptable for use as hip stems. Biocompatibility has already been established [66].

A.6 Boroaluminosilicate Ceramics

Synthetic mica is crystallised in a boroaluminosilicate glass matrix to form this material. It has good wear properties but biocompatibilty and biostability are yet to be established [66].

A.7 Silicon, Aluminium Nitride and Aluminium Oxide (SIALON)

This is made of hot-pressed silicon nitride, aluminium nitride and aluminium oxide. It has adequate friction and wear properties but still requires investigation as to its biocompatibilty and biofunctionality [66].

Appendix B

Amino Acids

Amino acids are the monomer units of proteins, i.e. all proteins are made up of a number of amino acids in varying combinations. The general structure of an amino acid is that of an amino group and a carboxyl group bonded to the same carbon atom. The nature of the side chains, referred to as R groups is the basis of the difference between various amino acids. With the exception of glycine, amino acids can exist in two forms. These are designated L and D and are stereoisomers i.e. non-superimosable mirror images. The amino acids found in proteins are all of the L form. Amino acids are classified by the nature of the side chain, most importantly whether the chains are polar or non-polar and the presence of an acidic or basic group on the side chain [106]. Individual amino acids can be linked together by the formation of covalent bonds. The bond is formed between the α-carboxyl group of one amino acid and the α-amino group of the next one. Water is eliminated during this process and linked amino acid residues remain. Bonds formed in this way are known as peptide bonds. In a protein many amino acids bond in this way to form a polypeptide chain [106]. The formation of a peptide bond is shown in figure B2.

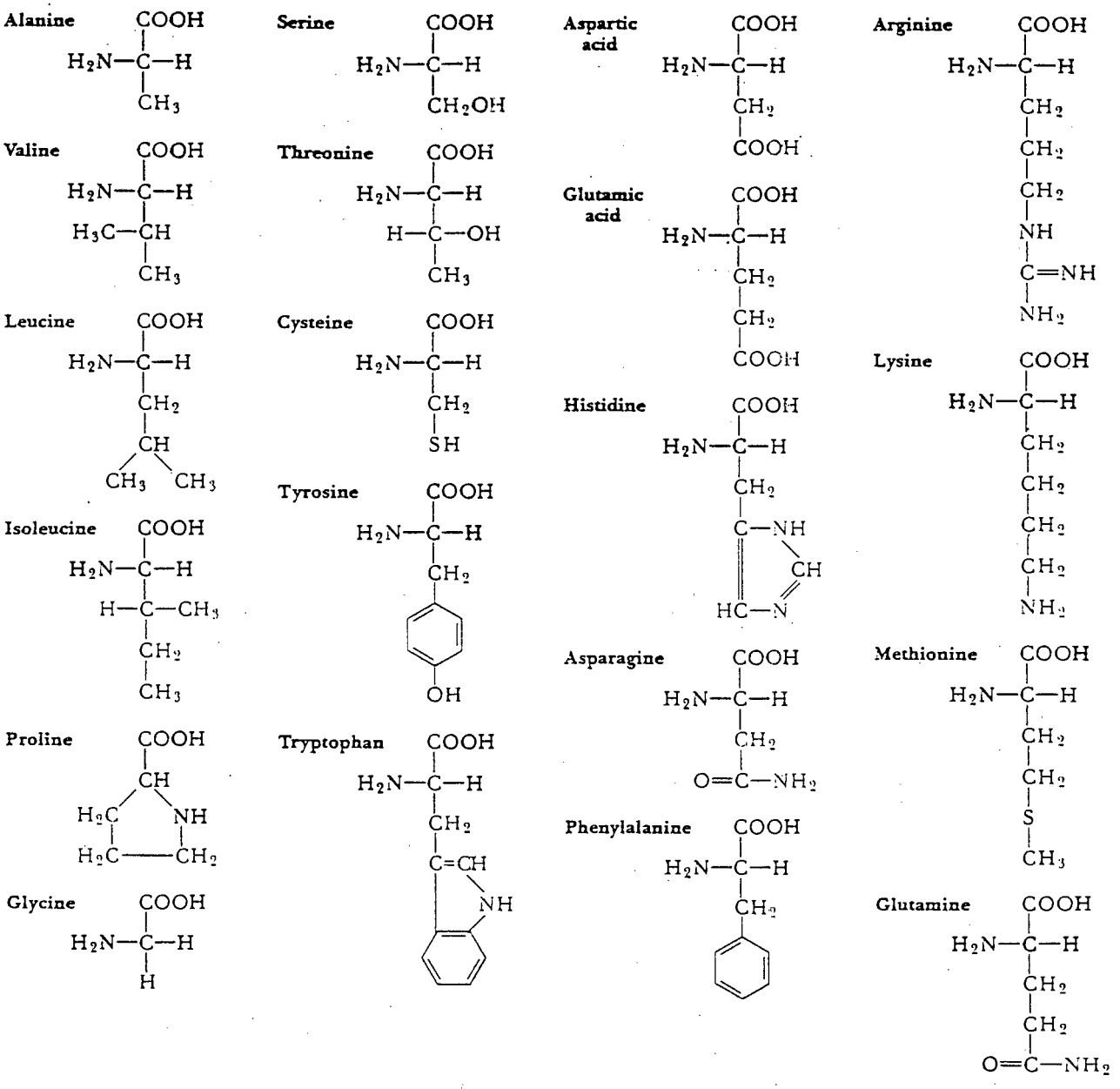

Figure B.1 *The 20 amino acids and their structures [106]*

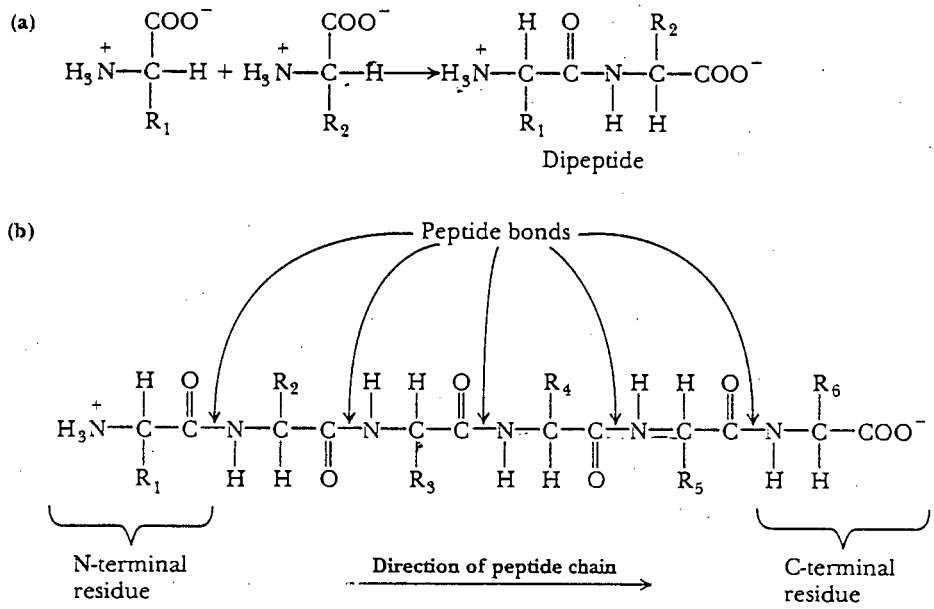

***Figure B 2** The formation of a peptide bond [106]*

The carbon nitrogen bond (formed when two amino acids are linked in a peptide bond) can be written as a single or double bond by shifting the position of an electron pair. The shifting of electrons in this manner is common in organic chemistry and results in resonance structures. These are structures which differ only by the position of the electrons. No resonance structure actually represents the bonding in a compound for which resonance structures can be written. All resonance structures contribute to the actual bonding. The peptide bond can be written as a resonance hybrid of two structures. One with a single bond between the carbon and the nitrogen and the other with a double bond between the carbon and the nitrogen. The peptide bond has a partial double bond character and so the peptide group that forms between two amino acids is planar. There is free rotation around the bonds between the α-carbon of a given amino acid residue and the amino nitrogen and the carbonyl carbon of that residue. There is no significant rotation around the peptide bond itself.

(An N-terminal amino acid is one with a free amino group. A C-terminal amino acid is an amino acid with a free carboxyl group)[106].

APPENDIX C

Polysaccharides

The simplest carbohydrates are known as monosaccharides. Monosaccharides are compounds that contain a single carbonyl group and two or more hydroxyl groups. Monosaccharides can undergo various reactions which include oxidation and esterification. The most important reaction is that of the formation of glycosidic linkages which result in oligosaccharides and polysaccharides. Monosaccharides are polyhydroxyaldehydes or polyhydroxyketones. It is possible for a sugar hydroxyl bond (ROH) to react with another hydroxyl (R'OH) to form an ester linkage (R'-O-R). This type of reaction frequently involves the -OH group bonded to the anomeric carbon of the sugar in its cyclic form. (Anomeric carbon is the carbonyl carbon of the open chain form of the sugar, it is the carbon that becomes a chiral centre in the cyclic form for monosaccharides). This newly formed bond is known as a glycosidic bond. Polysaccharides that occur in organisms are usually a combination of several types of monosaccharides. A polymer consisting of only one type of monosaccharide is known as a homopolysaccharide, while a polymer consisting of more than one type of monosaccharide is a heteropolysaccharide. Glucose is the most common monomer. There are usually only two types of molecules in a repeating sequence.

Hyaluronic acid is a heteropolysaccharide found in the connective tissue of animals. As a result of its highly viscous gelatinous consistency, it is known as a mucopolysaccharide. It is a polymer of two repeating units of two glucose derivatives, N-acetylglucosamine and glucuronic acid. Glucuronic acid is derived from glucose by the oxidation of the hydroxyl group at the C-6 carbon of glucose. The monomer units are linked together by alternating β (1$\rightarrow$ 3) and β (1 $\rightarrow$ 4) glycosidic bonds. Hyaluronic acid occurs in synovial fluid which is the lubricating fluid of joints [106].

APPENDIX D

Glycoproteins

Glycoproteins contain carbohydrate residues in addition to the polypeptide chain. Important examples of glycoproteins are involved in immune response. Antibodies which bind to an immobilise antigens (the substance attacking the organism) are glycoproteins. Carbohydrates play an important role as antigenic determinants, which are the portions of the antigenic molecule that antibodies recognise and to which they bind [106].

APPENDIX E

Properties of UHMWPE (Chirulen)

MedITECH

®Chirulen

Surgery

Under the trade name ®Chirulen, a specially pure form of ultrahigh-molecular-weight polyethylene (PE-UHMW) has been used as a semi-finished product for joint replacement surgery (see standards DIN 58834 and 58836).

Physical properties

The data quoted were determined on test specimens prepared from compression moulded sheet and film. Depending on the conditions of specimen preparation, individual measurements may deviate from these average values.

Property	Unit	Test method	Test specimen	®Chirulen
Density (of the homogeneously pressed material)	g/cm3	DIN 53479 method A	sheet	0,93
Viscosity number	ml/g	DIN 53728 sheet 4	concentration in decahydronaphthalene 0,0003 g/cm3	2300
Intrinsic Viscosity	ml/g	-	-	1920
Average molecular wt.	g/mol	-	-	$4{,}4 \cdot 10^6$
Yield value (150/10)	N/mm²	DIN 53493	dumbbell bar	0,25±0,05
Mechanical properties		(measured under standard climatic conditions 23°C, 50% RH)		
Yield stress	N/mm²	DIN 53455 ISO 527 testing rate: 50 [mm/min]	no. 3	≥ 20
Elongation at yield	%			≤ 20
Elongation at break	%			> 50
Tensile modulus	N/mm²	DIN 53457	test specimen no.3 of DIN 53455	720
Tensile creep modulus 1 hour value 1000 hour value	 N/mm² N/mm²	 DIN 53444 ISO 899		 460 230
Ball indentation hardness (value test load 365N)	N/mm²	DIN 53456 30-s-Wert	sheet, 4mm	38
Shore hardness D	-	DIN 53505 3 sec value	sheet, 6mm	63
Notched impact strength	mJ/mm²	DIN 53453	small standard test bar	no failure.
Notched impact strength (with 15° V-notch on both sides)	mJ/mm²	DIN 53453	120*15*10mm	≥ 200
Abrasion	-	Slurry method	sheet	100

MediTECH

Property	Unit	Test method	Test specimen	®Chirulen
Thermal properties				
Heat deflection temperature	°C	DIN53461,ISO75 method A	≥ 110*10*4mm	42
Vicat softening point	°C	DIN ISO 306 method B	10 * 10 * 4mm	80
Crystalline melting range	°C	differential thermal analysis	powder	130 – 135
Coefficient of linear expansion between 23°C and 80°C	1/K	DIN 53752	25 * 4 * 4mm	ca. $2 \cdot 10^{-4}$
Thermal conductivity at 23°C	W/m*K	resistance wire method	sheet, 10mm	0,41
specific heat at 23°C	kJ/kg*K	adiabatic calorimeter	powder	1,84
Electrical properties		(mesured under standartd climatic conditions 23°C, 50% RH)		
Volume resistivity	Ohm*cm	DIN 53482 VDE 0303 part 3	sheet, 1mm	$> 10^{14}$
Surface resistance	Ohm	DIN 53482 VDE 0303 part 3	sheet, 1mm	$> 10^{11}$
Dielectric strenght	kV/mm	DIN 53481 VDE 0303 part 2	sheet, 1mm	45
Relative transmittivity at 50 Hz	–	DIN 53483 VDE 0303 part 4	sheet, 1mm	2,1
at 1 MHz	–			3,0
Dissipation factor at 50 Hz	–		sheet, 1mm	$3,9 \cdot 10^{-4}$
Tracking CTI	comparative	DIN IEC 112		600
CTIM	index	VDE 0303 part 1	15 * 15 * 4mm	600
Arc resistance	rating	DIN 53484 VDE 0303 part 5	120*120*10mm	L4

This information is based on our present state of knowledge and is intended to provide general information on our products and their uses.
Therefore, it should not be construed as guaranteeing specific properties of the products described on their suitability for a particular application.

03/1994

REFERENCES

1. Cooper J R, Dowson D, Fisher J, *"Macroscopic and Microscopic Wear Mechanisms in Ultrahigh Molecular Weight Polyethylene"*, Wear, 162-164, 1993, p 378-384
2. Saikko V, *"Wear of Polyethylene Acetabular Cups against Zirconia Femoral Heads Studied in a Hip Joint Simulator"*, Wear, 176, 1994, p 207-212
3. Shanbhag A S, Jacobs J, Glant T, Gilbert J L, Black J, Galante J O, *"Composition and Morphology of Wear Debris in Failed Uncemented Total Hip Replacement"*, J Bone & Joint Surg, 76B, 1994, p 60-67
4. Willert H G, Semlitch M, *"Reactions of the Articular Capsule to Wear Products of Artificial Joint Prostheses"*, J Biomed Res., 11, 1977, p 157-164
5. Goldring S R, Schiller A L, Roelke M et al, *"The Synovial-like Membrane at the Bone-Cement Interface in Loose Total Hip Replacements and its Proposed Role in Bone Lysis"*, J Bone & Joint Surg [Am], 65-A, 1983, p 574-584
6. Maloney J, Jasty M, Harris W H, Galante J O, Callaghan J J, *"Endosteal Erosion in Association with Stable Uncemented Femoral Components"*, J Bone & Joint Surg [Am], 72-A, 1990, p 1025-1034
7. Howie D W, Vernon-Roberts B, Oakeshott R D, Manthey B, *"A Rat Model of Resorption of Bone at the Cement-Bone Interface in the Presence of Polyethylene Wear Particles"*, J Bone & Joint Surg [Am], 70-A, 1988, p 257-263
8. Goodman S B, Fornasier VL , Lee J, Kei J, *"The Histological effects of the Implantation of Different Sizes of Polyethylene Particles in the Rabbit Tibia"*, J Biomed. Mater Res., 24, 1990, p 517-524
9. Clarke I C (chairperson), Dorlot J-M, Graham J, Levine D J, Oonishi H, Rieu J, Rigney D, Schwartz G, Sedel L, Toni A, Zitelli J, *"Biomechanical Stability and Design : Wear"*, Position paper 8, Annals N. Y Academy of Sciences, 1988, p 292-296
10. Langkamer V G, Case C P, Heap P, Taylor A, Collins C, Pearse M, Solomon L, *"Systematic Distribution of Wear Debris After Hip Replacement- A Cause for Concern?"*, J Bone & Joint Surg., 74-B, No 6, Nov. 1992, p 831-839

11. Hernandez J B, Keating E M, Faris P M, Meding J B, Ritter M A, *"Polyethylene Wear in Uncemented Acetabular Components"*, J Bone & Joint Surg., 76-B, No 2, March 1994, p 263-266

12. Fisher J, Dowson D, Cooper J R, Jin Z M, Wroblewski B M, *"The Failure and Wear of UHMWPE in Artificial Joints"*, J Bone & Joint Surg., 75-B, 1993 : Sup III

13. Malcolm A J, *"Pathology of Longstanding Cemented Total Hip Replacements in Charnely's Cases"* , J Bone & Joint Surg., 70-B, 1988, p 153

14. McCrum N G, Buckley C P, Bucknall C B, **Principles of Polymer Engineering**, Oxford Sci. Publ, 1988

15. Crow J M G, **Polymers: Chemistry and Physics of Modern Materials**, 2nd edn, Blackie & Son Ltd. Chapman and Hall Inc., N Y, 1991.

16. Flory P J, Yoon D Y, *"Molecular Morphology in Semicrystalline Polymers"*, Nature, 272, 16 March, 1978, p 226-229

17. Meares P, **Polymers: Structure and Bulk Properties**, D Van Nostrand Company Ltd., London 1965

18. Fischer E W, *"Neutron-Scattering Studies on the Crystallization of Polymers"* Polym. J, 17, 1985, p 307-320

19. McCrum N G, Read B E, Williams G, **Anelastic and Dielectric Effects in Polymer Solids**, Wiley, N.Y., 1967

20. Vanderhart D L, *"Natural-Abundance C-13-C-13 Spin Exchange in Rigid Crystalline Organic Solids"* J Magn Reson., 72, 1987, p 13-47

21. Syi J-L, Mansfield M L, *"Solition Model of the Crystalline-Alpha Relaxation"* Polymer, 29, 1988, p 987-997

22. Schmidt-Rohr K, Spies H W, *"Chain Diffusion between Crystalline and Amorphous Regions in Polyethylene detected by ^{13}C NMR"*, Macromolecules, 24, 1991, p 5288-5293

23. Petermann I, Riek U, *"On the Plastic Deformation of Fibre Self-Reinforced Polymers"*, J Mat Sci, 22, 1987, p 1120-1126

24. Kestenbach H J, Petermann O, *"Micellular Morphology and its Plastic Deformation Behaviour in Ultra-high Molecular Weight Polyethylene"*, J Mat Sci, 29, 1994, p 6539-6542

25. Cho Myung H, Sadao H, Thein K, *"Crystal Twinning in Simultaneous Biaxial Stretching of Gelation-Crystallised Ultra-high Molecular Weight Polyethylene"*, J Mat Sci., 26, 1991, p 2507-2513

26. Suehiro K, Terashima T, Takayanagi M, *"Change of Mosaic Block Size of Bulk Polyethylene in Drawing Processes"*, J Mat Sci., 9, 1974, p 1563-1568

27. Pigeon M, Prud'homme R E, Pezolet M, *"Characterisation of Molecular Orientation in Polyethylene by Raman Spectroscopy"*, Macromolecules, 24, 1991, p 5687-5694

28. Peterlin A, *"Structure of Drawn Polymers"*, Technical Report AFML-TR-67-6 , US Air Force Materials Lab, Wright-Patterson, AFB, Ohio 1966

29. Zum Gahr K H, **Microstructure and Wear of Materials**, Tribology Series, V 10, Elsevier, Amsterdam, 1987

30. Rose W, Meurer Ch, *"Multiple Kinks in Lamellar Linear Polyethylene"* ,J Mat Sci, 16(4), 1981, p 883-888

31. Pietralla M, *"Twinning as a Fundamental Process in Polymer Crystal Orientation"*, Int J Polymeric Mater., 22, 1993, p 185-190

32. Marikhin V A, Myasinikova L P, **Supermolecular Structure of Polymers**, Kiminiya, Leningrad, 1978.(in Russian)

33. Guttman C M, DiMarzio E A, *"Polyethylene-like polymer between two plates-Connection to Gamblers Ruin Problem"*, Macromolecules, 15(2), 1982, p 525

34. Elyashevich G K, Karpov E A, Lavrentiev K V, Poddubny V I, Genina M A, Zabashta Y F, *"Changes in the Amorphous Phase of Polyethylene upon High Extension"*, Int J Polymeric Mater., 22, 1993, p 191-199

35. Ziatsev M G, Yaryukin S E, *"Thermodynamic Prediction of Molecular Morphology Parameters of Amorphous Regions of Worn Polymers"*, Int J Polymeric Mater., 22, 1993, p 33-40

36. Brydson J A, **Plastics Materials**, 4th edition, Butterworth Scientific, 1982

37. Noinville V, Vidal-Madjar C, Sebille B, *"Modelling of Protein Adsorption on Polymer Surfaces. Computation of Adsorption Potential"*, J Phys Chem, 99, 1995, p 1516-1522

38. Cherry B W, **Polymer Surfaces**, Cahn R W, Thompson M W, Ward I M (eds), Cambridge University Press 1981

39. Tabor D, *"Friction-The Present State of Our Understanding"*, J Lub Tech, ASME Trans, 103, 1981, p 169-179

40. Halling J, **Introduction to Tribology**, Wykenham Publ., London, 1976

41. Czichos H, *"Introduction to Friction and Wear"*, in **Friction and Wear of Polymer Composites** , K Friedrich (ed), Ch1, 1, Composite Materials Series, Amsterdam, Elsevier, 1986, p 1-23

42. Benabdallah S H, *"Shear Strength Resulting from Static Friction of Some Thermoplastics"*, J Mat Sci, 28, 1993, p 3149-3154

43. Marcus K, **Micromechanisms of Polymer Sliding Wear**, Thesis

44. J K Lancaster, *"Material-specific Wear Mechanisms: Relevance to Wear Modelling"*, Wear, 141, 1990, p 159-183

45. Tabor D, *"The Wear of Non-Metallic Materials: a Brief Review"*, from **The Wear of Non-Metallic Materials**, Proceedings of the 3rd Leeds-Lyon Symposium on Tribology, Sept. 1976, Mech. Eng.Publ, p 3-8

46. Gong D, Xue Q, Wang H, *"Physical Models of Adhesive Wear of Polytetrafluoroethylene and its Composites"*, Wear, 147, 1991,p 9-24

47. Buckley D H, **Surface Effects in Adhesion, Friction, Wear and Lubrication**, Tribology Series 5, Elsevier, N.Y., 1981

48. Briscoe B J, *"Wear of Polymers : An Essay on Fundamental Aspects"*, Trib Int., 14, Aug 1981, p 231-234

49. Zum Gahr K H, **Microstructure and Wear of Materials**, Tribology Series, V 10, Elsevier, Amsterdam, 1989

50. Lancaster J K, *"Abrasive Wear of Polymers"*, Wear, 14, 1969, p 223-239

51. Rose R M, Cimino W R, Ellis E, Grugnola A N, *"Exploratory Investigation on the Structure Dependence of the Wear Resistance of Polyethylene"*, Wear, 77, 1982, p 89-104

52. Jones W R (jr.), Hady W F, Grugnola A N, *"Effect of γ - Irradiation on the Friction and Wear of Ultra-high Molecular Weight Polyethylene"*, Wear, 70, 1981, p 77-92

53. Wineman A, *"Mechanical Response of Linear Viscoelastic Solids"*, MRS Bulletin, May 1991, p 19-23

54. McLaren K G, Tabor D, *"Viscoelastic Properties and the Friction of Solids. Friction of Polymers : Influence of Speed and Temperature"*, Nature, 197, 1963, p 856-858

55. Ludema K C, Tabor D, *"The Friction and Viscoelastic Properties of Polymeric Solids"*, Wear, 9, 1966, p 329-348

56. Briscoe B J, Tabor D, *"Friction and Wear of Polymers : The Role of Mechanical Properties"*, Br Polym Journal, 10, March 1978, p 74-78

57. Bahadur S, Stiglich J, *"The Wear of High-Density Polyethylene Sliding Against Stainless Steel Surfaces"*, Wear, 68, 1981, p 85-95

58. Dowson D, Harding R T, *"The Wear Characteristics of Ultrahigh Molecular Weight Polyethylene against a High Density Alumina Ceramic under Wet (distilled water) and Dry Conditions"*, Wear, 75, 1982, p 313-331

59. Hollander A E, Lancaster J K, *"An Application of Topographical Analysis to the Wear of Polymers"*, Wear, 25, No 2, 1973, p 155-170

60. Rose R M, Goldfield H V, *"On the Pressure Dependence of the Wear of Ultrahigh Molecular Weight Polyethylene"*, Wear, 92, 1983, p 99-111

61. Rose R M, Crugnola A, Ries M, Cimino R, Radin Paul, Radin E L, *"On the Origins of High* In Vivo *Wear Rates in Polyethylene Components of Total Joint Prostheses"*, Clin Orthop., 145, 1979, p 277-289

62. Komoto T, Tanaka K, *"Morphological Study of the Wear of Crystalline Polymers I: High Density Polyethylene"*, Wear, 75, 1992, p 173-182

63. Bonfield W, *"Hydroxyapatite-Reinforced Polyethylene as an Analagous Material for Bone Replacement"*, Annals NY Academy of Sciences, 1988, p 173-177

64. Callaghan J, *"Results of Primary Total Hip Arthroplasty in Young Patients"*, J Bone & Joint Surg., 75-A, No 11, Nov 1993, p 1728-1734

65. *Biomedical Stability and Design - Strength*, Annals N Y Academy of Sciences, Position Paper 7, 1988, p 287-291

66. Christel P, Meunier A, Dorlot J-M, Crolet J-M, Witvoet J, Sedel L, Boutin P, *"Biomechanical Stability and Design of Ceramic Implants for Orthopaedic Surgery"*, Annals N Y Academy of Sciences, 1988, p 234-255

67. Lewis G, Daigle K, *"Electrochemical Behaviour of Ti-6Al-4V Alloy in Static Biosimulating Conditions"*, Jnl Applied Biomaterials, 4, 1993, p 37-45

68. Agins H J, Alcock N W, Bansal M et al, *"Metallic Wear in Failed Titanium-Alloy Total Hip Replacements : A Histological and Quantitative Analysis"*, J Bone & Joint Surg [Am], 70-A, 1988, p 347-356

69. Lombardi A, Mallory T H , Vaughan B K, Drouillard P, *"Aseptic Loosening in Total Hip Arthroplasty Secondary to Osteolysis Induced by Wear Debris from Titanium Alloy Modular Femoral Heads"*, J Bone & Joint Surg [Am], 71-A, 1989, p 1337-1342

70. Robinson R P, Lovell T P, Green T M, Bailey G A, *"Early Femoral Component Loosening in DF-80 Total Hip Arthroplasty"*, J Arthroplasty, 1989, 4, p 55-64

71. Black J, Sherk H, Bonino J et al, *"Metallosis Associated with a Stable Titanium Alloy Femoral Component in Total Hip Replacement : A Case Report"*, J bone & Joint Surg [Am], 1990, 72-A, p 126-130

72. Witt J D, Swann M, *"Metal Wear and Tissue Response in Failed Titanium Alloy Total Hip Replacements"*, J Bone & Joint Surg. [Br], 1991, 73-B, p 559-563

73. Boehler M, Nahr K, Plank H(Jr), Walter A, Salzer M, Schreiber V, *"Long-term Results of Uncemented Alumina Acetabular Implants"*, J Bone & Joint Surg [Br], 76-B, 1994, p 53-59

74. Sedel L, *"Ceramic Hips"*, J Bone & Joint Surg [Br], 74-B, 1992, 331-332

75. C Clarke (chairperson), *"Biomechanical Stability and Design: Wear"*, Position Paper 8, Annals N Y Academy of Sciences, 1988, p 292-296

76. Katz J L (chairperson), *"Biomechanical Stability and Design : Stiffness and Remodelling"*, Annals N Y Academy of Sciences, 283-286

77. Cook S D, Barrat R L, Clemow A J T, *"Corrosion and Wear at the Modular Interface of Uncemented Femoral Stems"*, J Bone & Joint Surg [Br], 76-B, 1994, p 68-72

78. Wang A, Sun D C, Stark C, Dumbleton J H, *"Wear Mechanisms of UHMWPE in Total Joint Replacements"*, Wear, 181-183, 1995, p 245-249

79. Feller W, **An Introduction to Probability Theories and Its Applications**, 1, Wiley N.Y., 1968, p 175-190

80. Lennox D W, Schofield B H, McDonald D F, Riley L H, *"Aseptic Loosening in Various Prostheses"*, Clin Orthop & Rel Res, 225, 1987, p 171-191

81. Maloney W J, Peters P, Engh C A, Chandler H, *"Severe Osteolysis of the Pelvis in Association with Acetabular Replacement without Cement"*, J Bone & Joint Surg, 75-A, No 11, Nov 1993, p 1627-1635

82. Lee J M, Salvati E A, Betts F, DiCarlo E F, Dory S B, Bullough P G, *"Size of Metallic and Polyethylene Debris in failed Total Hip Replacements"*, J Bone & Joint Surg, 74-B, 1992, p 380-384

83. Escalas F, Galante J, Rostoker W, *"Biocompatibility of Materials for Total Joint Replacement"*, J Biomed. Res., 10, 1976, p 175-195

84. Johansen N A, Bullough P G, Wilson P D Jr, Salvati E A, Ranawat C S, *"The Microscopic Anatomy of the Bone-Cement Interface in Failed Total Hip Arthroplasties"*, Clin. Orthop., 218, 1987, p 123-135

85. Cohen J, *"Assay of Foreign Body Reaction"*, J Bone & Joint Surg [Am], 41-A, 1976, p 391-397

86. Matlaga B F, Yasenchak L P , Salthouse T B, *"Tissue Response to Implanted Polymers: the Significance of Sample Shape"*, J Biomed Mater. Res., 10, 1976, p 391-397

87. Salthouse T N, *"Some Aspects of Macrophage Behaviour at the Implant Interface"*, J Biomed Mater Res, 18 , 1984, p 395-401

88. Isaac G H, Atkinson J R, Dowson D, Wroblewski B M, *"The Role of Cement in the Long-term Performance and Premature Failure of Charnley Low Friction Arthroplasties"*, Eng Med, 15(1), 1986, p 19-22

89. Maloney W J, Jasy M, Harris W, Galante J O, Callaghan J J, *"Endosteal Erosion in Association with Stable Uncemented Femoral Components"*, J Bone & Joint Surg., 75-A, Aug 1990, p 1025-1034

90. Maloney W J, Peters P, Eng C A, Chandler H, *"Severe Osteolysis of the Pelvis in Association with Acetabular Replacement without Cement"*, J Bone & Joint Surg., 75-A, No 11, Nov 1993, p 1627-1635

91. Schmalried T P, Jasty M, Harris W H, *"Periprosthetic Bone Loss in Total Hip Arthroplasty. Polyethylene Wear Debris and the Concept of Effective Joint Space"*, J Bone & Joint Surg., 74-A, July 1992, p 849-863

92. Robert J, Quastel J H, *"Particles Uptake by Polymorphonuclear Leucocytes and the Ehrlich Ascites-Carcinoma Cells"*, Biochem J, 1963, 89, p 150-156

93. Glant T T, Jacobs J J, Monlar G, et al, *"Bone Resorption Activity of Particulate-Simulated Macrophages"*, J Miner Res., 1993, 8, p 1071-1079

94. Glant T T, Jacobs J J, *"Response of 3 Murine Macrophage Populations to Particulate Debris- Bone-Resorption Reaction Organ Cultures"*, J Orthop. Res., 12(5), 1994, p 720-731

95. Shanbag A S, Jacobs J J, Black J, Galante J O, Glant T T, *"Macrophage/Particle Interactions : The Effect of the Size, Composition and Surface Area"*, J Biomed Mater. Res., 1994, 28, p 81-90

96. Tabor D, **The Role of Surface and Intermolecular Forces in Thin Film Lubrication. Microscopic Aspects of Adhesion and Lubrication**, J M Georges (ed), Amsterdam, Elsevier, Tribology Series, 7, 1982, p 651-659

97. Avitzur B, *"Boundary and Hydrodynamic Lubrication"*, Wear, 139, 1990, p 46-76

98. Halling J (ed), **Principle of Tribology**, McMillan Press Ltd, London, 1983

99. **Lubrication Theory and Its Applications**, BP Trading Ltd, London, 1969

100. Meldahl A, *"Contribution to the Theory of the Lubrication of Gears and the Stressing of the Lubricating Flanks of Gear Teeth"*, Brown Boveri Rev., 28(11), 1941, p 374

101. Dowson D, *"Elastohydrodynamic and Micro-elastohydrodynamic Lubrication"*, Wear, 190, 1995, p 125-138

102. Kapsa P, Martin J, *"Boundary Lubricant Films : a review"*, Trib Int., 15(1), 1982

103. Swanson S A V, *"Mechanical Breakdown of Articular Cartilage in Osteoarthrosis"*, Paper V(1), from **The Wear of Non-Metallic Materials**, Proceedings of the 3rd Leeds-Lyon Symposium on Tribology, Sept 1976, Mech Eng Publ. Ltd., 1978, p 109-112

104. Unsworth A, Dowson D, Wright V, Koshal D, *"The Frictional Behaviour of Human Synovial Joints part 2 : Artificial Joints"*, J Lubr. Technol., July 1975, p 377-382

105. Unsworth A, *"The Effects of Lubrication in Hip Joint Prostheses"* Phys. Med. Biol., 23, 1978, p 253-268

106. Campbell M K (ed), **Biochemistry**, Saunders College Publishing, USA, 1991

107.Florkin M, Stoltz E (eds), **Comprehensive Biochemistry Proteins (part 1)**, 7 Elsevier, 1963

108.Nigam K M, Bujurke N M, Singh M P, Manohair K, *"Second-grade Fluid Film Lubrication in Hertzian Contacts with Reference to Synovial Joints"*, Wear, 84, 1983, p 261-274

109.Sinha P, Singh C, Prasad K R, *"Lubrication of Human Joints, a Microcontinuum Approach"*, Wear, 80, 1982, p 159-181

110.Prakash J, Sinha P, *"Lubrication Theory of Micropolar Fluids and its Application to a Journal Bearing"*, Int. J Eng Sci., 13, 1975, p 217-232

111.Linn F C, Radin E L, *"Lubrication of Animal Joints III, the Effect of Certain Chemical Alteration of the Cartilage and the Lubricant"*, Arth. Rheum., II, 1968, p 674-682

112.O'Kelly J, Unsworth A, Dowson D, Hall D A, Wright V, *"A Study of the Role of Synovial Fluid and its Constituents in the Friction and Lubrication of Human Hip Joints"*, Engng Med., 7, 1978, p 78-83

113.Berzen J, Birnkraut H W, Braun G, **"***Ultrahigh Molecular Weight Polyethylene (UHMW-PE): Application in Artificial Joints"*, British Polymer Journal, 10, Dec 1978, p 281-287

114.Fisher J, Dowson D, Hamdzah H, Lee H L, *"The Effect of Sliding Velocity on the Friction and Wear of UHMWPE for use in Artificial Joints"*, Wear, 175, 1994, p 219-225

115.Dowson D, Diab M M, Gillis B V, Atkinson J R, in Lee L H (ed.), *"Polymer Wear and its Control"*, American Chemical Society, series 287, 1985, p 171-187

116.McKellop H, Lu B, Benya P, 38th Ann Meet. Orthopaedic Research Society, Feb 17-20, 1992, Washington D C

117.Rol'nik V V , **Bird Embryology**, Academy of Sciences USSR, Israel Program of Scientific Translations, Jerusalem, 1970

118.Florkin M, Stotz E (eds), **Comprehensive Biochemistry**, 9, Elsevier Publ, Amsterdam, 1963

119.Sole B, personal communication

120.Dowson D, *"A Comparative Study of the Performance of Metallic and Ceramic Femoral Head Components in Total Hip Replacements"*, Wear, 190, 1995, p 171-183

121.Soltez U, *"Ceramics in Composites : Review and Current Status"*, Annals N Y Academy of Sciences

122.Saikko V, *"Wear and Friction Properties of Prosthetic Joint Materials Evaluated on a Reciprocating Pin-on-Flat Apparatus"*, Wear, 166, 1993, p 169-178

123.Kumar P, Oka M, Ikeuchi K, Shimizu T, Yamamaro T, Okumura H, Koloura Y, *"Low Wear Rates of UHMWPE against Zirconia Ceramic in Comparison to Alumina Ceramic and SUS 316L Alloy"*, J Biomed Mater Res., 25, 1991, p 813-818

124.Atkinson J R, Charnley J, Dowling J M, Dowson D, *"The Wear of Total Replacement Hip Joints in the Human Body - A Topographical Survey of the Surfaces of the Worn Acetabular Cups"*, Paper V from **The Wear of Non-Metallic Materials**, Mech Eng Publ Ltd, 1978, p 127-132

125.McKellop H A, Campbell P, Park S-Y, Schmalzried T P, Grigoris P, Amstutz H, Sarmiento A, *"The Origin of Sub-Micron Polyethylene Wear Debris in Total Hip Arthroplasty"*, Clin Orthopaedics Relat. Res., 137, 1995, p 3-20